

This book of contributed papers includes the original abstracts of lectures presented at the International Workshop “Nonequilibrium Processes in Combustion and Plasma Based Technologies” (Minsk, August 21 - 26, 2004).

Данный сборник содержит оригинальные тексты докладов, представленных на международный научный семинар “Неравновесные процессы в горении и плазменных технологиях” (Минск, 21 - 26 августа 2004г.).

Редакционная коллегия:

Е.А. Матвейчик, А.Н. Мигун, А.П. Чернухо

Рецензенты:

академик НАН Беларуси С.А. Жданок академик
НАН Беларуси А.Г. Шашков

Section 1. Elementary processes in plasma and combustion phenomena

DISSOCIATION AND RECOMBINATION PROCESSES OF CARBON MONOXIDE MOLECULES IN ELECTRICAL DISCHARGES

F. M. GRIGORIAN¹, I. V. KOCHETOV²

¹ VA.Fock Institute of Physics, St.Petersburg University, St.Petersburg, 198504, Russia

² Troitsk Institute for Innovation and Fusion Research, Moscow Region, 142190, Russia

The dynamics of CO molecule decomposition and regeneration has drawn increasing attention. Interest in this problem has been widely expanding. Processes involving CO molecules play an important role in gas discharge plasmas, plasma chemical technology, combustion, astrophysics and physics of atmospheres. Despite their importance many of the general characteristics of such processes are not yet well established.

In this work we present results of experimental and theoretical investigation of processes governing the concentration of carbon monoxide molecules in gas discharge plasmas in the wide range of experimental conditions. For the first time, simultaneous measurements of concentration of CO molecules and products of their decomposition (O, C, CO₂) and comparison of these concentrations with theoretical ones resulted in development schemes of the processes controlling the concentration of CO molecules for wide range of experimental conditions in gas discharge plasmas (including gas-flow and sealed-off discharges, as well). The dependence of a type of the dominant dissociation channel of experimental conditions has been analyzed. Rate constants for the process of heterogeneous recombination of C and O atoms leading to CO molecules regeneration were estimated. Their dependence on experimental parameters was studied.

The experimental setup was similar to that described in [1, 2]. The experiments were carried out with a 15-mm-diameter discharge tubes made of molybdenum glass or alund ceramics (Al₂O₃) and cooled with flowing water. The length of the discharge region was 50 cm. A DC discharge was ignited in He/CO and He/CO/Xe mixtures in the gas flow or in sealed-off volume. The concentrations of CO molecules and Xe atoms were 0.05-12% and 5-12%, respectively. The pressure was varied in the range 1-15 torr.

The mixture composition in the discharge tube was analyzed with an MSC-6 time-of-flight mass spectrometer. The time evolution of the concentrations of stable products in the discharge plasma was monitored by periodically analyzing gas samples. The emission from the positive column of the discharge in the spectral range of 200-3000 nm was recorded with a spectrometer. The analysis of the emission spectra allowed us to determine the populations of the vibrational levels of CO molecules, the gas temperature at the discharge axis and its radial profile (by analyzing the rotational structure of the bands of CO molecules), and the concentrations of the electronically excited particles in the gas discharge plasma.

Concentrations of C and O atoms in the discharge plasma were found in a similar way as it was done in [3]: concentrations of atoms in the ground state were calculated from the measured concentration of the atom in excited states. Experimental concentrations of CO, CO₂ molecules (measured by mass spectrometer) and C, O atoms were compared with theoretical ones.

The concentrations of CO molecules, plasma chemical molecular products CO₂, CO(a³Π), C₂O, C₂, O₂ and atoms C, O and metastable He and Xe atoms were calculated by solving a set of non-equilibrium balance equations taking in to account diffusion of the

species to the walls. Detailed description of the plasma chemical model used one can find in [2]. The rate constants for the processes with the participation of electrons were calculated by

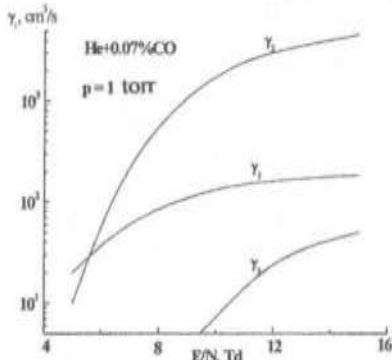


Fig. 1

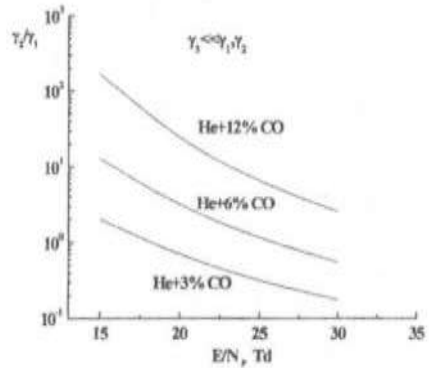


Fig. 2

numerically solving the kinetic Boltzmann equation for the electron energy distribution function (EEDF). In simulations, we took into account the scattering of electrons by the vibrationally excited CO molecules. The molecule distribution over vibrational levels was assumed to be Boltzmann one, and the vibrational temperature was taken from the experimental data. The used sets of cross sections and the technique of computing were described in detail in [1].

Investigation has shown that the main processes of CO dissociation in the discharge plasma in the whole range of examined experimental conditions were the following:



The rates of processes of (1), (2) and (3) are $v_1 = [\text{CO}] n_e k_1$; $v_2 = [\text{CO}] [\text{CO}^*(a^3\Pi)] k_2$;

$v_3 = [\text{CO}] [\text{He}^*(2^3S)] k_3$, (where $k_2 = 1.2 \cdot 10^{12} \text{ cm}^3/\text{s}$ [4], $k_3 = 2 \cdot 10^{12} \text{ cm}^3/\text{s}$ [5]). The relative contribution of each of these processes to CO decomposition strongly depends on the experimental conditions. Fig.1 and 2 illustrate relative efficiency ($\gamma_i = v_i/v_e$) for different cases.

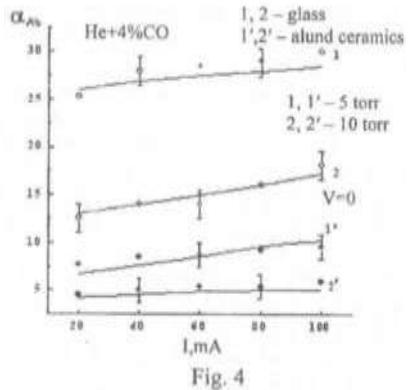
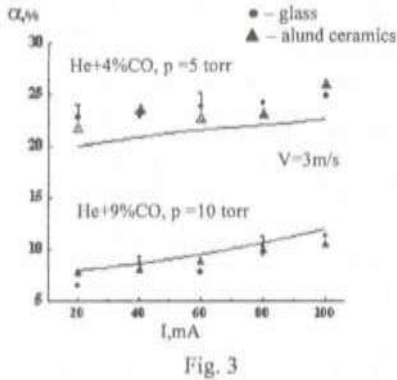
Experimental values for the degree of carbon monoxide decomposition were found to be in good agreement with theoretical ones (Fig. 3).

In sealed-off discharges, processes controlling CO concentration in plasma are more complicated. In this case, the CO concentration strongly depends on the rate of heterogeneous regeneration of CO molecules on the walls of the discharge tube. In [2] we have shown, that this formation of CO molecules can be ascribed to the process of heterogeneous recombination called Eley-Rideal mechanism (involves the reaction of adsorbed species A with an impinging gas-phase atom B) where C and O atoms take part:



and/or





with the following effective frequency:

$$k_{eff}^{CO} = \frac{k_{rec}^{CO} \frac{S}{V} v_{diff}}{k_{rec}^{CO} \frac{S}{V} + v_{diff}}; S, V \text{ are surface area and volume of the discharge tube; } v_{diff} = D/\Lambda^2 \text{ is}$$

frequency of the atom diffusion; D is the diffusion coefficient, $\Lambda = r/2.4$, r is the radius of the discharge tube, k_{rec}^{CO} is the rate constant of the heterogeneous recombination of C and O atom in He-CO mixtures in the molybdenum glass discharge tube was found to be $k_{rec}^{CO} = (6 \pm 2) \cdot 10^{18} / [CO]$ cm/s ($[CO]$ in cm^{-3}). The calculated CO

concentrations in a discharge as functions of the discharge current are shown in Fig. 4, which demonstrates good agreement between the experimental data and the calculated results obtained with allowance for the heterogeneous recombination of C and O atoms.

A comparison of the calculated and experimental results on the CO concentration in He-CO-Xe mixtures shows that the rate constant for heterogeneous recombination reaction (4) differs from that in He-CO mixtures; namely, it is $k_{rec}^{CO} = (2 \pm 0.5) \cdot 10^{19} / [CO]^{0.8}$ cm/s ($[CO]$ in cm^{-3}). The value is close to that measured in He-CO mixtures; however, the dependence of k_{rec} on the CO concentration is weaker, which can be related to the change in the wall properties under the action of the discharge plasma in He-CO-Xe mixtures.

Experiments have shown strong influence of the sort of walls material on the value of rate constant k_{rec} . In the alund ceramics discharge tube this rate constant was found to be 4 times higher than in the molybdenum glass discharge tube. Such a high efficiency of CO regeneration gives rise a rather low degree of CO decomposition in ceramics tube in comparison to molybdenum glass tube (Fig. 4). In contrast, in the case of gas-flow discharge (Fig.3), where heterogeneous recombination (4) does not control CO concentration, the degree of dissociation does not depend on the sort of wall material.

Special experiments carried out with electrodes made of other materials and with different surface areas showed that in sealed-off discharges, with all other factors being the same, variations in the electrode material and surface area do not affect the degree of the dissociation of CO molecules in plasma in the initial stage of a discharge ($t < 10$ h), so that our model can be used to predict the mixture composition in a discharge plasma.

For longer sustaining discharges, their parameters begin to depend on the electrode material and surface area. Variation in the concentrations of CO and plasmachemical products observed in this stage are caused by the processes that were not taken into account in the

above model (in particular, by the processes occurring at the discharge electrodes). Since the processes at the electrodes have not yet been studied even qualitatively, we did not attempt to incorporate the processes at the electrode surface in our model.

We have measured the time evolution of the degree of dissociation of CO molecules and the concentrations of the main products of plasmachemical reactions in the plasma of a sealed-off CO laser. A comparison of the calculated results with the experimental data on the concentrations of CO₂, C, and O in the initial stage of a discharge (for an operation time of less than 10 h) have shown that the plasmachemical model proposed in this study can be successfully used to predict the mixture composition in the plasma.

A comparison of the calculated and measured concentrations has shown that the main process leading to the regeneration of CO molecules in a sealed-off discharge is the heterogeneous recombination of C and O atoms. The rate constants for this process have been estimated under different conditions.

Authors express their gratitude to A.P. Napartovich for useful discussions.

This study was partially supported under grant N 04-02-16961 of Russian Foundation for Basic Research.

References

1. Grigorian G.M., Kochetov I.V. *Plasma Phys.Reports*. 2003, Vol.29, N.8, pp.709-714.
2. Grigorian G.M., Kochetov I.V. *Plasma Phys.Reports*. 2004, Vol.30, N.8. (in press).
3. Ionikh Yu.Z., Kuranov A.L., Ermolaev Yu.V. *Proc.6th All-Union Conf. Physics of Low- Temperature Plasma, Leningrad*. 1983 Vol.1, pp.86-88.
4. Ivanov E.E., Ionikh Yu.Z., Penkin N.P., Chernysheva N.V. *Khim. Fiz.* 1988, Vol.7, pp. 1694-1699.
5. Chang R.S., Setser D.W., Taylor G.W. *Chem.Phys.* 1978, Vol.35, pp.204-208.

LEVEL DESCRIPTION OF PHYSICAL AND CHEMICAL PROCESSES IN STRONG SHOCK WAVES

S.A. LOSEV

Institute of Mechanics, Moscow State University, 119192, Michurinsky prospekt, 1,
Moscow, Russia

Invited Lecture **Introduction**

Thermal and chemical equilibrium of a gas medium is considerably violated in strong shock waves. Under these conditions, the most appropriate description of kinetics of molecular dissociation and chemical exchange reactions is provided by the level (state-to-state) kinetic theory approach, which treats the variation of individual vibrational level populations of molecules in the absence of the Boltzmann distribution. Realization of such a method requires modelling of the elementary processes rate coefficients depending on the vibrational state of molecules involved in the reaction. In order to obtain reliable data on the state specific rate coefficients, the analysis of existing models of molecular collisions with chemical transformation has been carried out, and the level rate coefficients in equations of chemical kinetics have been determined (see [1], Chapter 4). As a result, a base of models has been developed; it includes empirical and discursive level models.

The level (or state-to-state) chemical kinetics may be of three types:

- initial level kinetics, when it is fixed initial vibrational states only of chemical reagents (example is the dissociation of diatomic molecules);
- final level kinetics, when it is fixed vibrational states only of products of reactions
- (example is the recombination with formation of diatomic molecules);
- full (state-to-state) level kinetics, when it is fixed initial states and also final states of chemical reagents and products of reactions.

In action the models of processes with initial level kinetics are more useful. The models with final level kinetics are less common, but there is only one model with full level kinetics (see below - the vibronic term model of electronic-nonadiabatic processes). The results of quasiclassical trajectory (QCT) method of collision dynamics are used for description of full level kinetics. The other problem is the modelling of electronic level kinetics and corresponding models for rate coefficients.

Some models for level kinetics

The review and examination of level rate coefficients models for diatomic molecules dissociation and decay of polyatomic molecules, bimolecular reactions of chemical exchange lead to the base of models; the part of this base includes the following models, where k_{dm} and k_{em} are the m -th vibrational level rate coefficients for dissociation and exchange reactions, respectively. Some of these models are the concrete definitions of thermal non-equilibrium two-temperature models (see [2]), Chapter 6) for the descriptions of several channels of chemical reactions with corresponding vibrational energy E_m on m -th vibration level.

For dissociation of diatomic molecules $A+B+M \rightarrow A+B+M$, *Marrone-Treanor model* leads to

$$k_{dm}(T) = k_d^0 \left\{ \frac{Q_v(T)}{Q_v(-U)} \exp \left[E_m \left(\frac{1}{T} + \frac{1}{U} \right) \right] \right\},$$

where $k_d^0(T)$ is the thermally equilibrium rate constant of dissociation, D_0 is the dissociation energy of diatomic molecule (in K), Q_v is the partition functions over vibrational states, E_m is the vibrational energy on the m -th vibrational level (in K), U is the model parameter [3]; usually $U = D_0/6$, but see below.

In accordance with the initial level kinetics *model of vibrational energy efficiency* (a_0 -model) [4] on the assumption that efficiency of translational energy of collision of reactants in activation energy E_a is complete, the level rate coefficients of exchange reactions are:

$$k_{em}(T) = A(T) \exp \left[-\frac{E_a - \alpha E_m}{kT} \bar{\theta}(E_a - \alpha E_m) \right],$$

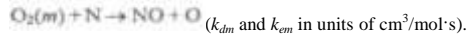
where α is the efficiency of vibrational energy E_m in activation of reaction, θ is Heaviside function ($\bar{\theta}(x) = 1$ for $x \geq 0$, $\bar{\theta}(x) = 0$ for $x < 0$). The pre-exponential factor $A(T)$ is close to the collision frequency per one concentration of particles (see [2], p.31). The values of the coefficient α are indicated in [4]; the examples are:

Reaction	$N_2(m)+O \rightarrow N+NO$	$O_2(m)+N \rightarrow O+NO$	$NO(m)+O \rightarrow N+O_2$	$O_2(m)+NO \rightarrow O+NO_2$
α	0.51	0.24	0.94	0.85

Warnatz model is based on the theory of chemically active collisions [5]. In accordance with this theory chemical reaction occurs when the energy of relative motion along the line between center of colliding particles exceeds the reaction threshold energy. Calculations [6] on the basis of Warnatz model indicate, that for initial level kinetics

$$\left. \begin{matrix} k_{dm} \\ k_{em} \end{matrix} \right\} = C(m+1)T^\beta \exp \left[-\frac{E - E_m}{kT} \bar{\theta}(E - E_m) \right],$$

where $E = D_0$ for dissociation reactions (D_0 - dissociation energy) and $E = E_a$ for exchange reactions (E_a - activation energy), θ is the Heaviside function (see above), $C = 2 \times 10^{13}$ and $\beta = 0$ for dissociation O_2 , $C = 1.14 \times 10^{15}$ and $\beta = -0.6$ for dissociation N_2 , $C = 4.17 \times 10^{12}$, $\beta = 0$ for reaction $N_2(m) + O \rightarrow NO + N$ and $C = 2 \times 10^9$, $\beta = 1.0$ for reaction



The calculation result for distributions of population density of vibrational levels for O_2 molecule (in molar fractions) behind a shock wave front in air is shown in Fig.1; initial temperature of air behind front of a normal shock wave in this example is equal to 22000 K, pressure before front is equal to 0.02 Torr. As it is seen from Fig.1, the population density of the excited vibrational levels initially (for about 2×10^{-6} s) grows because of vibrational energy exchange, and then it decreases as a result of chemical reactions. The steady-state equilibrium distribution of molecules O_2 over vibrational levels corresponds to temperature 5810 K.

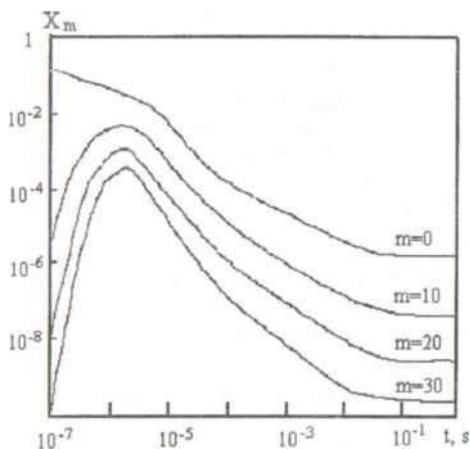


Fig.1. The time dependence of population density distribution over m vibrational levels of molecules O_2 (molar fractions x_m) behind a shock wave front in air

Semiclassical Macheret-Adamovich model [7] is the nonempirical model without adjustable parameters; see information about this model in [8].

The full level kinetics is investigated by A.Yu. Staiikovskiy [9] (see also [8]) using *vibronic term model* for exchange reactions $AB(m) + C \rightarrow A + BC(n)$, where values m and n are the vibrational levels number for corresponding molecules. In accordance with this model the transitions are the electronic-nonadiabatic process with the probabilities by Landau- Zener mode (see [1], Chapter 5). It is significant that this model is usable for full level kinetics, but it is only qualitative one for electronic-adiabatic processes and needs the additional parameters variations.

The description of the *information-theoretical approach (IT)*, *level modified model of vibrational energy efficiency (a_{mod} -model)*, *level modified CVCV-model* are considered in [10]. The purpose of these models is the simple universal relations between modified parameters using information about the energy fraction ξ_v , as the energy part which goes into vibrations of the molecule-product of reverse exothermic reaction, that is the molecule- reactant of direct endothermic reaction. The dependence of level rate constants $k(T, m)$ on vibrational energy E_m for modified CVCV-model is identical to CVDEV-model, see [11].

Application of QCT method results

By now many interesting and reliable results have been obtained in the solutions of dynamic collision problems by means of quasiclassical trajectory method (see [12-15] as examples). Although the problems of practical using of these results remain, because their presentations are limited to numerical and graphic demonstrations without simple analytical model approximation over gas temperature T and vibrational level number m . Only two initial level kinetics models: Losev γ -model [16] and Levitsky model [17] are the function-approximated results based on quasiclassical trajectory method. The simple formulas of these models are demonstrated in the text of other our paper in this school- seminar publication. The solution of dynamic problem for dissociation in shock waves were

used for this y -model. The results are in good agreement with data obtained by Esposito et al. [12] for this process.

The main problem is the verification of the reaction rate coefficient models on the basis of trajectory calculations. As the result of this verification we can allow that model parameters are not constant values but the functions are dependent on temperature T and vibrational level number m . The example of verification of Marrone-Treanor model parameter U in [3] using trajectory calculation [18] for dissociation reaction $N_2(m) + N \rightarrow 3N$ leads to: $U = \infty$ for $m > 45$ at low temperatures, $U = D_o / 6k$ for m about 20 at $T < 4000$ K, and for $m > 30$ at $T > 6000$ K, $U = 3T$ for $m > 20$ at $T > 6000$ K.

For simulation of elementary chemical reactions (dissociation, exchange reaction, process of vibrational relaxation) by QCT method the software complex "MD Trajectory" was created [15]. The main features of "MD Trajectory" are represented here:

- wide set of potential energy surface (PES) analytical functions such as Sorbie-Murrell, Aguado-Paniagua, Garcia-Lagana and different modifications of generalized LEPS model;
- capability of obtaining not only two-temperature but also state-to-state rate constants depending on vibrational states of reagent and product;
- determination of angle distribution of reaction products;
- determination of product distribution over vibrational and rotational levels;
- storage of coordinates and pulses along of trajectory for subsequent demonstration purposes.

Thus, software complex "MD Trajectory" is rather powerful tool for investigation of chemical reaction by QCT method especially for conditions hardly realized in experiment. Fig. 2 shows the results of this complex using as the example of realization of full level kinetics data but without analytical model approximation. Such approximations are absent, although being very important and necessary for solution of modelling problem in full level kinetics. These approximations must be short and simple expressions of models presentation with necessary accuracy and may be used in practical applicatons for complex gasdynamic problems. We are in need of simplicity, universality and accuracy for applications of QCT method results!

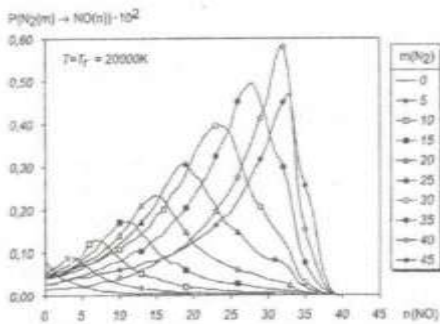


Fig. 2. The probabilities P of state-to-state transition: $m \rightarrow n$ for chemical exchange reaction $N_2(m) + O \rightarrow NO(n) + N$ on $T = 20000$ K

The role of level kinetics in shock wave investigations

The non-equilibrium kinetics, gas dynamics and transport processes behind strong shock waves are investigated in the framework of level approach. A set of governing equations consists of conservation equations for the momentum and the total energy and equations of detailed vibrational-chemical kinetics for the vibrational level populations of molecules and number densities of atomic species. Master equations have been solved for a stationary one-dimensional gas flow, and vibrational distributions and gasdynamic parameters in the relaxation zone have been found. These data have been used for the evaluation of the heat and mass transfer behind a shock wave. Different models of chemical reactions are tested, and the influence of a model on the distributions, species molar fractions and gas temperature is estimated. A comparison of the results obtained by means of the level approach with the ones based on the two-temperature and one-temperature kinetics (with thermal equilibrium vibrational distributions) shows an important role of state-to-state kinetics in the relaxation zone behind a shock wave [19,20].

The examples of results are obtained for a binary mixture N_2/N with dissociation, recombination and vibrational energy transitions. The transition probabilities are calculated using the SSH-theory generalized for anharmonic oscillators [21]. The Marrone-Treanor model [3] is applied for the computation of dissociation probability from each vibrational level. The conditions in the free stream are the following: initial temperature $T_0 = 293$ K, pressure $p_0 = 100$ Pa, Mach number $M_0 = 15$. A comparison of the temperature and the total energy flux found in various approaches is given in Figs.3,4. It is seen that the difference between vibrational distributions influences noticeably the gas temperature and the heat flux, particularly in a region of the relaxation zone close to the shock front where the processes of vibrational excitation is of importance.

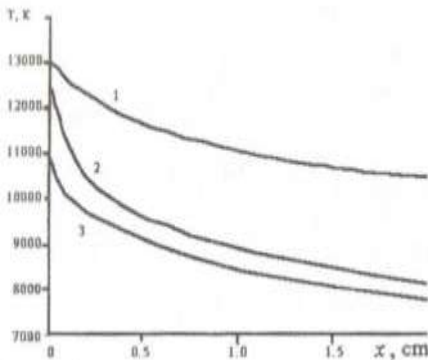


Fig. 3. Gas temperature T behind a shock wave as a function of x . 1 - level approach; 2 - two-temperature approach; 3 - one-temperature approach

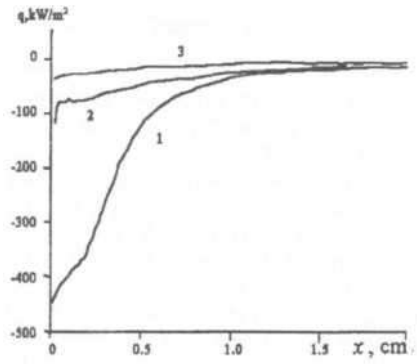


Fig. 4. Total heat flux q behind a shock wave as a function of x . 1 - level approach; 2 - two-temperature approach; 3 - one-temperature approach

These differences are explained by the underestimation the temperature value with the use of the two-temperature and one-temperature approaches because the quasi-stationary distribution is assumed to be immediately behind a shock wave front. These approaches do not consider the real delay of vibrational excitation at the start of relaxation zone.

The other effect of level kinetics is an excitation of specific electronic states of atoms and molecules in shock waves. The interesting result of non-equilibrium translational relaxation is the peak of radiation in Swan band of C₂ molecules from a region in front of shock waves in CO₂-N₂-Ar mixture (example see [22,23]).

Development of new electronic information system

The information support for mathematical modelling with the use of modern electronic communicative possibilities is very important now. It insures not only the application of the existing models but also the creation of new models with parameters values for these models. These systems include the needed database, software for specific scientific calculations, electronic journals, as well as electronic collections of materials not easily accessible, such as reports and preprints, protocols of experimental results, and so on.

The example of our electronic journal "Chemical and Physical Kinetics in Gas Dynamics" you can see at the site (<http://www.chemphys.edu.ru>): the results of some process modelling in strong shock waves are available in [23]. Such open scientific information systems are very perspective.

Conclusion

The level description of physical and chemical processes in shock waves yields a much better accuracy compared to two- and one-temperature approaches for the macroscopic parameters of flows. The problem is to develop a simple, reliable and universal model for full level kinetics on the base of the results of quasiclassical trajectory method. It is recommended to use more extensively the electronic information systems in solutions of the problems being discussed.

Acknowledgement

This work is supported by RFBR Grant N03-07-90037.

References

1. *Physical and Chemical Processes in Gas Dynamics: Cross Sections and Rate Constants for Physical and Chemical Processes*. Vol. 1. Progress in Astronautics and Aeronautics. Vol. 196, 2002.
2. *Physical and Chemical Processes in Gas Dynamics: Physical and Chemical Kinetics and Thermodynamics*. Vol. 2. Progress in Astronautics and Aeronautics. Vol. 197, 2004.
3. Marrone P.V., Treanor C.E., *Phys Fluids*, 1963, Vol. 6, N.9, P.1215.
4. Rusanov V.D., Fridman A.A., *Physics of Chemically Active Plasma*, Moscow: Nauka, 1984 (*in Russian*).
5. *Combustion Chemistry*, Ed. by W.C. Gardiner. Springer-Verlag, NY, 1984.
6. Wamatz J., Riedel U., Schmidt R., *Advanced in Hypersonic Flows*, Vol.2. *Modeling of Hypersonic Flows*. Boston, Birhauser, 1992.
7. Macheret S.O., Adamovich I.V., *J. Chem. Phys.*, 2000, Vol. 113, N 17, p. 7351
8. Losev S.A. *Nonequilibrium Processes and their Applications*. VI Intern. School-Seminar, Minsk, 2002, P. 23
9. Starikovskiy A. Yu., *Thesis in Physics and Mathematics*. Moscow Institute of Physics and Technology. 1999 (*in Russian*).
10. Gordiets B.F., Losev S.A., Capitelli M., Sergievskaya A.L., Kovach E.A., *Comparative modelling of endothermic reactions level rate constants*. 16th Intern. Symp. on Plasma Chemistry. 2003. Univ. Bari. CNR. Bari, P.236.

11. Seror S., Drugulet M.-C., Schall E., Zeitoun D.E., *AIAA-Paper* N.97-2556. 1997.
12. Esposito F., Capitelli M., *Chem. Phys. Letters*, 1999, Vol. 302, P.24.
13. Bose D., Candler G.V., *J. Chem. Phys.* 1996. Vol. 104. N 8, P.2825.
14. Esposito F., Capitelli M., *Chem. Phys. Letters*. 2002. Vol. 364, P. 180.
15. Pogobekjan M.Yu., Losev S.A. *Chem. Phys. Reports*, 2003, Vol. 22, N6, P.38.
16. Losev S.A., Sergievskaya A.L., Kovach E.A., Nagnibeda E.A., *Modern Problems of Combustion and its Applications*, IV Intern. School-Seminar. Minsk. 2001, p. 119.
17. Polak L.S., Goldenberg, M.Ja., Levitsky A.A. *Computer Methods in Chemical Kinetics*. Moscow: Nauka, 1984 (*in Russian*).
18. Capitelli M., Esposito F., Kustova E.V., Nagnibeda E.A. *Chem Phys. Letters*. 2000. Vol.330, P.207.
19. Nagnibeda E.A., Kustova E.V. *Kinetic Theory of Transport Processes and Relaxation in Non-equilibrium Flows of Reacting Gases*, Saint Petersburg Univ. Press, Saint Petersburg, 2003. (*in Russian*).
20. Kustova E.V., Nagnibeda E.A., Chikhaoui A., *Non-equilibrium Effects in Reaction Gas Flow*. 24 Inter. Symp. on Rare field Gas Dynamics. Bari, 2004.
21. Gordietz B., Zhdanok S., *Analytical Theory of Vibrational Kinetics of Anharmonic Oscillators, Nonequilibrium Vibrational Kinetics*, Ed. by M. Capitelli, Springer-Verlag, Berlin, Heidelberg, New York, Tokyo, 1986, P. 43-84.
22. Losev S.A., Kozlov P.V., Kuznetsova L.A., et al. *Proc. Third Europ. Symp. Aerothermodynamics for Space Venicles*, Noordwijk, 1998, P. 437.
23. Losev S.A., Kovach E.A., Pogobekjan M.Yu., Sergievskaya A.L. *Modelling of Physical and Chemical Processes in Strong Shock Waves*. Chemical and Physical Kinetics in Gas Dynamics. Electronic journal: www.chemphys.edu.ru. Vol. 1, 2003 (*in Russian*).

ROLE OF HETEROGENEOUS CHEMICAL REACTIONS AT FORMATION OF FILTRATION COMBUSTION WAVES

V.V. MARTYNNENKO, S.I. SHABUNJA, Ju.M. DMITRENKO, V.G. MINKINA

A.V. Luikov Heat and Mass Transfer Institute of NAS of Belarus 15, P. Brovka Str, Minsk, 220072, Belarus

Application of filtration combustion in manufacturing processes calls forth urgency of researches of physical phenomena in waves of filtration combustion (WFC). Along with optimization of existing processes the new technologies stipulated by intensive development of hydrogen power engineering suitable for making source of hydrogen of various productivity are developed. In particular the usage of WFC is considered to produce hydrogen at partial oxidation of methane in reactors with inert and catalytic fillings. The researches of WFC in case of rich fuel (methane-air) mixtures are conducted experimentally [1-3] and by numerical modeling [4]. As a rule simulation results give the qualitative description of the experiment, but good quantitative coincidence is not achieved yet.

The kinetics of chemical reactions is complex in case of rich mixtures because of an intercoupling of exothermal and endothermal processes. It is more difficult to clarify the importance of heterogeneous factor in case of rich mixtures because of more various yield composition. It should be easier in case of combustion of lean mixtures having equivalent ratio $\gamma < 1$, when the combustible mixture burns down to H_2O and CO_2 . Used model of homogeneous kinetics is tested for combustion in free space for mixtures at γ within range 0.6 - 1.6 [5]. Therefore it is possible to test the relevancy of applicability of homogeneous model at WFC simulation in case of lean mixtures, for example $\gamma = 0.6$.

The simulation of WFC in the experimental reactor is conducted to check the hypothesis of relevance of taking into account the heterogeneous factor in case of combustion of a lean mixture. As the model contains the parameters of experimental installation, which are badly determined; the series of methodical experiments on propagation of thermal wave in porous filling is conducted to realize the procedure of optimization refinement of these parameters. In the experiments preliminary heated filling in reactor is cooled by air of room temperature. The temperature is measured by six thermocouples equidistributed inside porous filling. The experiments are conducted at three values of airflow Q_a equal to 0.27, 0.55 and 2.21 1/s. Described above numerical procedure is used to calculate evolution of temperature. Obtained six functions of temperature on time in points corresponding to the position of thermocouples inside porous filling are compared with experimental data. During calculations the values of "badly determined" parameters of the model are selected to minimize the deviation of thermocouple measurements from calculated values.

The values of parameters obtained during minimization procedure are given in tab. 1. The graphs of calculated and measured temperature evolution are shown in Fig. 1. Dashed lines correspond to the measurements, and solid lines are the calculations using parameters from tab. 1. There is good coincidence both by the shape of curves, and the values of temperature. The maximum value of deviation does not exceed 30 °C.

Table 1. Parameters determined by optimization procedure

$c_{insul}\rho_{insul}$	λ_{insul}	ρ_y/ρ_{bulk}	λ_{insul}	$\alpha_{s,v}$	β_{sCond}	β_{sRad}
0.642·10 ⁶	0.129	0.428	0.129	0.510 [*]	0.138	0.3

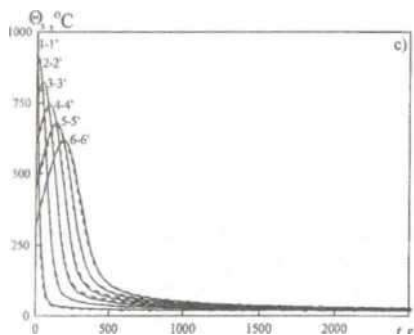
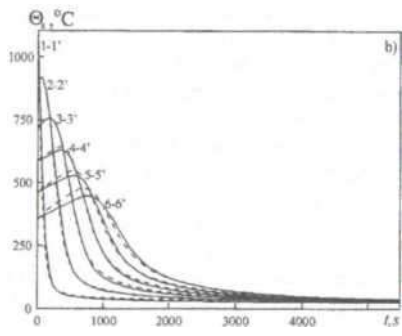
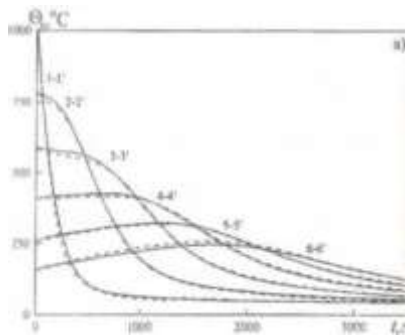


Fig. 1. Comparison of calculated (solid line) and measured (dashed line) temperatures by six thermocouples in porous filling for different values of: a - $Q_a = 0.27$ l/s, b - $Q_a = 0.55$ l/s and c - $Q_a = 2.21$ l/s

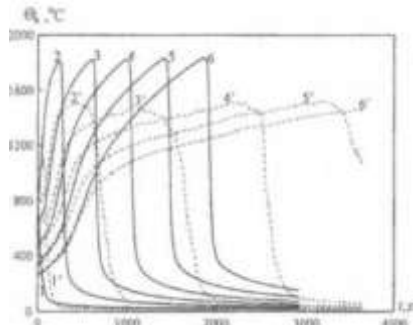
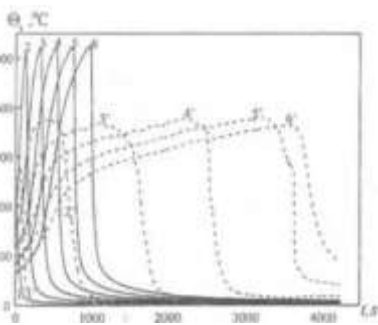


Fig. 2. Comparison of temperatures for mixture flow rate $Q_m = 0.94$ l/s at $\gamma = 0.6$ calculated by model of homogeneous chemistry (solid line) with experiment (dashed line)

Fig. 3. Comparison of measured temperatures (dashed line) with simulation (solid line) at usage $T = \max(T_g, \Theta)$ to calculate homogeneous reaction rate ($Q_m = 0.94$ l/s at $\gamma = 0.6$)

At calculations of WFC in case of lean fuel mixtures there are no difficulties, bound with simulation of mixture ignition using experimental initial distribution of temperature in a filling. However WFC formed in calculation has higher velocity and temperature in comparison with experimentally observed one. The example of experimental and calculated curves is shown in Fig. 2.

One more hypothesis based on only homogeneous nature of chemical processes is checked up. It is assumed that the homogeneous reactions start in the vicinity of the surface of a solid phase, where temperature is higher than mean temperature of gas. Therefore at simulation there is overstating of ignition threshold. In order to check such hypothesis the following calculation is conducted, when the rate of homogeneous reactions is calculated using temperature $T = \max(T_g, \theta_s)$. The behavior of curves in Fig. 3 demonstrates, though more early mixture ignition has taken place, calculated curves are still very far from experimental one.

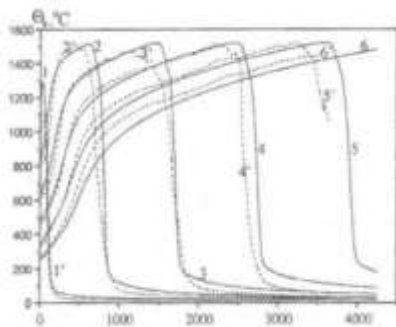


Fig. 4. Comparison of experiment (dashed line) at $Q_m = 0.94$ l/s and $\gamma = 0.6$ with calculations (solid line) where the model of homogeneous chemistry is supplemented by l modeling “heterogeneous” reaction

Since homogeneous kinetics is tested for $\gamma = 0.6$, the difference between calculations and experiments are attributed on influence of heterogeneous chemical reactions. The reality of such assumption is demonstrated by calculations, where the model of chemical processes is supplemented by reaction of “heterogeneous” type. It is not the case of simulation of actual processes on a surface of filling particles (adsorption, reactions, desorption). Reaction of “heterogeneous” type is perceived as the process with the following characteristics: the reaction rate is calculated by temperature of solid surface, the initial reactants are removed from gas at the temperature of gas media, and the reaction products having temperature of solid surface appear in gas. At such definition the heat of chemical process is redistributed between solid and gas media, while in homogeneous process it is entirely related to gas. The following reaction $\text{CH}_4 + 2\text{O}_2 = \text{CO}_2 + 2\text{H}_2\text{O}$ is used as modeling “heterogeneous” one. Arrhenius type relation is accepted to describe reaction rate. Corresponding coefficients are selected to adjust the calculation with the experiment. In Fig. 4 the result of such adjustment demonstrates good enough coincidence of simulation with the experiment. The shape of curves at stage of mixture preheating in calculation and experiment does not coincide. It means, that the used model describes well enough only the scale of power influence of heterogeneous reactions, but the chemical features of actual processes on solid surface are not characterized by such reaction. Success of the presented example is probably explained by the fact that in case of lean mixtures the yield contains CO_2 and H_2O only and introduced reaction does not affect the yield composition in WFC. In case of rich mixtures such coincidence of experiment with simulation hardly could be possible, as yield composition should be in a coincidence too. Though all reduced experimental data are obtained using filling of spheres

mudc of Al_2O_3 , there is no basis to consider that other materials will exhibit essentially weaker heterogeneous activity. Most likely, all solid materials at high temperatures will behave as weak catalysts. Experimental data [2] demonstrate, that in the fillings made of Al_2O_3 , SiO_2 and ZrO_2 WFC has similar behavior and close parameters.

In connection with so strong influence of heterogeneous processes on all important parameters of WFC all models using only homogeneous chemical kinetics should be considered with care. For the successful quantitative description of actual processes of filtration combustion it is necessary to develop the models of heterogeneous processes on solid surface at least for such often used non-catalytic materials as Al_2O_3 , ZrO_2 etc. Probably the simplified approaches such as demonstrated above could be applied in case of lean mixtures. However in case of chemical reactors working with rich mixtures, such models has to be more refined.

References

1. Zhdanok S.A., Kennedy L.A., Koester G. *Superadiabatic combustion of methane air mixtures under filtration in a packed bed II* Combust. Flame. 1995. Vol. 100. P. 221-231.
2. Gavriljuk V.V., Dmitrenko Ju.M., Zhdanok S.A., Minkina V.G., Shabunja S.I., Jadrevskaja N.L., Jakimovich A.D. *Investigation of process of conversion of methane into hydrogen in regime of single wave offiltration combustion IIIV* Minskij Mezhdunarodnyj Forum "Teplomassoobmen". T.4, MIF-IV, Mn. 2000. P. 21-31 (in Russian).
3. Bingue J.P., Saveliev A.V., Fridman A.A., Kennedy L.A. *Hydrogen production in ultrarich filtration combustion of methane and hydrogen sulfide* // Int. journal of hydrogen energy. 2002. Vol. 27. P. 643- 649.
4. Shabunja S.I., Martynenko V.V., Jadrevskaja N.L., Jakimovich A.D. // *Simulation of transient process of conversion of methane into hydrogen in wave of filtration combustion*. IFZH. 2001. T. 74, № 5. P. 7-12. (in Russian).
5. <http://homepages.vub.ac.be/~akonnov/science/mechanism/worksheets/testG1.html>

NONEQUILIBRIUM PLASMA-CHEMICAL IGNITION AND COMBUSTION IN SUPERSONIC FLOW OF HYDROGEN-OXYGEN MIXTURE WITH ELECTRONICALLY EXCITED SINGLET OXYGEN ACTIVATED BY ELECTRICAL DISCHARGE

V.V.NAUMOV¹, A.P.CHERNUKHO², A.N.MIGOUN², A.M.STARIK³, N.S.TITOVA³

¹Institute of Fundamental Problems for High Technology, Ukrainian Academy of Sciences Prospect Nauki 45, Kiev 03028 Ukraine ²A.V. Luikov Heat and Mass Transfer Institute of NAS of Belarus P. Brovka St. 15, Minsk 22072 Belarus ³P.I.Baranov Central Institute of Aviation Motors, SCR "Raduga" Aviamotomaya St. 2, Moscow 111116 Russia

Abstract

The numerical modeling of nonequilibrium plasma-chemical ignition/combustion in a supersonic flow of the H₂-O₂ mixture with the oxygen activated in an electrical discharge is presented. With a detailed plasma and chemical description of gas discharge and reactive flow dynamics, the effect of electronically excited singlet molecules $O_2(a^1\Delta_g)$ and $O_2(b^1\Sigma_g^-)$ on kinetics and mechanism of low-temperature initiation and intensification of supersonic detonation combustion is studied.

Introduction

The possibilities of promoting combustion by nonequilibrium excitation of internal vibrational and electronic degrees of freedom of reacting molecules in combustible gas mixtures is extensively discussed in the literature [1-3]. The excited molecules are chemically more active and can effectively accelerate the reaction kinetics due to a decrease of the barrier of endoergic reactions with excited molecules in contrast with non-excited reagents [4]. Principal enhancement of chain mechanism of combustion due to excited molecules, resulting in the reduction of the induction period, lowering of self-ignition temperature and extension of fuel flammability limits, is very attractive. Among novel approaches, two methods of non-thermal initiation, resonance laser-induced and plasma-assisted, are most promising [5]. This paper presents detailed numerical modeling of kinetics and mechanism of plasma-chemical initiation of combustion in a supersonic flow of the H₂/O₂ mixture under abundance of electronically excited singlet oxygen molecules, $O_2(a^1\Delta_g)$ and $O_2(b^1\Sigma_g^-)$, produced by the specific nonequilibrium high voltage electrical discharge.

Methodology

The analysis has been done for a scheme of the steady-state supersonic flow with an inclined shock wave [6]. A fuel, H₂, is mixed with an oxidizer, O₂, preliminary activated in an electric discharge. The flow parameters before the mixing are: temperature T₀ = 300-400 K, pressure P₀ = 10³-10⁵ Pa, Mach number M₀ = 2-8, shock front slope angle β = 20-30°. The O₂ discharge results in a sufficient amount of excited oxygen molecules, atoms, electrons, and numerous ions. After the discharge, the charged particles (e, O⁺, O₂⁺, O₄⁺, O⁻, O₂⁻, O₃⁻) rapidly disappear but the molecules $O_2(X^1\Sigma_g^-)$, $O_2(a^1\Delta_g)$, $O_2(b^1\Sigma_g^-)$, $O_2(B^3\Sigma_g^-)$, $O_2(A^1\Sigma_g^+, C^3\Delta_u, e^1\Sigma_g)$, atoms O(³P), O(¹D) and ozone O₃(¹A₁) remain active. A time of the mixing of discharge O₂- products and H₂ does not exceed τ_m = 10⁻⁸ s (mixing length L_m = 50 cm at M₀ = 6), so there is

practically an instantaneous mixing. After the induction period in the supersonic flow behind

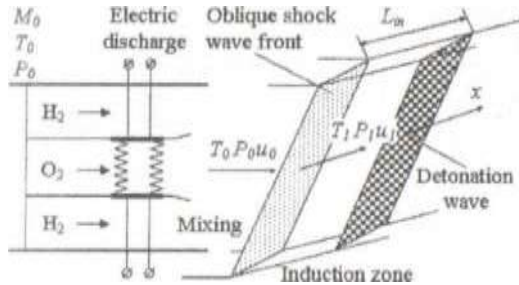


Fig. 1. Schematic of initiation of supersonic H₂/O₂ combustion

the shock front an ignition occurs and combustion goes on.

For modeling of the O₂ electric discharge, we applied a 0D kinetic+1D gasdynamic discharge model called PLASKIN [7]. This self-consistent model based on the kinetic Boltzmann equation for the electron energy distribution function (EEDF) in the standard 2TSH quasi-stationary approximation, coupled to the kinetic rate balance equations for reacting species,

combined with the continuity and transport equations, which were solved simultaneously in order to account a coupling between electron and heavy particle kinetics, involving vibrationally and electronically excited molecules. The plasma-chemistry kinetics includes all known electron-ion-molecular-atomic reactions, i.e. ionization, attachment, detachment, charge exchange, dissociation, recombination, vibrational excitation, de-excitation, etc. (over 100 elementary processes). The electron rate coefficients $k_e(E/N)$ and electron temperature T_e are derived on the basis of the calculated EEDF over a range of the reduced electric field E/N . Cross-sections for electron collisions and rate constants were collected from the reliable reference databases. A discharge cathode was assumed spatially homogenous; plasma was supposed quasineutral, i.e. $n^+ = n_e + n^-$.

For modeling of the H₂+O₂ combustion in the supersonic flow behind the inclined shock wave, we applied a 01D gasdynamic code [6] coupled with a detailed chemical kinetics involving normal H_2 , H, OH, H₂O, HO₂, H₂O₂, O₃(¹A₁), O₃(X³Σ_g⁻), O(³P) and electronically excited O(¹D), O₂(a¹Δ_g), O₂(b¹Σ_g⁻) species. An extended combustion mechanism consists of 76 reversible reactions. Vibrational V-V, V-T kinetics is considered in a mode approximation (model of local vibrational temperatures 7V). Rotational and translational kinetics is assumed to be in thermodynamic equilibrium. More details of modeling are given in [5-7].

Results and Discussions

According to the electrical discharge models, in a Droper O₂ discharge, which should be non-self-sustained at $E/N \approx 1.1 \cdot 10^{16} \text{ V} \cdot \text{cm}^{-2}$ ($T_e \sim 2 \text{ eV}$), both singlet oxygen states, O₂(a¹Δ_g) and O₂(b¹Σ_g⁻), are populated by the direct electron impact: 40% of energy goes to O₂(a¹Δ_g) (0.98 eV/state), 15

For illustration of discharge kinetics, Fig. 2 shows the typical evolution of O₂ plasma species along the discharge at $M_0 = 2$, $P_0 = 10^4 \text{ Pa}$, $T_0 = 300 \text{ K}$ with the specific energy deposition $E_t \approx 10^3 \text{ J/cm}^3$. Here, singlet oxygen participate in the E-E pooling $2 \text{ O}_2(a^1\Delta_g) \rightarrow \text{O}_2(b^1\Sigma_g^-) + \text{O}_2(X^3\Sigma_g^-)$ and in quenching collisions with O atoms and ozone O₃, those densities are proportional to pressure. O(³P) and O(¹D) atoms are produced by the electron impact dissociation. A rate of this process is a function of E/N , which depends on the discharge features and electron density. O₃ is produced in the three-body association $\text{O}(³P) + \text{O}_2(X^3\Sigma_g^-) + \text{M} \rightarrow \text{O}_3(^1A_1) + \text{M}$. Formation of O atoms is much shorter than that of O₃, and O₃ formation of is much faster than the gasdynamic transport, and so it may influence. Luckily, production of O₃ is suppressed by the fact two.

body reaction $O(^1D)+O_2 \rightarrow 2O_2(X^1\Sigma_g^-)$. Some O atoms recombines into the O_2 by the three-body reaction $O(^1P)+O(^1P)+M \rightarrow O_2+M$. While the $O_2(X^1\Sigma_g^-)$ is a dominant component, the $O_2(a^1\Delta_g)$ is a major long-lived excited state. In the post-discharge zone, due to the plasma decay, electrons disappear within a few microseconds, positive and negative ions are recombined and neutralized also quickly. Meantime, $O_2(a^1\Delta_g)$ remains sufficiently large for a time of milliseconds due its extra metastability [7]. A typical output from the O_2 discharge is following: $[O] \approx (1-7)10^{-2}$, $[O_2] = (1-5)10^{-2}$, $[O_2(b^1\Sigma_g^-)] \approx (1-5)10^{-3}$, $[O_2(a^1\Delta_g)] \approx (1-5)10^{-2}$, $[O_2(X^3\Sigma_g^-)] \approx 0.9$, $T_e \approx 800-1200$ K, and $T \approx 300-400$ K. It is really non-equilibrium and non-isothermai discharge composition.

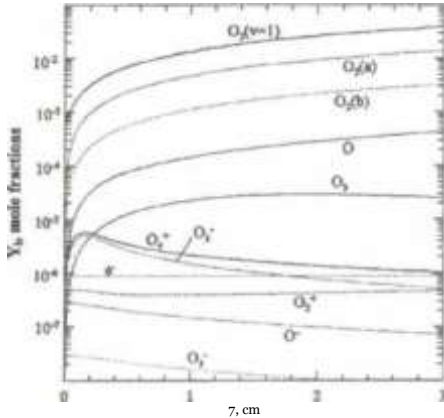


Fig. 2. Fractional yield in the O_2 gas discharge at $E/N \approx 1.1 \cdot 10^{19}$ V·cm⁻², $M_0 = 2$, $P_0 = 10^4$ Pa, $T_0 = 300$ K

For the combustion modeling, the stoichiometric mixture $H_2/O_2=2/1$ is taken as a common case for study. We consider the situation when a supersonic flow is moving through a shock wave front, a gas pressure and temperature are stepwise increasing, and it causes the acceleration of chemical reactions and subsequent ignition/combustion at some distance downstream. The presence of $O_2(a^1\Delta_g)$ and $O_2(b^1\Sigma_g^-)$ in the mixture with the H_2 accelerates the process strongly. For illustration of advanced combustion dynamics, Fig.3 shows the evolution of the main species responsible for the ignition of the H_2 in the flow at $M_0 = 6.5$, $\beta = 25^\circ$, $P_0 = 10^5$ Pa, $T_0 = 300$ K as with preliminary O_2 discharge activation ($E_d = 10^{-2}$ J/cm³) and without ($E_d \approx 0$). As is seen, even at a moderate discharge energy deposition, the excitation of O_2 gives rise to ignition of H_2 in the flow at a short distance of ~ 1 m from the primary shock front. Without O_2 pre-excitation, it will need, at least, of ~ 100 m.

Indeed, the O_2 discharge changes the kinetics and mechanism of combustion. Usually, H_2+O_2 combustion is initiated by the formation of OH radical and H and O atoms in the cycle of reactions: $H_2+O_2=2OH$, $OH+H_2=H_2O+H$, $H+O_2=OH+O$ and $O+H_2=OH+H$. The injection

of the singlet oxygen O_2^* ($O_2^*=O_2(a^1\Delta_g), O_2(b^1\Sigma_g^-)$) forms new pathways of the OH, O, H production in the reactions: $O_2^*+H_2=HO_2+H$, $O_2^*+H_2=2OH$, $O_2^*+H=OH+O$ and $O_2^*+O_2=2O_2+O$. Ozone also contributes: $O_3+H=OH+O_2$. All these reactions are of high kinetic rates. Hence, the excited O_2 causes a significant intensification of the chain-branching mechanism of initiation that results in a dramatic decrease of the induction and combustion zone lengths. The more is content of excited O_2 in the H_2/O_2 mixture, the better is the promoting effect (although it may be of non-linear character). A degree of this influence depends not only on the gas discharge energy E_d but also on the gas dynamic parameters behind the shock front P_1 and T_1 , which are determined by the initial values P_0 , T_0 , M_0 , and β

Summing the results of parametric modeling, Fig.4 shows the dependence of the

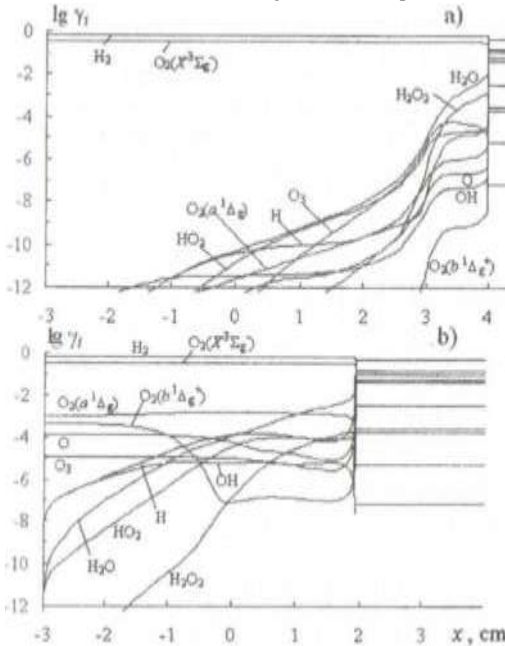


Fig. 3 Evolution of combustion species along the flow at $M_0 = 6.5$, $\beta = 25^\circ$, $P_0 = 10^4$ Pa, $T_0 = 300$ K, $H_2/O_2 = 2/1$ (a) without and (b) with electric discharge activation at $E_s = 1 \cdot 10^{12}$ J/cm².

experimental confirmation for our predictions but qualitatively analogous effect of the promoting influence of small $O_2(a^1\Delta_g)$ additions was the case in the lean ($\sim 7\% H_2$) premixed H_2/O_2 laminar flames [8].

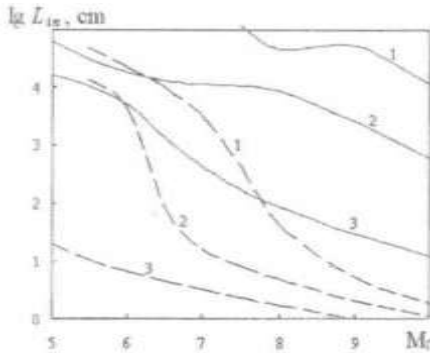


Fig. 4. Induction zone length L_{ind} vs. Mo in the flow at $\beta = 25^\circ$, $P_0 = 10^4$ Pa, $T_0 = 300$ K, $H_2/O_2 = 2/1$ at different $E_s = 0; 1 \cdot 10^{12}; 3 \cdot 10^{12}$ J/cm² (curves 1-3)

induction zone length, L_{in} (bench mark $gradT_{max}$) on the Mach number Mo at different values of the discharge energy E_s . One can see that discharge activation of O_2 results in the remarkable decreasing of L_{in} (by factor of 10^2 - 10^3) compared to conventional case. In the flow at $M_0 = 6.5$, $\beta = 25^\circ$ with $E_s = 10^{12}$ J/cm², the length L_{in} can be reduced to 1-2 m ($L_{in} \approx 100$ m at $E_s = 0$). An increasing of the discharge power makes it possible both initiating combustion at lower temperatures in the flow behind the shock wave and conducting detonation with a higher final temperature of the products. Even at a rather weak oblique shock in the flow at $M_0 = 5$, $\beta = 25^\circ$ when a temperature behind the shock front is $T_1 = 600$ K, the injection of excited O_2^* in concentration $\sim 1\%$ accelerates the ignition of H_2 and generates the detonation wave at a distance of ~ 1 m from the primary shock wave. As is known in the 'normal' $2H_2 + O_2$ mixture it is impossible to obtain detonation combustion under such conditions. There is no yet an

Nonequilibrium electric discharge excitation of molecular oxygen in the singlet states, $O_2(a^1\Delta_g)$ and $O_2(b^1\Sigma_g^+)$ provides the efficient plasma-chemical initiation of ignition and combustion of the H_2/O_2 mixture in the supersonic flow behind the inclined shock wave ($M_0 \geq 5$, $\beta \leq 30^\circ$). This is the result of the intensification of the chain mechanism of combustion due to new high rate channels of the formation of atoms H and O and radicals OH with the participation of electronically excited molecules $O_2(a^1\Delta_g)$ and $O_2(b^1\Sigma_g^+)$. Even a small amount of singlet oxygen (~1-3%) produced in an electric discharge with the specific energy deposition of $\sim 5 \cdot 10^3 \text{ J/cm}^3$, is more than enough. In the premixed H_2/O_2 flow at $M_0 \approx 6.5$, a temperature of initiation of combustion behind the shock front can be as low as 500-600 K. At that, the induction zone can be reduced by factor of 10^2-10^3 , and the length of the detonation combustion can be as short as 1 m. This gives a good possibility for effective control of ignition and combustion processes, particularly, in hypersonic aircraft engines.

Acknowledgments

The work is partially supported by the INTAS (Grants No. 00-556 and 03-61-4736) and by the Russian Foundation for Basic Research (Grants No. 02-02-16915 and 02-01-00703).

References

1. Brown R.C. *Combust.Flame*. 1985, Vol.62, pp.1-12; Fisher E.M. *Combust.Flame*. 1997, Vol. 108, pp. 127-138.
2. Starik A.M., Dautov N.G. *Dokl.Akad. Nauk*. 1994, Vol.336, pp.617-622; 1996, Vol.350, pp.757-762.
3. *Advanced Combustion Methods* /Ed. Weinberg F.J., London: Academic Press. 1986; *Alternative Approaches for Improved Combustion* /Eds. Wolfrum J., Wamatz J., PCI-IWR, Heidelberg. 2002.
4. Rusanov V.D., Fridman A. A. *Physics of Chemical Active Plasma*, Nauka, Moscow. 1984.
5. Starik A.M., Titova N.S. *Dokl.Akad.Nauk2001*, Vol.380, pp.332-337; 2003, Vol.391, pp.471-477.
6. Starik A.M., Titova N.S., *AIAA Paper 99-3637*. 1999; *Chem.Phys*. 2001, Vol.20, pp.17-25.
7. Naumov V.V., Starik A.M., Chemukho A.P., *et al* Proc. of Int.School-Seminar "Nonequilibrium Processes and their Applications", HMTI, Minsk, 2002, pp.62-66; Starik A.M., Titova N.S., *ibid*. 2002, pp.99-103.
8. Basevich V.Ya., Belyaev A.A. *Khim.Fiz*. 1989, Vol.8, pp. 1124-1127.

VERIFICATION OF THE REACTION LEVEL RATE CONSTANT MODELS ON THE BASIS OF TRAJECTORY CALCULATIONS

M.Ju. POGOSBEKIAN¹, S.A. LOSEV¹, A.L. SERGIEV SKA Y A ¹, B.F. GORDIETS²

Institute of Mechanics, M.V.Lomonosov Moscow State University, Moscow, Russia ²Physical Institute of Russian Academy of Science, Moscow, Russia

Description of the chemical reacting systems without thermal equilibrium between vibrational and translational freedom degrees of reacting molecules can be more accurately realized as a level chemical kinetics. This kinetics is described in terms of vibrational level populations of reagents and reactions products. This approach is strongly required for many applications in the fields of the combustion and plasma chemistry, laser systems, hypersonic (flows and etc. This issue comes into existence when characteristic time of investigated hydrodynamic flow τ_g , chemical reaction τ_c and vibrational relaxation τ , become of the same order.

Two-temperature approximation

The main problem in modeling the two-temperature kinetics of dissociation and exchange reactions is obtaining rate coefficients as functions of T and T_v : $k(T, T_v)$. The (arguably) better way to reveal the nonequilibrium nature of the reaction is to use a dimensionless nonequilibrium factor $Z(T, T_v) = k(T, T_v) / k^*(T)$. Here $k^*(T)$ is the rate coefficient at $T_v = T$ commonly called the equilibrium rate constant. A number of theoretical and empirical models have been suggested for $Z(T, T_v)$ in dissociation and exchange reactions [1,2]. Theoretical models differ in their assumptions regarding the roles of vibrational and translational modes in reactions, and in their description of vibrational states (quantum or classical harmonic oscillator or anharmonic oscillator).

For nonequilibrium exchange reactions, three models were chosen:

- α -model, or model of vibrational energy efficiency (case of harmonic oscillator model for vibrational excited molecule),
- Macheret formulas for endothermic exchange reactions proceeding directly (with no long-lived complex),
- Intuitive Park model.

When the reacting diatomic molecules are modeled by harmonic oscillators, both classical and quantum oscillators are considered. In both cases, the distribution of molecules among vibrational levels is assumed to be quasi-Boltzmann.

1. Quantum harmonic oscillator approximation ($T_v < \theta$):
for $0 < \alpha < 1$

$$Z(T, T_v) = \frac{1 - \exp(-\theta/T_v)}{1 - \exp(-\theta/T)} \cdot \frac{\exp\left(-\frac{E_x}{\alpha T_v}\right) - \exp\left(-\frac{E_x}{T}\right)}{\exp\left(-\frac{E_x}{T}\right) - \exp\left(-\frac{E_x}{\alpha T}\right)} \cdot \frac{\exp\left(-\frac{E_x}{\alpha T_v}\right)}{1 - \exp\left(-\frac{\theta}{T_v}\right)} \cdot \frac{\exp\left(-\frac{\alpha\theta}{T} - \frac{\theta}{T_v}\right) - 1}{1 - \exp\left(-\frac{\theta}{T}\right)}$$

for $\alpha = 1$

$$Z(T, T_v) = \frac{1 - \exp(-\theta/T)}{\left[1 - \exp(-\theta/T_v)\right] \left[\exp\left(\frac{\theta}{T} - \frac{\theta}{T_v}\right) - 1\right]} \frac{\theta}{E_a} \left[\exp\left(\frac{\theta}{T} - \frac{\theta}{T_v} - \frac{E_a}{T_v} + \frac{E_a}{T}\right) - 1 \right].$$

2. Classical harmonic oscillator approximation ($T_v > \theta$):

for $\theta < \alpha < 1$, $Z(T, T_v) = \frac{1 - \alpha \frac{\alpha T_v}{T} \exp\left(-\frac{E_a}{\alpha T_v}\right) - \exp\left(-\frac{E_a}{T}\right)}{\frac{\alpha T_v}{T} - 1 \exp\left(-\frac{E_a}{T}\right) - \alpha \exp\left(-\frac{E_a}{\alpha T_v}\right)}$,

for $\alpha = 1$, $Z(T, T_v) = \frac{T}{E_a} \left[\frac{T_v}{T_v - T} \exp\left(-\frac{E_a}{T_v} + \frac{E_a}{T}\right) + \frac{T}{T - T_v} \right]$.

The Macheret formulas have some restrictions. This model cannot be applied to the exothermic reactions and to the reactions of double exchange ($XY(v) + ZW \rightarrow XW + YZ$). It is also inapplicable to the reactions where reactants are in rotational disequilibrium. It is not recommended to apply Macheret formulas to the reactions proceeding through formation of intermediate long-lived complex, that is, to reactions $XY(v) + Z \rightarrow X + YZ$, if the stable molecule XYZ exists. The nonequilibrium factor $Z(T, T_v)$ in the Macheret formulas is given by the formulas:

- in the case of high temperatures ($T_v, T > \theta$)

$$Z(T, T_v) = \left[\frac{E_a - W}{\alpha_M T_v + (1 - \alpha_M) T} - \frac{W - E_a}{T} - \frac{E_a}{T} \right], \quad \alpha_M = \frac{m_x(m_y + m_z + m_z)}{(m_x + m_y)(m_y + m_z)}, \quad W = E_a \left(1 - \frac{f_v}{\alpha_M} \right)$$

- in the case of not very high temperatures ($T_v, T < \theta$)

$$Z(T, T_v) = \left[f_v \exp\left(-\frac{\theta}{T_v}\right) + (1 - f_v) \exp\left(-\frac{\theta}{T}\right) \right]^{n+s} \exp\left(\frac{E_a}{T}\right).$$

Here m_x, m_y, m_z are the masses of the X, Y and Z particles, respectively, α_M is the dimensionless mass ratio, W is the energy parameter (in K degrees), f_v is the dimensionless average fraction of the energy release in reverse reaction $X + YZ \rightarrow XY + Z$ converted into the vibrational excitation of XY , θ is the characteristic vibrational temperature of the reacting molecule XY. Experimental values of coefficient f_v for various specific reactions are listed in [2]. To obtain an estimate of f_v , this quantity should be varied within the range $0.3\alpha_M < f_v < \alpha_M$.

The model aims at estimation an effect of violated equilibrium over vibrational degrees of freedom for gas molecules on the rate of arbitrary chemical reactions involving vibrationally nonequilibrium molecules.

$$Z(T, T_v) = \left(T^s T_v^{1-s} \right)^n \exp\left[-\frac{E}{k} \left(\frac{1}{T^s T_v^{1-s}} - \frac{1}{T} \right) \right]$$

Here D_0 is dissociation energy, D^0 is bond-breaking energy, E_a is activation energy, n is exponent of the temperature factor in the pre-exponential factor in the generalized Arrhenius formula for $k^0(T)$, s is empirical model parameter. The empirical parameter s was assumed to be 0.5-0.6.

In the level kinetics the main problem is determination of the rate constants for corresponding chemical reactions. There are many theoretical and semiempirical models of the level rate constants. Such models are mainly developed for description of the dissociation processes and to a less degree for exchange reactions. The most of them use some adjusted parameters, which have to be determined from experimental results or other estimates. There are few experimental results especially at the high temperatures. On the other hand, the rather reliable data about potential energy surface (PES) permit to calculate the level rate constants by solving the problem of the collision dynamics. Each model has own set of restrictions on reaction type, kind of reagents, temperature range applicability and etc. Therefore the selection of the most adequate model is very important problem [3, 4].

The description of the information-theoretical approach, level modified model of vibrational energy efficiency (a-model), level modified CVCV model are considered in [5]. The purpose of these models is the simple universal relations between modified parameters using information about the energy fraction ν , as the energy part which goes into vibrations of the molecule-product of reverse exothermic reaction, that is the molecule- reactant of direct endothermic reaction.

γ -model and Levitsky model are the function-approximated results based on the solutions of particular dynamic collision problem by means of quasiclassical trajectory method. In accordance with Losev γ -model for process of dissociation $AB(\nu) + M \rightarrow A + B + M$:

$$k_{dv}(T) = k_d^0(T) \exp\left(\frac{\gamma E_v}{T}\right) \frac{\left[1 - \exp(\gamma-1) \frac{\theta}{T}\right] \left[1 - \exp\left(-\frac{D_0}{T}\right)\right]}{\left[1 - \exp(\gamma-1) \frac{D_0}{T}\right] \left[1 - \exp\left(-\frac{\theta}{T}\right)\right]}, \quad E_v \leq D_0, \quad k_d^0(T) = A \exp(-D_0/T) [1 - \exp(-\theta/T)],$$

where θ is the characteristic vibrational temperature, A [cm^3/mols] is pre-exponential factor in the Arrhenius form for the equilibrium rate constant, γ is model parameter (other notation see above). Values of this model parameters and coefficients for dissociation of $N_2(\nu) + O \rightarrow N + N + O$ are $A = 7.1 \times 10^{18}$, $\gamma = 0.8$, $D_0 = 113000$ K, $\theta = 3354$ K.

The results of calculation in [6,7] are approximated by Levitsky model, so

$$\left. \begin{aligned} k_{dv} \\ k_{cv} \end{aligned} \right\} = A(T) \left[\frac{E - \alpha E_v - \beta (E - \alpha E_v)}{\beta T} \right] \quad \text{where } E = D_0 \text{ for dissociation reactions (} D_0 \text{ - dissociation energy) and } E = E_a \text{ for exchange reactions (} E_a \text{ - activation energy); } \alpha, \beta \text{ are the parameters describing participation of vibrational and translational energies in reactions. For } N_2(m) + O \rightarrow N + N + O \text{ parameters of this model are (} E \text{ is in Kelvin) } \alpha =$$

Verification of models

The basic method for deriving of the recommendations on models applicability consists in carrying out of the wide spectrum of the numerical experiments. Both detailed studying of each model, and comparison of several models in identical conditions can be fulfilled in the framework of numerical experiments. Such approach is realized in the software complex "KINTVT" developed in Institute of Mechanics MSU [8].

The other way for models verification can be based on the comparison with the results of quasiclassical trajectory (QCT) calculations. For investigation of the elementary chemical reactions by QCT method the "MD Trajectory" software complex was created and

successfully applied [9]. The optimization of trajectory code for more efficient utilization of the modern supercomputer clusters has been performed.

Some results of investigation of models and verification of model parameters in two-temperature approximation are given on Fig 1-4. On Fig 1,2 the dependence of the nonequilibrium factor and two-temperature rate constant of $\text{CO} + \text{N} \rightarrow \text{CN} + \text{O}$ on temperature at

different value of vibrational temperature are shown. All this results are obtained by QCT method. The next two figures (Fig.3,4) represent comparison of various model results with the QCT results for this reactions at different values of vibrational temperatures. There are comparison between QCT calculations and some theoretical models for two exchange reactions $\text{CO} + \text{N} \rightarrow \text{CN} + \text{O}$ and $\text{N}_2 + \text{O} \rightarrow 2\text{N} + \text{O}$ on Fig. 5,6. Investigation on level factor

$k_v(T)/k_0(T)$ for dissociation $\text{N}_2 + \text{O} \rightarrow 2\text{N} + \text{O}$ calculated by y-model at the different translational temperatures $T = 3000, 4000, 6000, 8000\text{K}$ as the function of vibrational level and calculated by Marrone-Treanor model with parameter $U = 3T$ at the same translational temperatures are represented on Fig.7,8. Fig 9 shows dependence level factor $k_v(T)/k_0(T)$ for

dissociation $\text{N}_2 + \text{O} \rightarrow 2\text{N} + \text{O}$ calculated by Marrone-Treanor model with parameter $U = D/6$ on vibrational levels at the different translational temperatures. Fig. 10 shows comparison between QCT calculations and two theoretical models (a-model and IT one). Level factors $k_v(T)/k_0(T)$ for dissociation $\text{N}_2 + \text{O} \rightarrow \text{NO} + \text{N}$ at the fixed translational temperature $T = 10000\text{K}$ was compared.

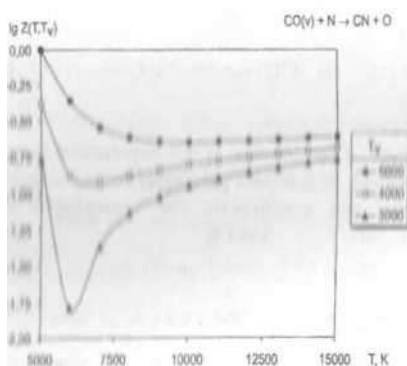


Fig. 1. Nonequilibrium factor $Z(T, T_v) = \frac{k(T, T_v)}{k(T, T_v = T)}$ for exchange reaction $\text{CO} + \text{N} \rightarrow \text{CN} + \text{O}$ at the fixed vibrational temperatures $T_v = 3000, 4000, 5000\text{K}$ as the function of translational one. QCT calculation results

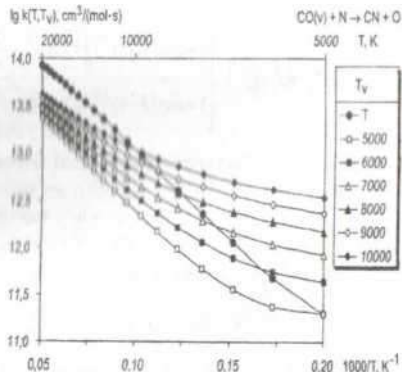


Fig. 2. One-temperature and two-temperatures rate constants for exchange reaction $\text{CO} + \text{N} \rightarrow \text{CN} + \text{O}$ at the different vibrational temperatures $T_v = 5000, 6000, 7000, 8000, 9000, 10000\text{K}$ as function of translational one, QCT calculation results

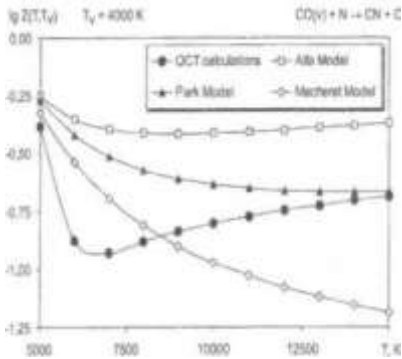


Fig. 3. Nonequilibrium factor $Z(T, T_v) = \frac{k(T, T_v)}{k(T, T_v = T)}$ for exchange reaction $\text{CO} + \text{N} \rightarrow \text{CN} + \text{O}$ at the fixed vibrational temperature $T_v = 4000$ K as the function of translational one

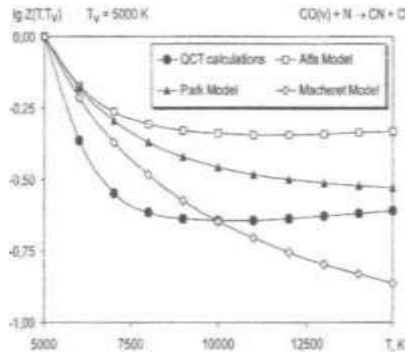


Fig. 4. Nonequilibrium factor $Z(T, T_v) = \frac{k(T, T_v)}{k(T, T_v = T)}$ for exchange reaction $\text{CO} + \text{N} \rightarrow \text{CN} + \text{O}$ at the fixed vibrational temperature $T_v = 5000$ K as the function of translational one

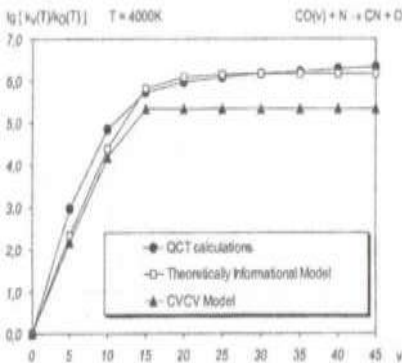


Fig. 5. Level factor $\frac{k_v(T)}{k_0(T)}$ for exchange reaction $\text{CO} + \text{N} \rightarrow \text{CN} + \text{O}$ at the fixed translational temperature $T_v = 4000$ K as the function of vibrational level

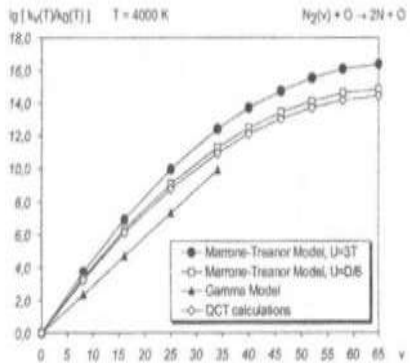


Fig. 6. Level factor $\frac{k_v(T)}{k_0(T)}$ for dissociation $\text{N}_2 + \text{O} \rightarrow 2\text{N} + \text{O}$ at the fixed translational temperature $T_v = 4000$ K as the function of vibrational level

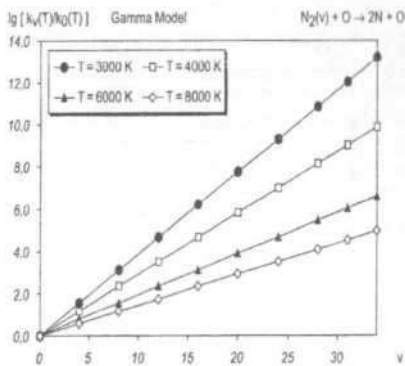


Fig. 7. Level factor $k_v(T)/k_0(T)$ for dissociation $N_2 + O \rightarrow 2N + O$ calculated by γ - model at the different translational temperatures $T = 3000, 4000, 6000, 8000$ K as the function of vibrational level

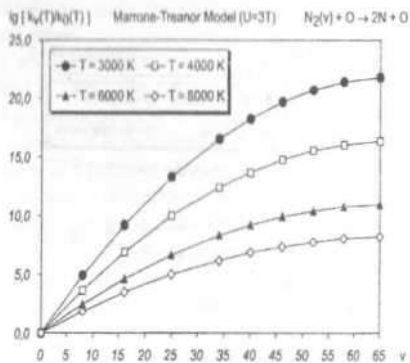


Fig. 8. Level factor $k_v(T)/k_0(T)$ for dissociation $N_2 + O \rightarrow 2N + O$ calculated by Marrone-Treanor model with parameter $U = 3T$ at the different translational temperatures $T = 3000, 4000, 6000, 8000$ K as the function of vibrational level

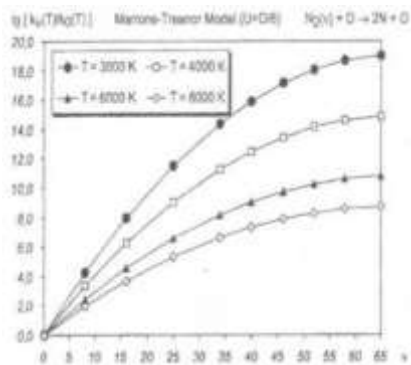


Fig. 9. Level factor $k_v(T)/k_0(T)$ for dissociation $N_2 + O \rightarrow 2N + O$ calculated by Marrone-Treanor model with parameter $U = D/6$ at the different translational temperatures $T = 3000, 4000, 6000, 8000$ K as the function of vibrational level

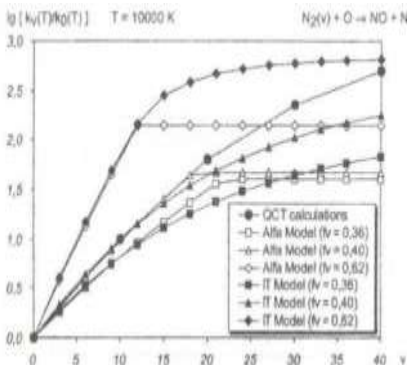


Fig. 10. Level factor $k_v(T)/k_0(T)$ for dissociation $N_2 + O \rightarrow NO + N$ at the fixed translational temperature $T = 10000$ K as the function of vibrational level. Comparison between QCT calculations and two theoretical models for various parameters $f_v = 0.36, 0.4, 0.62$

References

0. Kovach E.A., Losev S.A., Sergievskaya A.L. *Two-Temperature Kinetic Models for Dissociation of Molecules in Strong Shock Waves*. Chem. Phys. Repts. 1995, Vol. 14, N9, pp.1353-1387.
1. *Physical and Chemical Processes in Gas Dynamics: Computerized Handbook*: Ed. by Chemyi G.G. and Losev S.A. *Physical and Chemical Processes in Dynamics*. Moscow Univ. Press. Moscow. 1995, Vol.1.
2. Losev S.A., Sergievskaya A.L., Kovach E.A., Nagnibeda E.A., Gordiets B.F., *Mathematical Modelling*. 2003, Vol.15, N6, pp.72-82, (in Russian).
3. Gordiets B.F., Losev S.A., Sergievskaya A.L., Kovach E.A. *16th International Symposium on Plasma Chemistry*, Taormina, Italy. June 22-27, 2003, Abstract and full-paper CD: Ed. by d'Agostino R., Favia P., Fracassi F., Palumbo F., Univ. of Bari, CNR, Bari. 2003, pp.236-242.
4. Gordiets B.F., Losev S.A., Sergievskaya A.L., Kovach E.A., *Rate constants of chemical reactions with vibrational excited molecules*. Khim.Fizika. 2004, Vol.1, (in Russian).
5. Wamatz J., Riedel U., Schmidt R. *Advanced in Hypersonic Flows, Modeling Hypersonic Flows*. Birhauser, Boston. 1992, Vol.2.
6. Losev S.A., Sergievskaya A.L. *Mathematical Modeling of Physico-Chemical Processes in Gases with Information Support*. AIAA-Paper N 98-2954, 11.(1998).
7. Pogosebikyan M.Ju., Losev S.A. *Development of parallel software complex "MD Trajectory" based on MPI technology. Book of Abstracts, XIV European Conference on Dynamics of Molecular Collisions, Istanbul, , p.56 (2002)*.
8. Pogosebikyan M.Ju., Losev S.A. *Investigation of the reaction $CO+N \rightarrow CN+O$ by quasiclassical trajectory method using "MD Trajectory" software complex*. Chem. Phys. Repts. 22, N.6, 38-46 (2003) (in Russian).

HYDROGEN-OXYGEN REACTIONS ASSISTED BY $\text{OH}(^2\Sigma^+)$, $\text{O}(^1\text{D})$ and $\text{O}_2(^1\Delta)$ FORMATION

O.V. SKREBKOV, S.P. KARKACH, A.L. SMIRNOV

Institute of Problems of Chemical Physics RAS, Chemogolovka 142432, Russia

Introduction

The combustion of hydrogen (or hydrocarbons) is accompanied by the emission of ultraviolet light due to transitions of excited $\text{OH}^*(^2\Sigma^+)$ radicals to their ground states $\text{OH}(^2\Pi)$, and monitoring for this emission has been used long ago in the investigation practice as a method for determining the ignition-delay time. Since the $\text{OH} \rightarrow \text{OH}^*$ excitation energy is about 47000 K, the question arises, what is the formation mechanism for excited OH^* radicals at low temperatures ~ 1000 K, and what is the role of other electronically excited particles, such as $\text{O}^*(^1\text{D})$ and $\text{O}_2^*(^1\Delta)$, possessing lower excitation energies. Answers to these questions are of importance for the search of alternative approaches to improve combustion, in particular, for efficient ways of influencing the ignition process. On the other hand, the problems of detailed understanding the hydrogen-oxygen reaction remains one of central in modern combustion chemical physics; in particular, the mechanism of chain initiation and new developments in this field were discussed in recent publications [1-6].

In this paper, we focus on the theoretical analysis of mechanism for ignition-combustion processes in hydrogen-oxygen mixture with allowance for electronically excited OH^* , O^* , and O_2^* particles, and vibrational nonequilibrium for initial H_2 and O_2 molecules. To rectify the kinetic scheme, results of *ab initio* analysis are widely used; in particular, rate constants for essential reactions were held near the theoretically suggestible levels.

Experimental

Herein, we deal the following experimental results: (i) our shock tube experiments [5] (incident shock waves, emission spectroscopy monitoring OH^* radical, stoichiometric $\text{H}_2 + \text{O}_2 + \text{Ar}$ mixtures), (ii) the shock tube experiments [7] (reflected shock waves, absorption spectroscopy monitoring OH radical, rich on hydrogen $\text{H}_2 + \text{O}_2 + \text{Ar}$ mixtures), and (iii) the shock tube experiments [3] (reflected shock waves, absorption spectroscopy monitoring O atoms, lean on $\text{H}_2 + \text{O}_2 + \text{Kr}$ mixtures).

Theory

Theoretical consideration involves the following two aspects: (i) *ab initio* analysis intended to identification of some reactions as elementary ones and to independent estimate for their rate constants, (ii) kinetic calculations including further refinement of some rate constants as a result of fitting the calculated values to experimental ones.

For a number of systems, extensive *ab initio* analysis was carried out with use of GAMESS program package, employing CASSCF (complete active space self-consistent field) method, in various active spaces. Most accurate energy and frequency estimates for use in frames of CTST (conventional transition state theory) were performed employing high-level post-SCF methods from GAUSSIAN package, within the energy prediction scheme proposed earlier [2]. This scheme was also adapted to MCQDPT2 (multiconfiguration quasi-degenerate perturbation theory, 2nd order) energy calculations. To a number of

activationless reactions, CASSCF-based VTST (variational transition state theory) was applied.

General formulation of problem for the chemically- and vibrationally-nonequilibrium flow of multicomponent gas mixture has been given previously [8,9]. Presently, the problem is simplified to isothermal one because, for greatly diluted mixtures, the heat effects can be neglected. In this case, it is enough to integrate two Landau-Teller equations. We have the analytical dependencies for vibrational temperatures of molecular hydrogen and oxygen:

$$E_k(t) = E_k^0 - [E_k^0 - E_k(0)] \cdot \exp(-t/\tau_{vib}), \quad T_k(t) = \theta_k / \ln\{[1 + E_k(t)]/E_k(t)\}, \quad k = \text{H}_2, \text{O}_2$$

The effect of vibrational nonequilibrium on the chemical reaction rates was calculated in terms of the model [8, 9] as following:

$$k_r(T, T_k) = \kappa_r(T, T_k) k_r^0(T), \quad \kappa_r(T, T_k) = \exp \left[\frac{E_r}{k} \left(\frac{1}{T} - \frac{\sum_i \beta_{ri}^2}{i} \right) \right],$$

$$E_r = \begin{cases} E_r^A - (\xi_r + 4)kT/2, \\ 0, & E_r \leq 0. \end{cases}$$

The multiplier $\kappa(T; T_k)$ takes into account acceleration or slowing-down from vibrational nonequilibrium. Here, T_k is the vibrational temperatures; $k_r^0(T)$ is the equilibrium rate constant of the r^{th} reaction; E_r^A is the activation energy; E_r is the vibrational portion of E^A , ξ_r is the number of rotational degrees of freedom of reagents; here, $\beta_{ri} = 1$ (We suppose the uniform energy distribution on vibrational degrees of freedom).

Results and discussion

Table 1. The reactions with participation of O_2^* , O^* and OH^* in $(2\text{H}_2 + \text{O}_2) + \text{Inert Gas}$ mixture at $1000 \leq T \leq 2500 \text{ K}$, $2.0 \geq p \geq 0.3 \text{ atm}$

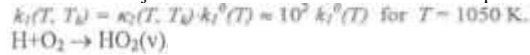
r	Reactions	$k_r^0(T)(\text{incm}^3, \text{mole}, \text{s})$
1	$\text{HO}_2 + \text{H}_2 \leftrightarrow \text{OH}^* + \text{H}_2\text{O}^{\text{a)}}$	$3.0 \cdot 10^{15} (T/298)^{-1.7} \exp(-19000/T)^{\text{c)}$
2	$\text{O}^* + \text{H} + \text{M} \leftrightarrow \text{OH}^* + \text{M}$	$7.0 \cdot 10^{15} (T/298)^{-1 \text{ c)}$
3	$\text{O} + \text{H} + \text{M} \leftrightarrow \text{OH}^* + \text{M}$	$1.0 \cdot 10^{16} (T/298)^{-1} \exp(-12000/T);$ $\text{M} = \text{OH}: 2.0 \cdot 10^{15} (T/298)^{-1 \text{ c)}$
4	$\text{OH}^* + \text{M} \leftrightarrow \text{OH} + \text{M}$	$\text{M} = \text{H}_2\text{O}: 2.2 \cdot 10^{14} \exp(-276/T); \text{H}_2: 1.0 \cdot 10^{12};$ $\text{M} = \text{O}_2: 6.0 \cdot 10^{12}; \text{Ar}: 1.3 \cdot 10^{11} \cdot (T/298)^{0.5 \text{ c)}$
5	$\text{OH}^* + \text{O}_2 \leftrightarrow \text{O}_3 + \text{H}$	$4.0 \cdot 10^{13} (T/298)^{0.5 \text{ c)}$
6	$\text{OH}^* + \text{H}_2\text{O} \leftrightarrow \text{H}_2\text{O}_2 + \text{H}$	$7.5 \cdot 10^{12} \exp(-276/T)^{\text{c)}$
7	$\text{OH}^* + \text{H}_2 \rightarrow \text{H}_2\text{O} + \text{H}$	$8.8 \cdot 10^{13} (T/298)^{0.5 \text{ c)}$
8	$\text{OH}^* + \text{O}_2 \rightarrow \text{HO}_2 + \text{O}$	$2.0 \cdot 10^{13} (T/298)^{0.5 \text{ c)}$
9	$\text{OH}^* \rightarrow \text{OH} + \text{h}\nu$	$1.4 \cdot 10^6$
10	$\text{HO}_2 + \text{H} \rightarrow \text{H}_2\text{O} + \text{O}^*$	$2.3 \cdot 10^{13} (T/298)^{0.438} \exp(-678/T)^{\text{c)}$
11	$\text{O}^* + \text{H}_2 \leftrightarrow \text{OH} + \text{H}$	$\approx 8 \cdot 10^{13} \exp(20000/T)$
12	$\text{O}^* + \text{M} \leftrightarrow \text{O} + \text{M}$	$\text{M} = \text{H}_2: 1.0 \cdot 10^{14}; \text{M} = \text{O}_2: 2.0 \cdot 10^{11}; \text{Ar}: 2.0 \cdot 10^{11}$
13	$\text{H} + \text{HO}_2 \leftrightarrow \text{H}_2 + \text{O}_2^*$	$6.5 \cdot 10^{11} (T/298)^{1.671} \exp(-3162/T)^{\text{b)}$
14	$\text{O}_2^* + \text{M} \leftrightarrow \text{O}_2 + \text{M}$	$\text{M} = \text{H}_2: 2.7 \cdot 10^6; \text{O}_2: 1.0 \cdot 10^6; \text{Ar}: 3.0 \cdot 10^5$

Notes to Table 1:

- a) Here and below the double arrow means the brief writing for two reactions (forward, r, and reverse, r'); $K_f = k_f/k_r$, K_r is the equilibrium constant.
- b) Our CTST (Conventional Transition State Theory), VTST (Variational Transition State Theory), or LST (Landau Statistical Theory) estimations.
- c) Fitted with experiment.

In the table, there are the reactions and/or rate constants marked out by the heavy type. It is the new kinetic information obtained in the course of our work as a result of theoretical estimations and/or fitting with experiment.

The formation of electronically excited hydroxyl-radical OH* is caused by the reactions 1 - 3 and 4' - 6', the absolutely main reaction is the reaction 1 with participation of vibrationally excited radical HO₂(v); the major source of HO₂(v) is the recombination process



In accordance with our estimations, the possible vibrational nonequilibrium effect increases the equilibrium rate constant, $k^0(T)$, of 2+3 orders at low temperatures. So,

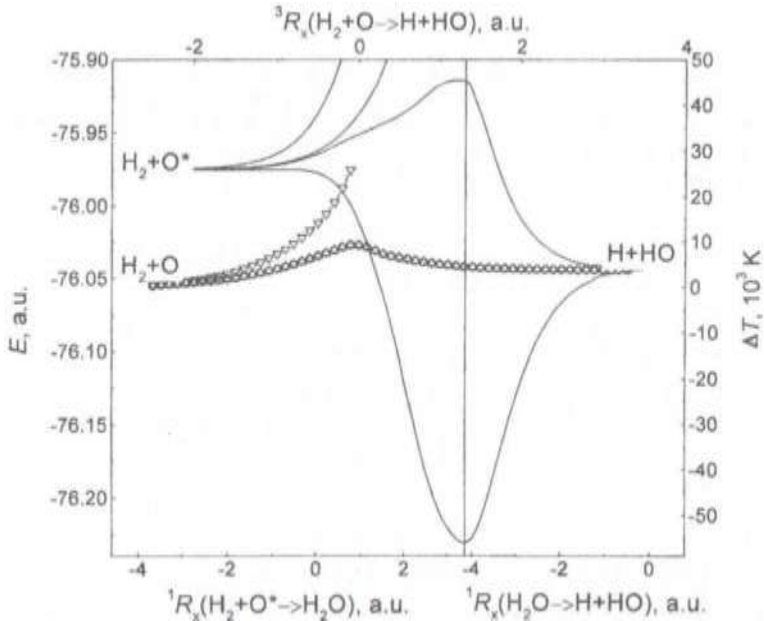


Fig. 1. *Ab initio* reaction pathways from $\text{H}_2 + \text{O}$, $\text{H}_2 + \text{O}^*$ to $\text{H} + \text{HO}$. On the triplet potential surface (triangles), there is well known chain branching reaction $\text{H}_2 + \text{O} \rightarrow \text{OH} + \text{H}$ possessing direct mechanism

The corresponding direct mechanism reaction on the singlet potential surface, $\text{H}_2 + \text{O}^* \rightarrow \text{H} + \text{OH}$, is not valuable due to high activation barrier. Note, that the paramount reaction on the singlet potential surface is the water-producing one $\text{H}_2 + \text{O}^* \rightarrow \text{H}_2\text{O}$.

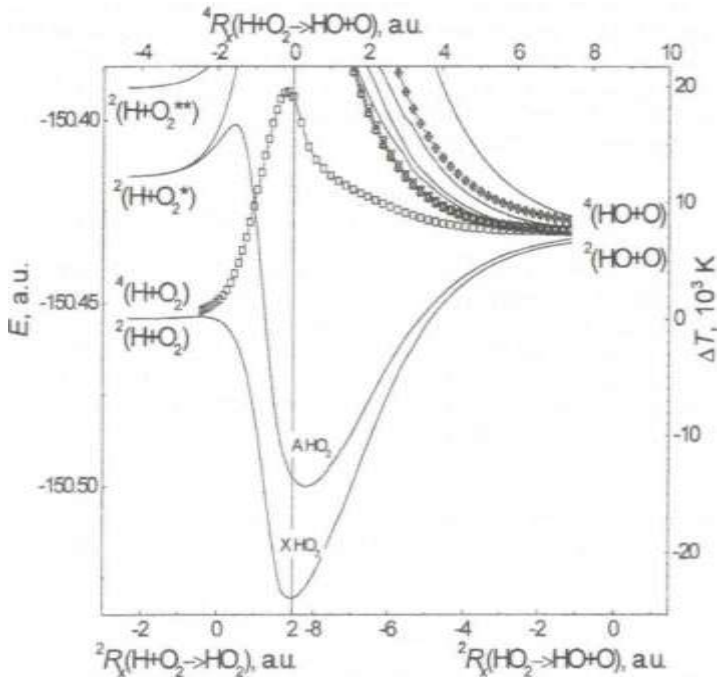


Fig 2. The ground (O_2 & $X HO_2$) and some electronically excited ($O_2^* = O_2(a^1 \Delta_g)$, $O_2^{**} = O_2(b^1 \Sigma_g^-)$, ΛHO_2) terms of HO_2 system

Note, that the direct mechanism chain branching reaction (a) $O_2 + H \rightarrow OH + O$ reveals very high activation barrier about 20000 K (that differs drastically from the literary value, $6500 \div 11000$ K, by different authors [10]; the heat effect of this reaction being 8300 K). For effective chain branching, we propose indirect mechanism which includes the formation of vibrationally excited hydroperoxy radical, $HO_2(v)$:

The kinetic calculations with the reactions (a 1) + (a 4) instead of the reaction (a) and with an estimation of HO_2 vibrational nonequilibrium effect were carried out for $1000 \leq T \leq 1400$ K. The results showed the present mechanism preference for the interpretation of experiments [3,5,7] by the single kinetic scheme.

Particular attention was paid to the analysis of initiating reactions, which are of crucial importance at early stages of the process. Because of obvious discrepancy between literary and recent theoretical data for initiating reactions, they were analyzed carefully. Most unambiguous is reaction $H_2 + O_2 \leftrightarrow H + HO_2$ estimated, with close results, both experimentally and theoretically. At high temperatures T more then 2000 K, reaction $H_2 + M \leftrightarrow 2H + M$

becomes principal. At low temperatures ($T < 1000$ K) and high pressures ($p > 1$ atm), the initiation mechanism of chemical transformation in the hydrogen - oxygen system is not understood now; in our opinion (*ab initio* calculations), it realize via long-lived $\{O_2 \cdots O_2\}$, $\{O_2 \cdots H \cdots HO_2\}$, and $\{O_2 \cdots HO_2\}$ intermediates. The H_2O_4 molecular system is the most complicated for *ab initio* analysis. But because of the most important for ignition at low temperatures, this system is our main priority.

Conclusions

- (i) HO_2 is the overwhelmingly important intermediate component for chain branching and OH^* formation.
- (ii) The correct kinetic calculations with account of the superequilibrium vibrational excitations of $HO_2(v)$ and its relaxation are necessary.
- (iii) Further elaboration of the physically adequate mechanism of initiation, especially at low temperatures and high pressures, is still actual. In this relation, detailed topological analysis of intermediate complex $\{H_2O_4\}$ is necessary. This includes search for the saddle and minimizing structures on the lowest singlet, triplet and quintet terms of H_2O_4 and their (quasi)crossings.

Acknowledgments

This work was supported by RFBR (Grant N 04-03-32678), Presidium RAS (BR Programme N 1 by coordination O.M. Nephedov) and INTAS (Programme INTAS N 03-51-4736).

References

1. Blumenthal R., Fieweger K., Komp K.H., Adomeit G. and Gelfand B.E. *Proc. 20th Int. Symp. on Shock Tubes and Waves*, 1996, p. 935.
2. Karkach S.P., Oshero V.I., *J. Chem. Phys.* 1999, Vol.1 10, p.1 1918.
3. Michael J.V., Sutherland J.W., Harding L.B. and Wagner A.F. *Proceedings of the Combust. Inst.* 2000, Vol. 28, p. 1471.
4. Filatov M., Reckien W., Peyerimhoff S.D. and Shaik S. *J. Phys. Chem. A* 2000, Vol. 104, p. 12014.
5. Skrebkov O.V., Miagkov Ju.P., Karkach S.P., Vasil'ev V.M. and Smirnov A.L., *DAN* 2002, Vol.383, p.1.
6. Skrebkov O.V., Karkach S.P., Vasil'ev V.M., Smirnov A.L. *Chem. Phys. Lett.* 2003, Vol.375, p.413.
7. Ryu S.-O., Hwang S.M., Rabinowitz M.J. *J. Phys. Chem.* 1995, Vol. 99, p.13984.
8. Vasil'ev V.M., Kulikov S.V., Skrebkov O.V. *Prikl. Mekh. Tekhn. Fiz.* 1977, Vol.4, p. 13.
9. Skrebkov O.V., Kulikov S.V., *Chem Phys.* 1998, Vol.227, p.349.
10. Mallard W.G., Westley F., Herron J.T., Hampson R.F., *NIST Chemical Kinetics Database Ver. 6.0. NIST Standard Reference Data. Gaithersburg, MD, 1994.*

STUDY OF NONEQUILIBRIUM AIR PLASMA FLOW IN TRANSVERSE ARC DISCHARGE

V.Ya. CHERNYAK, V.V. NAUMOV², I.L. BABICH¹, V.V. YUKHIMENKO¹,
Yu.V. WOEWODA¹

¹Kiev National Taras Shevchenko University, Radiophysical Faculty Prospect Acad. Glushkova 4/5,
Kiev 01028 Ukraine

²Institute of Fundamental Problems for High Technology, Ukrainian Academy of Sciences Prospect Nauki
45, Kiev 03028 Ukraine

Spectroscopic characterization of air plasma in electric arc discharges is of permanent interest in many labs because of various important applications in materials processing, plasma chemical and biotechnologies. In this paper we report about spectroscopic studies of a specific regime of air plasma flow in the transverse arc discharge. A free jet of atmospheric air ran from the nozzle across two coaxial electrodes and formed a bright crescent-shaped arc as well as a highly reactive afterglow. For diagnostics, we applied a method of absolute emission UV-VIS-NIR spectroscopy, equipped by modern fast PC-operated CCD-based MOSA instrumentation and etalon spectral lamps. Measurements were performed in different sections along the jet under the variation of discharge parameters and flow rates. Both copper and carbon electrodes were utilized in order to see difference. Within available spectrum of wavelengths (200-1100 nm) we conducted monitoring of all remarkable emissions and identified all basic atomic lines of N, O, H as well as molecular bands of NO, N₂, O₂, OH, CO, CN. On this base, we draw curves of changes of emissions' intensity along the jet depending on the discharge power and flow velocity.

We recognized nitride oxide NO γ system ($A^2\Sigma^+ - X^2\Pi$: (0-1) 236.3 nm, (0-2) 247.1 nm, etc); oxygen O₂ Shumann-Runge bands ($B^2\Sigma_u^- - X^2\Sigma_g^-$: (0-14) 337.0 nm); nitrogen N₂⁺ 1st negative system ($B^2\Sigma_u^- - X^2\Sigma_g^+$: (0-0) 391.4 nm, (0-1) 428.0 nm, (0-2) 470.9 nm, (1-0) 358.2 nm, (2-1) 356.4 nm, etc); N₂ 2nd positive system ($C^2\Pi_u - B^3\Pi_g$: (0-0) 337.1 nm, (0-1) 357.7 nm, (0-2) 380.5 nm, etc) and a very weak N₂ 1st positive system ($B^3\Pi_g - A^3\Sigma_u^+$: 570-750 nm) Under

the LTE assumption, we determined the excitation temperature of nitrogen molecules from the emissivity of N₂ 2⁽⁺⁾ bands using the Boltzmann plot. The excitation temperature of oxygen atoms is calculated from the emissivity of OI lines at 777.3 nm, 884.6 nm and 926.0 nm. Besides, the electronic density is deduced from the Stark broadening of the H Balmer α line at 656.3 nm. There were a lot of CuI lines in case of copper electrodes but the electronic temperatures obtained from the relative intensities of CuI 324.7 nm and 327.4 nm was out of the LTE as well as CuI 521.8 nm and 515.3 nm due to the overlap with N₂⁺(1) bands. The interference of the N₂ 2⁽⁺⁾ system precluded diagnostics of the OH (A-X) at 308 nm. The temperature of heavy particles undertaken through the partially resolved emission of N₂⁺ 1⁽⁻⁾ bands turned out also not equal to the gas temperature T_g . It differed from the temperature of vibrationally excited molecules more then twice. This evidences about the strong non-

isothermal conditions. Therefore, usual two-temperature approach with T_e for electrons and T_g for heavy particles is not valid in this case. Another character effect is an “ignition” of the molecular emission downstream the arc resulted from the kinetic non-equilibrium conditions. The highest temperature (~ 1.5 eV) is measured in the center of the arc. In the afterglow zone, the temperature T_e decreases rapidly while the temperature of excited metastable molecules T_{exc} keeps longer. Then increasing an arc discharge current, the temperature T_{exc} becomes larger. At a larger flow rate the gradient T_{exc} becomes smaller.

We see that even small variations in plasma conditions due to spatial and temporal instability, decomposition, contamination, etc can produce large visual changes in the spectral emission, which is functionally related with the temperatures and concentrations of components, so spectroscopy could serve as a powerful tool for diagnostics and characterization of nonequilibrium plasma.

ELECTRON COOLING AND ION HEATING EFFECTS IN AR PLASMA-WALL INTERFACE

A. CENIAN¹, A. CHERNUKHO²

¹The Szwedalski Institute of Fluid-flow Machinery, Polish Academy of Sciences,
80-952 Gdansk, Fiszerka 14; Poland, cenian@imp.gda.pl

²A.V. Luikov Heat and Mass Transfer Institute of NAS of Belarus P. Brovka Street 15, 220072 Minsk,
Belarus

Abstract

The electron cooling and ion heating processes in a positive column of an Ar DC discharge are discussed here. The Particle-In-Cell Monte Carlo (PIC MC) method is used which describes the kinetics of electron and ions in plasma-wall interface.

Introduction

The problems related to a plasma-wall interface, important in the case of Langmuir probes, ambipolar diffusion, etc., still attracts much attention during the last years (e.g. Chabert 2000; Kono 2001; Kawamura and Ingold 2001; Franklin 2003; Stenovskiy 2003). Most of the respective theoretical considerations are based on the assumption of constant T_e/T_i ratio in whole plasma volume and Boltzmann profile of electron in plasma wall interface.

In contrast, Kono (2001) and Kawamura and Ingold (2001) modelled both electron and ion kinetics. Kono (2001) has developed a 1d2v (1D displacement 2D velocity) PIC-MC model for a spherical probe immersed in a plasma bulk. The charged species (electrons as well as positive and negative ions) gradually fill an empty simulation box due to the thermal particle flux from ambient plasma. All particles move in the electric field determined by a probe bias and a space charge. The ion collisions are treated in a simplified manner, i.e. the velocity of a colliding particle is replaced by the random thermal velocity corresponding to the temperature of that specie. The temperatures of undisturbed plasma are related by relations, $T_e = T_i = T_0/100$. The substantial differences in multi-sheath formation in fluid model (based on above stated assumptions) and PIC MC model were reported, even for weakly collisional case. It was related to the chaotic oscillation of potential barrier observed in the PIC MC model.

Cenian et al. (2003) have modified 1d3v (1D displacement 3D velocity) PIC-MC model of electropositive plasma in the system of cylindrical-symmetry proposed by Kawamura and Ingold (2001). The 3D trajectories were calculated in that model but only radial (1D) dependence of charge distribution was taken into account in Poisson's equation (in relation to assumed cylindrical symmetry). The model was used to study the electron cooling and ion heating effects in positive column of Ar DC discharge at plasma-wall interface and in the sheath of a Langmuir probe immersed in Ar plasma. Some important implications for plasma theory will be discussed.

The model description

Model of plasma-wall interface in Ar discharge positive-column

A low-pressure ($p \leq 1$ torr) Ar-plasma of positive column, surrounded by a nonconducting wall of cylindrical-symmetry (tube radius $R = 1$ cm) is considered. The MC

trajectories of “quasi-particles” representing a large number of electrons and Ar^+ ions are calculated. They move in the electric field determined by a solution of Poisson’s equation and the densities of charged “quasi-particles” determined in grid points of a simulation box.

The real collisions of electron and ions with an Ar atom described by the cross sections sets compiled by Phelps (1994, 1997) are considered. The ionization, elastic and excitation processes are taken into account while simulating electron trajectories. The elastic processes (isotropic and backscattering) are considered when ion trajectories are calculated.

An assumed axial current is sustained by the axial electric field ($E_j(r) = \text{const}$), i.e. E_z is derived by requirements that impact ionization rate equals the charge losses due to the plasma-wall interactions. When the electron balance is not fulfilled the E_z value is changed and the procedure is continued until the steady-state conditions are established.

The MC trajectories for “super particles” are calculated using “null collision method” (Cellierud, 1968). Arbitrary collision frequency was chosen in such a way that the mean free path $\lambda_p < 0.002 R$. It has enabled the correct inclusion of field evolution into the equation of motion. In order to accelerate the computations, the Bessel profiles (instead of uniform ones) of charged-particle densities were assumed for the initial condition with arbitrary coordinates and velocities. The fixed electron energy distribution and thermal ion energy distribution were applied.

The particles crossing the simulation-box boundary were removed from a simulation. The simulation box was divided by 250 points of computational grid were charged particle densities and Poisson equation was solved. The space separation of the grid was chosen to decrease inversely proportional to the distance from the cylindrical symmetry axis ($(Ar_s - R/r_s)$). The azimuthal symmetry and uniformity in the axial direction was assumed, i.e. although MC trajectories were calculated in 3 dimensions only the radial distribution of charged particle densities was considered in the 1D Poisson’s equation.

The simulation algorithm works as follows. The calculation of charged particle trajectories is interrupted at the chosen time steps and the charged species concentrations at the points of computational grid are being determined. When the new radial profiles of potential and electric field are calculated, by solving the Poisson’s equation, the trajectory simulations are continued. The whole procedure is repeated, as long as the steady-state profiles are established.

Already introductory investigations (Cenian et al., 2003) proved that this model could be useful to study fundamental problems of plasma-wall interactions, including plasma neutrality, Bohm criterion and sheath formation.

Model of a probe immersed in Ar plasma

The plasma-probe interactions are studied in a system with cylindrical symmetry, related to an infinitely long cylindrical probe, $2r_p$ in diameter, immersed in a continuum, nonflowing, electro-positive plasma. The effects of a positive column DC field (directed along the probe symmetry axis) can be taken into account. For the sake of simplification, the whole plasma volume is separated into two different zones: Sheath-Pre-Sheath (SPS) zone and a ring-shaped volume around it (called later “buffer zone”) - see Fig. 1. The minimum radius of the SPS zone depends strongly on the probe bias voltage as will be discussed later. The motion of charged particles in both zones is described by the MC trajectories.

The concentration of charged particles in the buffer zone is kept constant by assuming that the particles reflect specularly at the boundaries i.e. at the boundary with the SPS zone and at an external boundary given by r_b (radius of buffer zone). The neutral plasma of the “buffer” zone is described by the electron (T_e) and ion (T_i) “effective” temperatures (see

Godyak, 1993). The Maxwell distributions were generally assumed as the initial conditions but other distribution may be easily introduced as well. As the simulations continue the charged particle distribution changes radically (as will be discussed later in the sheath region). Initially, the charged particles are uniformly distributed in the whole considered space, i.e. buffer and SPS zones. Later, the charged particle densities begin to decay in the close vicinity of the probe, due to the constant flux towards the probe and absorption (followed by recombination) on the probe surface. On the other hand, there is a continuous thermal influx of new charged particles from the buffer zone to the SPS zone. This flux is simulated by the creation of a new particle entering the SPS zone with the same velocity as the particle from the buffer zone, which was reflected from the border with the SPS zone. When a particle is crossing the same boundary but from the SPS side, it is removed from the simulation.

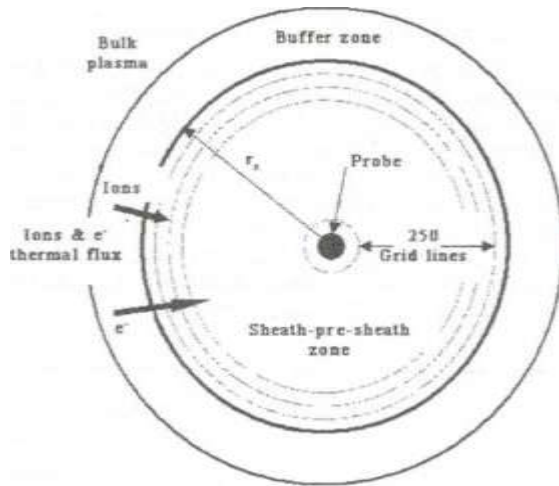


Fig. 1. Scheme of the considered zones in PIC model

The described procedure allows determining the thermal flux from the buffer to the SPS zone and it keeps constant the ionization degree in the buffer zone. It was checked that the described procedure is simpler but gives the same results as the one used previously (Cenian et al. 2003). It should be here noted that the flux from the buffer into the SPS zone is higher than that in the opposite direction giving a netto thermal influx to the SPS zone.

The charged-particle MC trajectories in the SPS zone are determined by the Newtonian equations for particles motion in an electric field. It is possible to take into account both the axial-field of the DC plasma column as well as the radial field generated by the probe-bias and the space-charge density (through the Poisson equation evaluated in 250 grid points) - see Fig. 1.

The probe surface is assumed to be fully absorptive both for electrons and ions, i.e. a particle is removed from the simulation (absorbed on the probe surface and recombined) when its trajectory passes the probe-wall coordinate (i.e. when $r < r_p$). The difference between the number of absorbed electrons and ions determines the probe current.

The electrons take part in different collision processes with the target Ar gas atoms, described by cross sections for elastic and excitation processes as well as ionization according

to Phelps (1997). The Ar^+/Ar collisions are described by cross sections for elastic collisions: isotropic and backscattering(charge transfer) processes proposed by Phelps (1994).

The standart null-collision method is applied (Skullerud, 1968) when calculating MC trajectories. When the decision about the real collision is made the velocity components of the Ar atom are determined using the rejection method as discussed by Robertson and Sternowsky (2003) for the velocity-weighted Maxwellian distribution of Ar atoms. They show that the use of this distribution increases the rate of collisions with the high relative velocity and so, decreases the ion mobility (especially at low E/N) and increases the diffusivity. The determination of target velocity enables to decide (using random number generator) what type of collision took place (see e.g. Piscitelli et al. 2003).

Results and discussion *Plasma-*

wall interface in Ar discharge positive-column

The positive column of the Ar discharge with $[\text{Ar}] = 10^{21} \text{ m}^{-3}$ and $I_z = 10 \text{ mA}$ was considered. It was shown already by Kawamura and Ingold (2001) that resulted E_z values agree reasonably well with experimental results (Groos 1934; Ferreira and Loureiro 1985) for Ar discharges under pressure range $0.4 < p < 40 \text{ Pa}$. At higher pressure agreement is worse due to the neglect of other than direct-ionization processes. It is well known (see e.g. Bogaerts and Gijbels, 1999) that at 75 Pa, more than 20% of the ionization processes results from other channels than direct ionization. At still higher pressures the associative ionization processes and production Ar_2^+ ions cannot be neglected (Petrov and Ferreira, 1999).

The self-consistently determined electron temperature and ionisation density in the centre of positive column were, $T_e \sim 5.3 \text{ eV}$ and $4 \cdot 10^{15} \text{ m}^{-3}$, respectively. So, $\lambda_D \sim 0.2 \text{ mm}$ in this case.

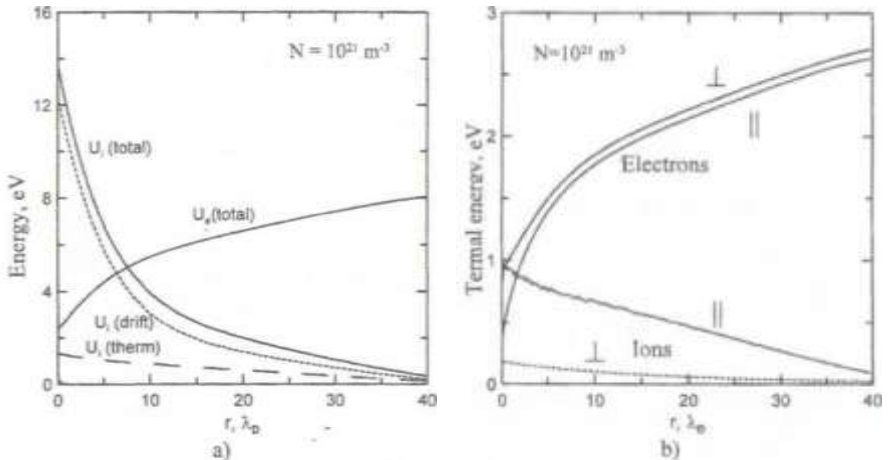


Fig. 2. Spatial profiles of electron and ion kinetic and thermal energies; thermal energies are calculated per degree of freedom in radial (||) and transversal (⊥) directions

Fig. 2 presents spatial profiles of electron and ion kinetic energies. It was confirmed that the electron energy has mainly thermal - chaotic - character (the fine small curve near $r =$

0 in Fig. 2 a represent its drift - ordered component) and quite rapidly decline toward tube wall. In contrast, the thermal part of ion kinetic energy increases - ions heat up - in the plasma-wall interface. So, although, the thermal energy of ions is generally much lower than the electron energy in the centre of a positive column of electric discharges, however, due to observed electron cooling and ion heating effects at plasma-wall interface of the considered Ar discharge, the U_e/U_i relation can change significantly across the tube radius. The radial component of the ion thermal energy can even exceed the radial component of the electron thermal energy - see Fig. 2 b. It should be noted that the transversal component of the ion thermal energy is significantly lower than the radial one. It can be explained by a significant decrease of cross-sections for elastic (isotropic) collisions for higher ion energies typical in the sheath region. At the same time, the back scattering component of cross sections decreases only slightly. It leads to much stronger scatter of ion energies in radial than in transversal direction. In contrast, "electron effective temperatures" in both directions are almost equal (see \perp and \parallel components of electron thermal energy). The ion heating effect at the plasma-wall interface results from ion collisions, which disperse energy gained from the radial ambipolar field. Electrons are de-accelerated by the same field in the radial direction and collisions help to cool down also the energy in the transversal direction. The both effects can have pronounce consequences for the discussion about the ambipolar diffusion - see (Franklin, 2003).

Probe immersed in Ar plasma

The probe model has been verified using the results of probe measurements in an Ar plasma of a standard double-plasma machine as described by Stemovsky et al. (2003). The experimental results related to current-voltage characteristics partly presented in Stemovsky et al. (2003) have been kindly supplied by dr.Z.Stemovsky (Stemovsky, 2004) - see erratic line in Fig. 3.a. The crosses represent PIC MC results of the model described here and broken line correspond to the modified OML model of Stemovsky et al. (2003). The considered case is related to that described by Stemovsky et al. (2003) in Fig. 7a. i.e. a probe in a plasma under the conditions described by the parameters $r_p/\lambda_D = 0.26$ and $\lambda_D/\lambda_{mfp} = 0.04$, where λ_D is

the Debye length and λ_{mfp} is mean free path. It means that although the thicker probe ($r_p = 313 \mu\text{m}$) is considered a thin probe approximation ($r_p/\lambda_D < 0.5$) in weakly-collisional case can still

be applied. The measured by Stemovsky et al. (2003) gas pressure was 1.3 mTorr and the ions were supposed to be in equilibrium with the gas (room) temperature $T = 0.025 \text{ eV}$, in agreement with some LIF measurements in similar plasma devices. The charged particle density (in the bulk plasma - here "buffer zone"), $[Ar^+] = 7.15 \times 10^7 \text{ cm}^{-3}$, was derived by

using the Druyvesteyn method as presented by Godyak et al. (1993). The electron temperature, $T_e = 1.9 \text{ eV}$, was derived from the retarding part of the experimental probe- characteristic. Taking into account that the gas density (at room temperature) is of the order of $4.3 \times 10^{13} \text{ m}^{-3}$, the ionization degree α is about 2×10^{-6} and λ_D is 1.21 mm under the present conditions.

The profiles of ion (dashed line) and electron (solid line) thermal-energies are shown in Fig. 3. The results prove that the T_e/T_i ratio could not be considered constant in the plasma sheath region (et least for radius $r < 4 \lambda_D$ around the probe). Moreover, the ion and electron thermal-energies ("effective temperatures") become comparable in this region. The last is far from our intuitive expectation about the electron temperature being much larger than the ion one ($T_e/T_i \gg 1$) It should be noted that the electron cooling effect at the plasma sheath around the probe is much less pronounce than in the above considered case. It must be related to smaller electron energy and much lower pressure.

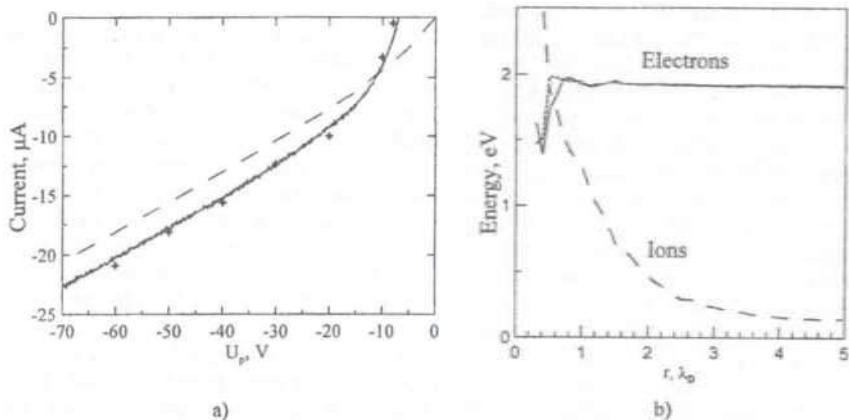


Fig. 3. Probe characteristic (a) and spatial profiles (b) of electron and ion energies in sheath region of the probe

Conclusions

The strong effects of electron cooling and ion heating have been found in the plasma- wall interface. The effect of electron cooling is smaller in the case of probe immersed in the low pressure plasma described by lower electron temperature. The both effects can have pronounce consequences for the discussion about the ambipolar diffusion - see (Franklin, 2003) and probe modeling.

Acknowledgments

We acknowledge a financial support from the bilateral Belarus - Polish cooperation program and the 4T10B 01922 Project of Polish Committee for Scientific Researches.

References

1. Bogaerts A. and Gijbels R. *J. Appl. Phys.* 1999, Vol.86, p. 15.
2. Cenian A., Chernukho A. and Leys C. *Radiation Phys. and Chem.* 2003, Vol.68, p.109.
3. Chabert, P., Sheridan, T.E. *J.Appl.Phys.* 2000, Vol.33, p.1854.
4. Ferreira C.M. and Loureiro J. *J. Appl. Phys.* 1985, Vol.57, p.82.
5. Franklin R.N. *J. Phys. D Appl. Phys.* 2003, Vol.36, p.828.
6. Godyak V.A. et al. *J.Appl.Phys.* 1993, Vol.73, p.3657.
7. Groos O. *Z. Phys.* 1934, Vol.88, p.741.
8. Kono A. *J.Phys.D: Appl.Phys.* 2001, Vol.34, p.1083.
9. Kawamura E. and Ingold J.H. *J Phys.D: Appl. Phys.* 2001, Vol.34, p.3150.
10. Petrov G.M. and C. M. Ferreira *Phys. Rev. E.* 1999, Vol.59, p.3571.
11. Phelps A.V. *J. Appl. Phys.* 1994, Vol.76, p.747.
12. Phelps A.V., 1997, the cross section (10/15/97) available on http://jila.colorado.edu/collision_data/electronneutral/electron.txt Piscitelli et al., *Phys. Rev. E.* 2003, Vol.68, p.46408.
13. Stemowsky Z. et al. *J.Appl.Phys.* 2003, Vol.94, p.1374.
14. Skullerud H.R. *J.Phys. D.* 1968, Vol.1, p.1567.

MODELING OF CF₄ DESTRUCTION IN ATMOSPHERIC PRESSURE MICROWAVE DISCHARGE

A.P. CHERNUKHO¹, A.N. MIGOUN¹, S.A. ZHDANOK¹, J.C. ROSTAING², J. PERRIN²

¹A.V. Luikov Heat and Mass Transfer Institute of NAS of Belarus 15, P. Brovka Str, Minsk, 220072, Belarus, chem@itmo.by

²Air Liquide Recherche et Developement, Boite Postale 126 Les Loges-en-Josas, 78354 Jouy-en-Josas, France, jean-christophe.rostaing@airliquide.com

Microwave plasma of atmospheric pressure has been the object of special interest over last decade due to their effective use in different applications, such as: excitation sources for elemental analysis [1], purification of noble gases [2] and many others. The present work is devoted to the use of this type of discharge to the abatement of perfluorinated compounds [3]. Here we present the numerical investigation of destruction of CF₄ in nitrogen with small admixtures of oxygen. The main attention is focused on the kinetic peculiarities of the process. Discharge peculiarities of the system are a subject of another work, presented in the current book [4]. One can find there the detailed description of creation and maintenance of microwave discharge plasma in fast flow gas system.

Model description

The following 51 species in C-F-O-N element space have been taken into account in the kinetic modeling of CF₄ conversion process: F, F₂, N, N₂, O, O₂, O₃, NO, NO₂, NO₃, N₂O,

Our previous investigations on SF₆ destruction in microwave discharge have shown that charged species do not significantly change chemical kinetics of the destruction process and the process itself has thermal character. Therefore, charged species are not taken into account in presented kinetic model.

We assume all reactions to be reversible. Direction of a reaction having most reliable data on rate constant within temperature range 300 - 6000 K has been selected as a forward direction of the reaction. Rate constants of forward reactions are given in modified Arrhenius form and principle of detailed balance is used for reverse rate constants calculation. Thermodynamic data has been taken mainly from [5], and kinetic data - from [5-7].

Table 1 presents all elementary chemical reactions and their rate constants that were included into kinetic mechanism.

Mathematically the task is formulated in two-dimensional steady-state approximation in cylindrical geometry where radial diffusion of the chemical component is taken into account. It was assumed that main part of discharge energy goes to thermal heating of gas flow. This is caused by low values of reduced electric field that are typical for microwave discharge. Radial profile of energy input and characteristic length of discharge were parameters of the task and taken from numerical results of [4]. Schematic diagram of the considered experimental discharge device has been described in the same article.

Present calculations have been performed using the following parameters of the setup: tube diameter D = 8mm, initial CF₄ mole fraction [CF₄]⁰ = 0.1-1% and initial mole fraction of oxygen [O₂]⁰ = 1.5 [CF₄]⁰.

N	Reaction	Rate constant, [molecule, cm, sec]	N	Reaction	Rate constant, [molecule, cm, sec]
1	2	3	1	2	3
1	$CF_3 + F(+M) \rightarrow CF_3(+M)$ (M=Ar) Low pres.lim.	$2.66 \cdot 10^{14} e^{-4504/T}$ $2.99 \cdot 10^{22} T^{-3.04} e^{-1545/T}$	39	$C + NO \rightarrow CN + O$	$3.30 \cdot 10^{11}$
2	$CF_2 + F(+M) \rightarrow CF_2(+M)$ (M=Ar) Low pres.lim.	$2.00 \cdot 10^{11}$ $3.96 \cdot 10^{21} e^{-2465/T}$	40	$C + NO \rightarrow CO + N$	$4.70 \cdot 10^{11}$
3	$CF_2 + O \rightarrow COF_2 + F$	$3.30 \cdot 10^{11}$	41	$C + N_2 + M \rightarrow CN + M$	$3.10 \cdot 10^{13}$
4	$COF_2 + F(+M) \rightarrow CF_2O(+M)$ Low pres.lim.	$4.17 \cdot 10^{12} e^{-4076/T}$ $3.80 \cdot 10^{25} T^{-3.06} e^{-440/T}$	42	$C + N_2 + O \rightarrow CN + NO$	$8.00 \cdot 10^{12}$
5	$CF_2 + O \rightarrow CF_2O$	$1.03 \cdot 10^{12}$	43	$C + F_2 \rightarrow CF + F$	$2.82 \cdot 10^{12} e^{-354/T}$
6	$CF_2 + O_2(+M) \rightarrow CF_2OO(+M)$ Low pres.lim.	$1.00 \cdot 10^{13}$ $1.16 \cdot 10^{21} e^{-1499/T}$	44	$2C(+M) \rightarrow C_2(+M)$ Low pres.lim.	$2.16 \cdot 10^{11}$ $2.20 \cdot 10^{23} e^{-2000/T}$
7	$CF_2 + O_2 \rightarrow CF_2O + O$	$3.75 \cdot 10^{15} e^{-114} e^{-10819/T}$	45	$C_2 + O \rightarrow CO + C$	$6.00 \cdot 10^{10}$
8	$CF_2 + NO_2 \rightarrow CF_2O + NO$	$5.00 \cdot 10^{12}$	46	$C_2 + O_2 \rightarrow 2CO$	$1.50 \cdot 10^{11} e^{-493/T}$
9	$CF_2 + NO_2 \rightarrow COF_2 + NOF$	$2.40 \cdot 10^{12}$	47	$2C_2 \rightarrow C_3 + C$	$5.30 \cdot 10^{10}$
10	$CF_2 + N_2O \rightarrow CF_2O + N_2$	$2.32 \cdot 10^{11} e^{-12073/T}$	48	$C_2 + N_2 \rightarrow 2CN$	$2.50 \cdot 10^{11} e^{-5100/T}$
11	$CF_2 + O_2 \rightarrow CF_2O + O_2$	$9.30 \cdot 10^{13}$	49	$CN + O \rightarrow CO + N$	$3.16 \cdot 10^{15} e^{-8.24} e^{-364/T}$
12	$CF_2 + F_2 \rightarrow CF_2F + F$	$9.30 \cdot 10^{13}$	50	$CN + O_2 \rightarrow CNO + O$	$1.20 \cdot 10^{11} e^{-2017/T}$
13	$CF_2 + CF_2(+M) \rightarrow C_2F_4(+M)$ Low pres.lim.	$1.55 \cdot 10^{11} e^{-808/T}$ $2.30 \cdot 10^{26}$	51	$2CN(+M) \rightarrow C_2N_2(+M)$ Low pres.lim.	$9.44 \cdot 10^{23} T^{-2.61} M=N_2$ $3.00 \cdot 10^{11}$
14	$2CF_2(+M) \rightarrow C_2F_4(+M)$ Low pres.lim.	$2.71 \cdot 10^{15} e^{-7.26} e^{-3547/T}$ $1.56 \cdot 10^{28} e^{-1124/T}$	52	$CN + CNO \rightarrow CN + CO$	$3.00 \cdot 10^{11}$
15	$CF_2 + CF_2OF \rightarrow CF_2 + CF_2O$	$3.30 \cdot 10^{19}$	53	$CN + CO_2 \rightarrow CNO + CO$	$1.57 \cdot 10^{11} e^{-1999/T}$
16	$CF + F(+M) \rightarrow CF_2(+M)$ Low pres.lim.	$1.00 \cdot 10^{11}$ $3.00 \cdot 10^{21}$	54	$CN + N \rightarrow N_2 + C$	$1.00 \cdot 10^{10}$
17	$CF_2 + O \rightarrow FCO + F$	$1.16 \cdot 10^{10} e^{-507/T}$	55	$CN + N + M \rightarrow CN + M$	$2.76 \cdot 10^{12}$
18	$CF_2 + O_2 \rightarrow COF_2 + O$	$2.20 \cdot 10^{11} e^{-13192/T}$	56	$CNO + N \rightarrow CN + NO$	$4.50 \cdot 10^{10} e^{-0.99} e^{-8655/T}$
19	$CF_2 + NO_2 \rightarrow COF_2 + NO$	$7.52 \cdot 10^{13}$	57	$CN + NO \rightarrow N_2 + CO$	$1.43 \cdot 10^{11} e^{-1667/T}$
20	$CF_2 + F_2 \rightarrow CF_2F + F$	$8.32 \cdot 10^{14}$	58	$CN + NO_2 \rightarrow CNO + NO$	$4.00 \cdot 10^{11} e^{-1867/T}$
21	$2CF_2(+M) \rightarrow C_2F_4(+M)$ CO/1.5/CO2/2/Ar/0.7/	$1.09 \cdot 10^{10} e^{-3547/109/T}$ $3.60 \cdot 10^{20} T^{-2.57} M=N_2$	59	$CN + NO_2 \rightarrow CO_2 + N_2$	$6.14 \cdot 10^{10} e^{-3.75} e^{-1737/T}$
22	$CF + O \rightarrow CO + F$	$6.64 \cdot 10^{11} e^{-503/T}$	60	$CN + NO_2 \rightarrow CO + N_2O$	$8.20 \cdot 10^{10} e^{-0.75} e^{-1737/T}$
23	$CF + O_2 \rightarrow FCO + O$	$3.32 \cdot 10^{11} e^{-965.89/T}$	61	$CN + N_2O \rightarrow CN + N_2$	$1.00 \cdot 10^{11} e^{-1728/T}$
24	$CF + N \rightarrow CN + F$	$3.90 \cdot 10^{11}$	62	$CN + N_2O \rightarrow NCN + NO$	$6.40 \cdot 10^{11} T^{-5.6} e^{-1860/T}$
25	$CF_2O + O_2 \rightarrow COF_2 + FOO$	$1.00 \cdot 10^{10} e^{-5600/T}$	63	$NCN + O \rightarrow CO + N_2$	$1.66 \cdot 10^{11}$
26	$CF_2O + CO \rightarrow CF_2 + CO_2$	$4.00 \cdot 10^{10}$	64	$NCN + O \rightarrow CN + NO$	$1.66 \cdot 10^{10} e^{-1094/T}$
27	$CF_2O + CO \rightarrow COF_2 + FCO$	$2.00 \cdot 10^{15}$	65	$NCN + O_2 \rightarrow CNO + CNO$	$1.66 \cdot 10^{11} e^{-2519/T}$
28	$CF_2O + NO \rightarrow COF_2 + NOF$	$3.70 \cdot 10^{11} e^{-1107/T}$	66	$CCN + O \rightarrow CO + CN$	$6.00 \cdot 10^{12}$
29	$CF_2O + NO_2 \rightarrow COF_2 + NO_2F$	$3.20 \cdot 10^{12}$	67	$CCN + N \rightarrow 2CN$	$1.00 \cdot 10^{10}$
30	$CF_2O + F \rightarrow CF_2OF$	$5.80 \cdot 10^{11}$	68	$C_2N_2 + O \rightarrow CN + CNO$	$7.60 \cdot 10^{11} e^{-4466/T}$
31	$CF_2O + O_2 \rightarrow CF_2OO + O_2$	$2.00 \cdot 10^{12} e^{-1500/T}$	69	$CNO + M \rightarrow CN + CO + M$	$3.65 \cdot 10^{10} e^{-2750/T}$
32	$C + O \rightarrow CO + M$	$2.00 \cdot 10^{14}$	70	$CNO + O \rightarrow CO + NO$	$7.50 \cdot 10^{11}$
33	$C + O_2 \rightarrow CO + O$	$9.63 \cdot 10^{11} e^{-280/T}$	71	$CNO + O \rightarrow N + CO_2$	$1.33 \cdot 10^{11} e^{-1288/T}$
34	$C + C_2N_2 \rightarrow CN + CCN$	$3.00 \cdot 10^{11}$	72	$CNO + O_2 \rightarrow NO + CO_2$	$2.32 \cdot 10^{12} e^{-1084/T}$
35	$C_2 + N \rightarrow C + CN$	$5.00 \cdot 10^{10}$	73	$2CNO \rightarrow 2CO + N_2$	$4.28 \cdot 10^{11} e^{-549/T}$
36	$C + CO + M \rightarrow C_2O + M$	$6.30 \cdot 10^{12}$	74	$CNO + N \rightarrow N_2 + CO$	$3.30 \cdot 10^{11}$
37	$C + CO_2 \rightarrow 2CO$	$1.00 \cdot 10^{15}$	75	$CNO + NO \rightarrow CO + N_2 + O$	$7.61 \cdot 10^{12}$
38	$C + N + M \rightarrow CN + M$	$9.40 \cdot 10^{13}$	76	$CNO + NO \rightarrow CO + N_2O$	$7.61 \cdot 10^{10} T^{-3} e^{-470/T}$
			77	$CNO + NO \rightarrow N_2 + CO_2$	$9.63 \cdot 10^{10} T^{-3} e^{-470/T}$
			78	$CNO + NO_2 \rightarrow 2NO + CO$	$2.88 \cdot 10^{10} e^{-1983/T}$
			79	$CNO + NO_2 \rightarrow N_2O + CO_2$	$5.93 \cdot 10^{10} T^{-3.65} e^{-1647/T}$
			80	$CNO + N_2O \rightarrow N_2 + NO + CO$	$5.00 \cdot 10^{12}$
			81	$CNO + F \rightarrow NF + CO$	$9.21 \cdot 10^{12}$
			82	$FCO + O \rightarrow CO_2 + F$	$4.98 \cdot 10^{11}$

1	2	3	1	2	3
83	$\text{FCO}+\text{F}(\text{+M})\rightleftharpoons\text{COF}_2(\text{+M})$ Low pres. lim.	$1.66\cdot 10^{-12}$ $2.70\cdot 10^{-12}\text{T}^{-3}$	125	$\text{FO}+\text{NO}_2\rightleftharpoons\text{FOO}+\text{NO}_2$	$1.00\cdot 10^{-12}$
84	$\text{FCO}+\text{F}_2\rightleftharpoons\text{COF}_2+\text{F}$	$1.10\cdot 10^{-11}\text{e}^{-1450\text{T}}$	126	$\text{FOO}+\text{O}+\text{M}\rightleftharpoons\text{FO}+\text{O}_2$	$5.00\cdot 10^{-11}$
85	$2\text{FCO}\rightleftharpoons\text{COF}_2+\text{CO}$	$3.70\cdot 10^{-11}\text{e}^{-1460\text{T}}$	127	$\text{F}_2+\text{O}+\text{M}\rightleftharpoons\text{F}_2\text{O}+\text{M}$	$1.06\cdot 10^{-10}\text{T}^{-4.02}$
86	$\text{FCO}+\text{O}_2\rightleftharpoons\text{CO}_2+\text{F}+\text{O}$	$3.32\cdot 10^{-11}\text{e}^{-13198\text{T}}$	128	$\text{F}_2\text{O}+\text{NF}_2\rightleftharpoons\text{NF}_2+\text{FO}$	$5.05\cdot 10^{-12}\text{e}^{-11120\text{T}}$
87	$\text{C}_2\text{O}+\text{CO}+\text{M}\rightleftharpoons\text{C}_2\text{O}_2+\text{M}$	$2.00\cdot 10^{-23}\text{T}^{-3.4}$	129	$2\text{NF}\rightleftharpoons 2\text{F}+\text{N}_2$	$3.50\cdot 10^{-12}$
88	$\text{C}_2\text{O}_2+\text{O}\rightleftharpoons\text{C}_2\text{O}+\text{CO}_2$	$4.10\cdot 10^{-14}$	130	$\text{F}+\text{NF}+\text{M}\rightleftharpoons\text{NF}_2+\text{M}$	$3.40\cdot 10^{-27}\text{T}^{-3.82}$ M=Ar
89	$\text{CO}+\text{O}(\text{+M})\rightleftharpoons\text{CO}_2(\text{+M})$ CO/1.875/CO2/3.75/Ar/0.88	$2.66\cdot 10^{-14}\text{e}^{-1498\text{T}}$ $1.70\cdot 10^{-13}\text{e}^{-1510\text{T}}$ M=N ₂	131	$\text{NF}_2+\text{O}\rightleftharpoons\text{F}+\text{NOF}$	$1.25\cdot 10^{-11}$
90	$\text{CO}+\text{F}(\text{+M})\rightleftharpoons\text{FCO}(\text{+M})$ (M=N ₂) CO/1.5/CO2/2/Ar/0.7	$5.50\cdot 10^{-13}$ $8.52\cdot 10^{-29}\text{T}^{-4.4}$ 2457	132	$\text{NF}+\text{FO}\rightleftharpoons\text{NF}_2+\text{O}$	$2.50\cdot 10^{-10}$
91	$\text{CO}+\text{O}_2\rightleftharpoons\text{CO}_2+\text{O}$	$4.15\cdot 10^{-12}\text{e}^{-2454\text{T}}$	133	$2\text{O}+\text{M}\rightleftharpoons\text{O}_2+\text{M}$ O/71/O2/20/NO/5/N2/5/N5	$2.76\cdot 10^{-31}\text{T}^{-1}$ M=Ar
92	$\text{CO}+\text{N}_2\text{O}\rightleftharpoons\text{CO}_2+\text{N}_2$	$4.17\cdot 10^{-10}\text{e}^{-2148\text{T}}$	137	$\text{N}_2+\text{O}\rightleftharpoons\text{NO}+\text{N}$	$3.00\cdot 10^{-10}\text{e}^{-18295\text{T}}$
93	$\text{CO}+\text{NO}_2\rightleftharpoons\text{CO}_2+\text{NO}$	$1.50\cdot 10^{-10}\text{e}^{-17000\text{T}}$	138	$\text{N}+\text{O}_2\rightleftharpoons\text{NO}+\text{O}$	$1.50\cdot 10^{-14}\text{e}^{-3271\text{T}}$
94	$\text{CO}+\text{FO}\rightleftharpoons\text{CO}_2+\text{F}$	$1.25\cdot 10^{-11}$	139	$\text{NO}+\text{M}\rightleftharpoons\text{N}+\text{O}+\text{M}$ (M=Ar) N2/1.5/NO/3/	$1.60\cdot 10^{-9}\text{e}^{-5425\text{T}}$
95	$\text{CO}+\text{F}_2\rightleftharpoons\text{FCO}+\text{F}$	$4.00\cdot 10^{-10}\text{e}^{-8600\text{T}}$	140	$2\text{NO}\rightleftharpoons\text{N}_2+\text{O}_2$	$2.50\cdot 10^{-17}\text{e}^{-3680\text{T}}$
96	$\text{CO}+\text{F}_2\text{O}\rightleftharpoons\text{FCO}+\text{FO}$	$4.64\cdot 10^{-11}\text{e}^{-12700\text{T}}$	141	$\text{N}_2\text{O}(\text{+M})\rightleftharpoons\text{N}_2+\text{O}(\text{+M})$ (M=Ar) O2/1.4/N2/1.7/NO/3/N2O/3.5/	$1.26\cdot 10^{-12}\text{e}^{-2311\text{T}}$ $6.62\cdot 10^{-10}\text{e}^{-2841\text{T}}$
97	$\text{CO}_2+\text{N}\rightleftharpoons\text{CO}+\text{NO}$	$3.20\cdot 10^{-12}\text{e}^{-1710\text{T}}$	142	$\text{N}_2\text{O}+\text{O}\rightleftharpoons\text{N}_2+\text{O}_2$	$1.66\cdot 10^{-10}\text{e}^{-1471\text{T}}$
98	$\text{C}_2\text{O}+\text{O}\rightleftharpoons 2\text{CO}$	$8.64\cdot 10^{-11}$	143	$\text{N}_2\text{O}+\text{O}\rightleftharpoons 2\text{NO}$	$1.15\cdot 10^{-10}\text{e}^{-1461\text{T}}$
99	$\text{C}_2\text{O}+\text{O}_2\rightleftharpoons 2\text{CO}+\text{O}$	$3.32\cdot 10^{-11}$	144	$\text{N}_2\text{O}+\text{N}\rightleftharpoons\text{N}_2+\text{NO}$	$1.66\cdot 10^{-11}\text{e}^{-1084\text{T}}$
100	$\text{C}_2\text{O}+\text{O}_2\rightleftharpoons\text{CO}+\text{CO}_2$	$3.32\cdot 10^{-11}$	145	$\text{N}_2\text{O}+\text{NO}\rightleftharpoons\text{N}_2+\text{NO}_2$	$4.57\cdot 10^{-10}\text{e}^{-2161\text{T}}$
101	$\text{CF}_2\text{O}+\text{CO}\rightleftharpoons\text{CF}_2\text{O}+\text{CO}_2$	$5.00\cdot 10^{-10}$	146	$\text{NO}+\text{O}(\text{+M})\rightleftharpoons\text{NO}_2(\text{+M})$ (M=N ₂) NO2/6.2/NO/1.8/O2/0.8/N2O/4.4/CO2/0/	$2.16\cdot 10^{-6}\text{T}^{-0.78}$ $1.30\cdot 10^{-23}\text{T}^{-1.97}$ 76/7
102	$\text{C}_2\text{F}_4+\text{O}\rightleftharpoons\text{CF}_2+\text{COF}_2$	$3.16\cdot 10^{-13}\text{T}$	147	$\text{NO}+\text{O}(\text{+CO}_2)\rightleftharpoons\text{NO}_2(\text{+CO}_2)$ Low pres. lim.	$2.16\cdot 10^{-6}\text{T}^{-0.75}$ $1.10\cdot 10^{-25}\text{T}^{-2.16}$ 82M/
103	$\text{CF}_2\text{CO}+\text{O}\rightleftharpoons\text{COF}_2+\text{CO}$	$1.66\cdot 10^{-11}\text{e}^{-403\text{T}}$	148	$\text{NO}_2+\text{O}\rightleftharpoons\text{NO}+\text{O}_2$	$6.50\cdot 10^{-12}\text{e}^{-123\text{T}}$
104	$\text{FCCO}+\text{F}\rightleftharpoons\text{CF}_2+\text{CO}$	$4.98\cdot 10^{-11}$	149	$\text{NO}_2+\text{N}\rightleftharpoons\text{N}_2\text{O}+\text{O}$	$1.40\cdot 10^{-12}$
105	$\text{FCCO}+\text{O}\rightleftharpoons\text{FCO}+\text{CO}$	$1.66\cdot 10^{-10}$	150	$\text{NO}_2+\text{N}\rightleftharpoons 2\text{NO}$	$1.66\cdot 10^{-12}$
106	$\text{C}_2\text{F}_2+\text{F}\rightleftharpoons\text{CF}_2+\text{CF}_2$	$4.98\cdot 10^{-11}$	151	$\text{NO}_2+\text{NO}\rightleftharpoons\text{N}_2\text{O}+\text{O}_2$	$1.66\cdot 10^{-12}\text{e}^{-3019\text{T}}$
107	$\text{F}+\text{O}_2(\text{+M})\rightleftharpoons\text{FOO}(\text{+M})$ (M=N ₂) Low pres. lim.	$2.40\cdot 10^{-13}$ $1.10\cdot 10^{-20}\text{T}^{-1}$	152	$2\text{NO}_2\rightleftharpoons 2\text{NO}+\text{O}_2$	$6.56\cdot 10^{-12}\text{e}^{-1188\text{T}}$
108	$\text{F}+\text{F}_2\text{O}_2\rightleftharpoons\text{FOO}+\text{F}_2$	$3.60\cdot 10^{-14}$	153	$\text{NO}_2+\text{NO}\rightleftharpoons 2\text{NO}_2$	$1.80\cdot 10^{-11}\text{e}^{-170\text{T}}$
109	$\text{F}+\text{NO}(\text{+M})\rightleftharpoons\text{NOF}(\text{+M})$ Low pres. lim.	$1.00\cdot 10^{-11}$ $8.30\cdot 10^{-32}$	154	$\text{NO}_2+\text{O}(\text{+M})\rightleftharpoons\text{NO}_2(\text{+M})$ (M=N ₂) O2/0.8/CO2/0/	$2.21\cdot 10^{-11}$ $4.10\cdot 10^{-20}\text{T}^{-4.08}$ 1242/
110	$\text{F}+\text{FOO}\rightleftharpoons\text{F}_2\text{O}_2$	$8.80\cdot 10^{-13}$	155	$\text{NO}_2+\text{O}(\text{+CO}_2)\rightleftharpoons\text{NO}_2(\text{+CO}_2)$ Low pres. lim.	$2.21\cdot 10^{-11}$ $3.70\cdot 10^{-20}\text{T}^{-5.94}$ 1144/
111	$\text{F}+\text{NF}_2(\text{+M})\rightleftharpoons\text{NF}_2(\text{+M})$ (M=N ₂) Low pres. lim.	$4.66\cdot 10^{-17}\text{e}^{-372200\text{T}}$ $1.60\cdot 10^{-13}\text{e}^{-2586\text{T}}$	156	$\text{NO}_2(\text{+M})\rightleftharpoons\text{NO}+\text{O}_2(\text{+M})$ Low pres. lim.	$2.50\cdot 10^{-9}\text{e}^{-6895\text{T}}$ $4.50\cdot 10^{-17}\text{e}^{-2137\text{T}}$
112	$\text{F}+\text{F}_2\text{O}\rightleftharpoons\text{FO}+\text{F}_2$	$8.52\cdot 10^{-14}\text{e}^{-488\text{T}}$	157	$\text{NO}_2+\text{NO}_2\rightleftharpoons\text{NO}+\text{NO}_2+\text{O}_2$	$2.00\cdot 10^{-17}\text{e}^{-1810\text{T}}$
113	$\text{F}+\text{NO}_2\rightleftharpoons\text{FO}+\text{NO}_2$	$3.00\cdot 10^{-11}$	158	$\text{NO}_2+\text{O}\rightleftharpoons\text{NO}_2+\text{O}_2$	$1.70\cdot 10^{-11}$
114	$\text{F}_2+\text{O}\rightleftharpoons\text{FO}+\text{F}$	$4.30\cdot 10^{-13}\text{e}^{-115\text{T}}$	159	$2\text{NO}_2\rightleftharpoons 2\text{NO}_2+\text{O}_2$	$8.50\cdot 10^{-17}\text{e}^{-245\text{T}}$
115	$\text{F}_2+\text{NO}\rightleftharpoons\text{NOF}+\text{F}$	$6.91\cdot 10^{-15}\text{e}^{-1130\text{T}}$	160	$\text{N}_2\text{O}_4(\text{+M})\rightleftharpoons 2\text{NO}_2(\text{+M})$ Low pres. lim.	$4.05\cdot 10^{-14}\text{T}^{-1.1}$ 6447/
116	$\text{F}_2+\text{NO}_2\rightleftharpoons\text{NO}_2\text{F}+\text{F}$	$2.64\cdot 10^{-12}\text{e}^{-258\text{T}}$	161	$\text{N}_2\text{O}_4+\text{O}\rightleftharpoons\text{N}_2\text{O}_5+\text{O}_2$	$2.00\cdot 10^{-12}$
117	$\text{F}_2+\text{NF}_2\rightleftharpoons\text{NF}_2+\text{F}$	$4.34\cdot 10^{-12}\text{e}^{-685\text{T}}$	162	$\text{NO}_2+\text{NO}(\text{+M})\rightleftharpoons\text{N}_2\text{O}_2(\text{+M})$ Low pres. lim.	$2.66\cdot 10^{-15}\text{T}^{-1.4}$ $2.76\cdot 10^{-15}\text{T}^{-1.7}$
118	$\text{FO}+\text{O}\rightleftharpoons\text{F}+\text{O}_2$	$5.00\cdot 10^{-11}$			
119	$\text{FO}+\text{N}\rightleftharpoons\text{F}+\text{NO}$	$1.30\cdot 10^{-11}$			
120	$\text{FO}+\text{N}\rightleftharpoons\text{O}+\text{NF}$	$1.30\cdot 10^{-11}$			
121	$\text{FO}+\text{NO}\rightleftharpoons\text{NO}_2+\text{F}$	$8.00\cdot 10^{-10}\text{T}^{-0.58}$			
122	$2\text{FO}\rightleftharpoons 2\text{F}+\text{O}_2$	$8.50\cdot 10^{-11}$			
123	$2\text{FO}\rightleftharpoons\text{F}+\text{FOO}$	$5.00\cdot 10^{-13}$			
124	$\text{FO}+\text{NF}_2\rightleftharpoons 2\text{F}+\text{NOF}$	$3.80\cdot 10^{-12}$			

1	2	3	1	2	3
163	$N_2O_3+O\leftrightarrow 2NO_2$	$4.50\cdot 10^{-13}$	168	$NF_2+NF_2(+M)\leftrightarrow N_2F_4(+M)$	$3.00\cdot 10^{-13}$
164	$2N+M\leftrightarrow N_2+M$	$8.30\cdot 10^{-34}e^{490/T}$		Low pres.lim.	$1.00\cdot 10^{-32}$
165	$2F+M\leftrightarrow F_2+M$	$3.80\cdot 10^{-29}T^{-2}e^{-315/T}$	169	$NO_2+NO_3(+M)\leftrightarrow N_2O_5(+M)$	$2.00\cdot 10^{-12}$
166	$NF+N_2F_2\leftrightarrow NF_2+N_2+F$	$1.00\cdot 10^{-12}$		Low pres.lim.	$1.30\cdot 10^{-21}T^{-3.5}$
167	$NF_2+NF\leftrightarrow N_2F_2+F$	$2.40\cdot 10^{-12}$			

Results and discussion

Thermodynamically CF_4 is stable in presence of oxygen up to T-1200 K. Increase of temperature results in consequent change of potential main conversion products as follows: COF_2 , CO_2 , CO (see Fig.1). Noticeable amount of CN and C appear under temperatures higher than 5000 K. To add, main carbon containing specie in temperature range from 2500 to 6000 K is CO .

As a rule, products composition is different from equilibrium values under real conditions. Mainly, this is caused by limited residence time of gas mixture in hot zone of the reactor. Fig. 2 shows numerical results of CF_4 conversion kinetics in isothermal conditions for two temperatures: 2500 K and 5000 K. Characteristic residence time in discharge region of the considered experimental device, that is in the range $\tau_{res} = 3e^{-3}e^{-3} s$ and depends on operation regime, is also shown in the figure. It is seen that under 2500 K temperature residence time is not long enough even for half decomposition of CF_4 , while for 5000 K this time is an order of magnitude higher than required one for complete CF_4 decomposition.

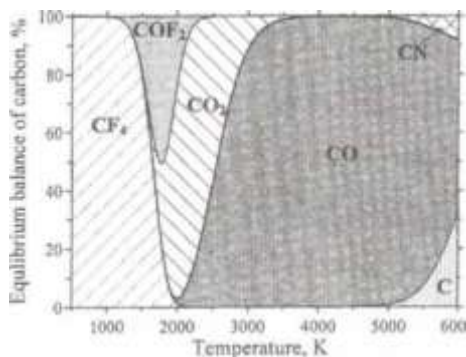


Fig.1. Balance of carbon in equilibrium

$N_2/O_2/CF_4=97.5/1.5/1.0$ mixture

temperature higher than 3000 K is required for effective process organization. Note that much higher times are required to reach equilibrium product content (see curve 4, Fig.3). This is mainly connected with transformation of CF_4 decomposition products. Under high temperatures establishment of equilibrium is limited by dissociation of N_2 , which is main part if the mixture.

Gas flow in discharge zone under real experimental conditions is characterized by huge radial nonuniformity, which is caused by specific nature of gas heating by microwave field and cooling of discharge tube which is necessary to prevent its damage. Along with high temperature central part (maximum energy input is not necessary occurs at the axis of the reactor), where temperature reaches 5000-6000 K [8] and decomposition process runs very fast, there are cold parietal zones of the flow, where chemical transformations does not run at

Fig. 3 shows temperature dependence of CF_4 decomposition characteristic times. One can see that under the considered conditions

fast, there are cold parietal zones of the flow, where chemical transformations does not run at all. This is the main reason of difficult complete CF_4 decomposition even for high discharge specific energy inputs.

Our calculations have shown that radial diffusion can partly compensate this effect by transfer of reagents from cold to hot zones; however, total positive input of this process does not exceed 10-15%.

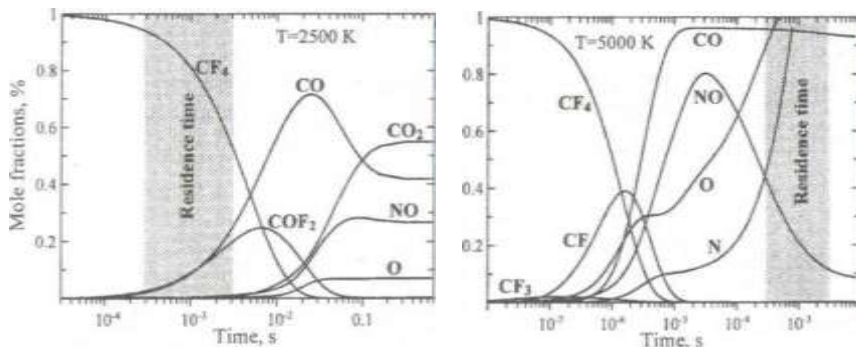


Fig.2. Isothermal kinetic of CF_4 destruction in $N_2/O_2/CF_4=97.5/1.5/1.0$ mixture: P-1 atm

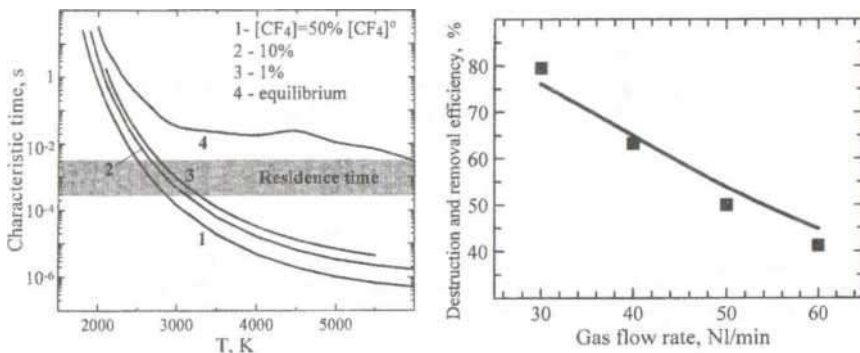


Fig.3. Characteristic times of CF_4 destruction Fig.4. Theoretical and experimental data on in isothermal conditions process: mixture - CF_4 destruction in microwave discharge: $N_2/O_2/CF_4=97.8/1.2/1.0$; P=1 atm W=4000 W; initial mixture - $N_2/CF_4/O_2=99.75/0.1/0.15$

Fig. 4, 5 present part of the results of numerical modeling using full 2D model. It is seen that results of calculations of destruction and removal efficiency are in a good agreement with experimental data (see Fig.4). Fig.5 shows the flow averaged kinetic curves for a few experimental regimes. It is seen, that destruction and removal efficiency is a monotonically rising function. That means that there is no even partial reconstruction of CF_4 from decomposition products in afterglow zone. Note, that for e.g. SF_6 such kind of reconstruction is possible.

One can see that main part of CH_4 is decomposed in discharge zone of the reactor ($z < 4$ cm). Intensity of the process reduces in afterglow. The process stabilize to the end of the discharge tube ($z = 15$ cm) and CF_4 concentration reaches its final value. This occurs due to cooling of the tube, which removes almost half of the energy obtained from discharge.

Further cooling of the gas occurs in heat exchanger ($z = 15$ -200 cm). Chemical transformations continue in this zone (see Fig.5b), while CF_4 mole fraction remains unchanged since they do not influence CF_4 , and connected mainly with transformations of conversion products (CO , CO_2 , CF_3OF , CF_2O) and recombination of atomic components (O , N , F).

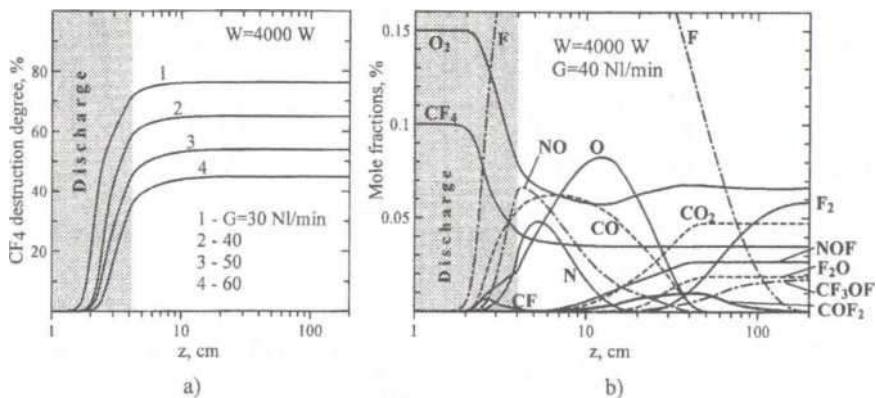


Fig.5. Kinetics of CF_4 destruction in microwave discharge reactor: initial mixture - N_2 , $\text{CF}_4/\text{O}_2=99.75/1.0/1.5$; $P=1$ atm

Conclusion

The kinetic model of high temperature CF_4 conversion process in N-O-C-F element space is developed. The thermodynamic and kinetic analysis of CF_4 destruction process has been done. A series of 2D numerical calculations of CF_4 destruction in microwave plasma reactor has been performed for different experimental conditions. Good agreement with experimental data has been obtained.

References

1. Woskov P.P., Hadidi K, Borrás M.C., Thomas P., Green K. and Flores G.J. Rev. Sci. Instrum. 1999, Vol.70, p.489.
2. Rostaing J.C., Bryslebout F. et al. C. R. Acad.Sci. Ser. IV, Paris. 2000, Vol.1, p.99.
3. Kabouzi Y., Moisan M. et al. J. Appl. Phys. 2003, Vol.93, pp.9483-9496.
4. Rolin M.N., Shabunya S.I., Rostaing J.C., Perrin J. Proc. Int. Workshop "Nonequilibrium processes in combustion and plasma based technologies", Minsk, 2004, (current book of abstracts).
5. NIST Chemical WebBook, <http://webbook.nist.gov/chemistry>
6. A. Konnov mechanism, <http://gopher.ulb.ac.be/~akonnov/science/mechanism/main.html>
7. Princeton mechanism, <http://www.princeton.edu/~cklaw/kinetics/>
8. Kabouzi Y., Calzada M.D. et al. J. Appl. Phys. 2002, Vol.91, pp.1008-1019.

PHYSICS AND APPLICATIONS OF UNDERWATER PLASMAS

F. DE BAERDEMAEKER, C. LEYS

Department of Applied Physics, Research Unit Plasma Technology,
Faculty of Engineering, Ghent University, Rozier 44, B-9000 Ghent, Belgium e-mail:
Christophe.Leys@UGent.be

Abstract

In the past few years, the research on underwater plasmas has become more and more important within the field of plasma sciences, but in comparison with the broad knowledge of gas discharges, the physics of underwater plasmas is still largely unknown. One of the reasons for this increased interest is the potential of such plasmas for several technological problems, for instance in the fields of water cleaning, medicine, sterilization and surface treatment and synthesis of polymers.

The oxidation of organic pollutants dissolved in water is an attractive method for water treatment, because it finally results in the conversion of the organic pollutants into compounds without secondary disposal requirements. Unfortunately, the direct reaction of organic pollutants with oxygen at ambient temperature is usually too slow to be of practical interest; and the use of higher temperatures is, especially for the treatment of low level organic pollutants, prohibitively expensive.

So-called advanced oxidation processes (AOPs) are processes that involve the input of energy - chemical, electrical or radiative (e.g. by high energy electron beams or γ -rays) - into the water to produce highly chemically active species (especially OH radicals), which then oxidize organic pollutants at ambient temperature. But also this method of water treatment involves a significant energy expense.

The need for an energy efficient method for the production of highly chemically active species in water has, in view of several potential applications such as water treatment, motivated research on the application of atmospheric non-thermal plasmas generated in water or above water surface: under the influence of the applied electrical field a non-equilibrium is established among electrons and heavy species (ions, neutral molecules) and a substantial part of the supplied electrical energy is funneled into the production of radicals through electron-molecule collisions. Various electrode configurations are possible. Both DC excitation and various types of AC excitation with either short or slowly rising voltage pulses have been studied (see e.g. [1]). However it should be said that, in comparison with the broad knowledge on gas discharges, the physics of underwater discharges is still largely unknown.

DC discharges generated above the water surface generate radicals in the discharge which then react with ambient air, creating a gaseous mixture of ozone, nitrogen oxides and nitric acid aerosols that subsequently dissolve in the water and react with the organic contaminants [2, 3]. An apparent deficiency of discharges above the water surface is that only a thin surface slab of water can be treated. This is why attempts are being made to generate underwater discharges.

Pulsed positive streamer corona discharges generated in water have been widely studied. Using a needle-plate electrode geometry, oxidation of low level phenol in water, removal of micro-organisms, production of OH, H and O radicals and production of H_2O_2 molecules have been demonstrated [1, 4-7]. Sharp needles, however, are quickly eroded and have a limited lifetime. In addition, the discharge of a single needle occupies only a very limited volume. Therefore, it is necessary to develop electrode configurations that produce larger plasma volumes.

Using a coaxial (flow-through) electrode geometry (also referred to as wire-cylinder geometry) in which the central electrode is coated by a thin layer of porous ceramics (2-5 % porosity, thickness of 0.2-0.3 mm), a large number of filamentary discharge channels can be generated at relative moderate applied voltage (order of 20 kV), filling almost homogeneously the electrode gap. Production of OH, H and O radicals, oxidation of Fe^{2+} and Fe^{3+} ions, production of hydrogen peroxide H_2O_2 molecules and degradation of phenol have been demonstrated with this concept that allows a wide variety of geometrical configurations and dimensions [1].

An interesting type of underwater discharge, which is not in direct contact with the electrodes, is the diaphragm discharge [8]. Diaphragm discharges can be sustained by DC or short to relatively slowly rising AC (50 Hz, 10 kV) voltages. If the pin-hole length to pin-hole diameter ratio is several times higher than one, the discharge scheme is referred to as a capillary underwater discharge [9]. In such a discharge scheme, the current is, at some point along its path between two submerged electrodes, flowing through a narrow bore in a dielectric material. When the current density is sufficiently high, local boiling and subsequent vapor breakdown, results in the formation of a plasma within this pin-hole. OH, H and O radicals are generated and at the same time the pin-hole emits an intense directed jet of vapor bubbles inside the surrounding water volume. Using an AC (50 Hz) excitation voltage, a stable plasma regime with one microsecond discharge pulse per half cycle, can be established in a broad range of conductivities (20 fxs.cm^{-1} - $10 \text{ ms}\cdot\text{cm}^{-1}$). The capillary discharge concept is easily scalable to a multi-channel configuration and offers the attractive possibility of pumping the water through the active discharge volume.

Next to the field of water treatment, underwater electrical discharges are also studied in connection to applications in medicine. In underwater spark discharges, i.e. high voltage/high current discharges between two submerged needle electrodes, a thermal plasma channel is formed, which emits ultraviolet light. The expansion of the plasma channel generates intense shock waves. Those underwater spark discharges have been extensively studied for the development of extracorporeal shock wave lithotripsy, a noninvasive method for the treatment of kidney stones [10,11]. With similar plasma sources, studies have also been made on the role of cavitation in cancer cell damage [12].

Other potential applications of plasmas generated underwater can be found in the sterilization of submerged objects like medical tools, and in the underwater surface treatment and synthesis of polymers [13].

References

1. Sunka P., Babicky V., tlupek M., Lukes P., Simek M., Schmidt J., Cemak M. *Plasma Sources Sci. Technol.* 8, 258-265. (1999).
2. Goheen S.C., Durhlan D.E., McCulloh M., Heat W.O. *Proc. 2nd Int. Symp. on Chemical Oxidation (Nashville, TN)*, 356. (1992).
3. Maximov A.I., Kuzmin S.M. *Proc. 5th Symp. on High Pressure Low Temperature Plasma Chemistry, Hakone V (Milovy, Brno)*, 282 .(1996).
4. Clements J.S., Sato M., Davis R.H. *IEEE Trans. Ind. Appl.* 23,224 (1987).
5. Joshi A.A., Locke B.R., Arce P., Finnay W.C. *Hazardous Mater.* 10, 3 .(1995).
6. Sato M., Oghiyama T., Clements J.S. *IEEE Trans. Ind. Appl.* 32, 106. (1996).
7. Sun B., Sato M., Clements J.S. *J. Electrostat.* 39,189 (1997).
8. Monte M., De Baerdemaeker F., Leys C., Maximov A.I. *Czech. J. Phys.* 52, D724-730 (2002).
9. De Baerdemaeker F., Monte M., Leys C. *Czech. J. Phys.* 54, C1062-1067. (2004).
10. Müller M. *Biomedizinische Technik* 35, 250. (1990).

11. Takayama K. Springer-Verlag, Berlin, 1992, Vol. II, P.1 163.

12. Sunka P.. *Phys. Plasmas* 8(5), 2587-2594 (2001).

IV Prat F., Chapelon J.Y., Ponchon T., Abou El Fadil F., Theilliere G., Pansu D., Berger F., Cathinghol D. *Proc. of 18th Int. Symp. on Shock Waves (Sendai 1991)*, edited by K. Takayama Springer-Verlag, Berlin, 1992, Vol. II, P.1163.

OBJECT-ORIENTED APPROACH TO GAS PHASE CHEMICAL KINETICS MODELING

A.N. MIGOUN, E.A. MATVEICHYK, A.P. CHERNUKHO, S.A. ZHDANOK A.V. Luikov Heat and Mass

Transfer Institute of NAS of Belarus

Numerical algorithms and methods are the subject of worldwide interest. Researchers have developed huge amount of numerical code during several last decades. Quite big part of program codes is written in different versions of Fortran programming language. Fortran language is known to be linear one. This fact does not fit modern approaches to complex software programming. Object oriented programming is one of the ways to obtain flexible, easily extendable, reusable and optimized code. This article describes new, object-oriented chemical kinetics class library for gas phase chemical kinetics modeling.

C++ programming language was selected as the basis.

Two main goals have been taken into account during software library development - flexibility and high speed of computations. High speed of computation can be achieved by high differentiation of the whole library into separate blocks and further blocks optimization, while flexibility was obtained by implementation of special algorithm that will be described below.

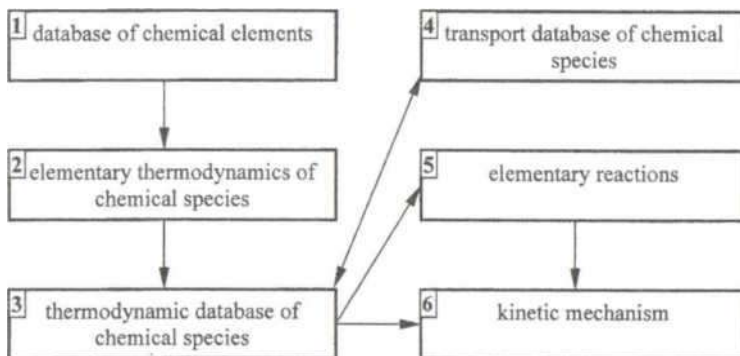


Fig.1. Structure of chemical kinetics class library

Structure of chemical kinetics class library is presented in Fig. 1. Module 1 contains information about chemical elements names and weights and set of functions for effective elements manipulation. Module 2 is responsible for creation of objects that calculate temperature dependences of thermodynamic properties. Objects created by module 2 are stored in module 3. Set of functions for effective work with set of chemical elements is also included in module 3. Fours module is responsible for creation and initialization of objects for transport properties calculation. Objects for chemical reaction rate calculation are managed by module 5. Module 6 serves as storage of the objects that were created by module 5. Modules number 2, 4 and 5 are consequently subdivided into several blocks in order to achieve flexibility and possibility of deep optimization of calculations for every definite case.

All popular thermodynamic databases make use of ASCII text format to define species properties. There are three frequently used specie formats, namely: Chemkin [1], NASA [2]

mul Shomate [3]. Our class library must support these three formats and allow other formats In he easily implemented. To achieve this goal we have developed special class CFactory that implements universal mechanism of objects creation from any STL input stream. Definition of the class and related stuff is shown below.

First, let us define three auxiliary types that describe pointer to service functions:

```
typedef int (*LPESTIMATE)(istream& in, ostream& pLog);
typedef CFactory* (*LPCREATE)(istream& in, UINT& nError, ostream& pLog); typedef const strings
(*LPID)();
```

All object types in the library that are supposed to be created from an input stream must have such companion functions, `LPESTIMATE` points to a function that should explore input stream from its current position and report weight coefficient, which is the measure of an object presence probability, `LPCREATE` points to a function that creates an object and returns its pointer. The third pointer was defined for logging purposes and defines a function that returns text identifier of an object type. Thus, algorithm of objects creation can be formulated as follows:

- a) Register all objects
- b) Let all objects to explore input stream by making call to all registered estimation functions
- c) Define the object that reports highest weight coefficient
- d) Create the object by making call to corresponding `LPCREATE` function
- e) Repeat from b until end

Interface of the class that implements described algorithm was defined as follows:

```
class CFactory {
public:
    virtual ~CFactory();
    static int Register(LPESTIMATE estimate, LPCREATE create, LPID id); protected:
    CFactory() {};
    static CFactory* Create(istream& in, int& nError, ostream& pLog);
};
```

Let us consider how this algorithm works for calculation of thermodynamic properties of chemical species. Usually, three main thermodynamic properties of specie must be known as functions of temperature: specific heat capacity at constant pressure, entropy and enthalpy. Other specie properties, e.g. name, weight, charge etc., are also must be usually known. Therefore, we can formulate an abstract interface class that describes generic chemical specie:

```
class CSpecie : public CFactory { public:
    static CSpecie* Create(istream& in, int& nError, ostream& pLog) ;

    virtual ~CSpecie() {}; virtual string Name() const = 0; virtual double
    Charge() const = 0; virtual double Weight() const = 0; virtual int
    Phase() const = 0; virtual double Entropy(double dT) const = 0;
    virtual double Enthalpy(double dT) const = 0; virtual double
    HeatCapacity(double dT) const = 0; protected:
    CSpecie() {};
    CSpecie(const CSpecieS);
};
```

The class inherits from `CFactory`, has protected constructors and pure virtual functions and, therefore, cannot be explicitly instantiated. To make use of these classes we need several more classes that implement creation, initialization and properties calculation for every supported specie type formats. For example, classes that implement Chemkin specie behavior were defined as follows: `class CChemkinSpecieLite : public CSpecie {`

```
public:
    virtual ~CChemkinSpecieLite() {};

    static int Estimate(istream& in, ostream* pLog);
    static CSpecie* Create(istream& in, UINT& nError, ostream* pLog); static const strings ID() {
    return m_strID; };

    virtual string Name() const { return m_strName; }; virtual string Formula() const;
    virtual string Comment() const { return m_strComment; }; virtual double Charge()
    const { return m_nCharge; }; virtual double Weight() const { return m_dWeight; };
    virtual int Phase () const { return m_enumPhase; }; virtual double Entropy(double
    dT) const; virtual double Enthalpy(double dT) const; virtual double HeatCapacity
    (double dT) const;

protected:
    CChemkinSpecieLite() {};
    CChemkinSpecieLite(const CChemkinSpecieLiteS);
};

class CChemkinSpecie : public CChemkinSpecieLite {
public:
    virtual ~CChemkinSpecie() {};

    static int Estimate(istream& in, ostream* pLog);
    static CSpecie* Create(istream& in, UINT& nError, ostream* pLog); static const strings ID() {
    return m_strID; };

    virtual double Entropy(double dT) const; virtual double
    Enthalpy(double dT) const; virtual double
    HeatCapacity(double dT) const;

protected:
    CChemkinSpecie() {};
    CChemkinSpecie(const CChemkinSpecieS);
};
```

The difference between classes `CChemkinSpecieLite` and `CChemkinSpecie` is that first one supports species with one temperature interval and second inherits one temperature interval implementation and supports additional temperature interval [1]. Implementation of both classes has been optimized to achieve high speed of properties calculation.

To make any class derived from `CFactory` work one should register it. For example, for `CChemkinSpecie` class it may look as follows:

```
CFactory::Register(CChemkinSpecie::Estimate, CChemkinSpecie::Create, CChemkinSpecie::ID);
```

ЛII internal classes register automatically at program startup. Note that user does not need to recompile whole library to make it work with external user-definer object types.

After registration of a class user can create objects of that type by making call to Create function of CSpecie class. Example of user code is shown here:

```
ifstream stream("input.dat");
vector<CSpecie*> species; while
(stream.good()) {
    if (CSpecie* pSpecie = CSpecie::Create(stream, nError))
        species.push_back(pSpecie);
    else
        break;
}
for (i=0; i<species.size (); i++) {
    cout << "H298(" << species[i]->Name() << ") = "; cout
    << species[i]->Enthalpy(298) << endl;
}
```

If input file contains supported species descriptions vector `species` will be populated by pointers to objects that implement corresponding species behavior. Then user can loop though all species in vector and obtain any property described in CSpecie interface by the same way independently of real type of the specie object.

The same idea was implemented for calculations of transport properties and reactions rate constants.

Conclusion

New approach to gas phase chemical kinetics modeling has been shown. Chemical kinetics class library has been developed and implemented in C++ programming language.

Acknowledgements

This work has been done under the support of INTAS Grant No. 03-51-4736 and belarussian state program of oriented fundamental research "Hydrogen 16".

References

1. Kee R.J., Rupley F.M. and Miller J.A. *Chemkin-II: A Fortran Chemical Kinetics Package for the Analysis of Gas-Phase Chemical Kinetics*, Sandia Report SAND89-80090. UC-401, September 1989.
2. McBride B.J., Zehe M.J. and Gordon S. *NASA Glenn Coefficients for Calculating Thermodynamic Properties of Individual Species*, NASA report TP-2002-211556, September 2002.
3. NIST chemical webbook, <http://webbook.nist.gov/chemistry>

NUMERICAL SIMULATION OF IONS KINETICS IN METHANE/AIR PREMIXED LAMINAR FLAME

A.N. MIGOUN¹, A.P. CHERNUKHO¹, N.S. TITOVA², A.M. STARIK², A. CENIAN³,
S.A. ZHDANOK¹

¹A.V. Luikov Heat and Mass Transfer Institute of NAS of Belarus, migoun@itmo.by ²Central Institute of Aviation Motors of RAS ³Institute of Fluid-Flow Machinery, Polish Academy of Sciences

Introduction

It is known from numerous literatures that under a certain conditions chemi-ionization processes can noticeably ionize a flame. This article is intended to investigate ions formation in stoichiometric methane/air premixed laminar flame. This work is the continuation of the work presented in [1], Contrary to that work, present investigations are based on detailed chemical kinetics of neutral and charged particles interactions.

Model description

Kinetics of neutral species transformation has been taken from [2], while kinetics of excited CH and charged species has been taken from [3]. Two kinetic mechanisms have been prepared in CHEMKIN format [4] to make use of previously developed software for kinetics investigation that supports the format: first includes only neutral species transformations while second contains first one and extends it by charged species kinetics.

Contrary to [2] we used another rate constant for methyl radicals recombination reaction which provides better fit to experimental data. The constant has been set according to [5] and Troe form [6] of pressure dependence has been declared using the following coefficients:

$$\alpha = 100, T^{***} = 8, T^* = 115, T^{**} = 6000.$$

Neutral species thermodynamic data has been taken from NASA database [7]. Data on thermodynamic properties of charged species has been taken mainly from [7,8]. Data on the rest species properties has been compiled using electron affinity and ionization potentials and principle of similarity.

Developed kinetic mechanisms have been tested against [2, 3] and have shown good agreement with theoretical and experimental data.

There is lack of data on transport properties of charged species in literature. Moreover, developed mathematical model does not take into account ambipolar character of charged species diffusion, which has significant influence on species transport when charged species concentrations are high enough. It is known flame under consideration to be the case. Therefore, the following technique of calculation of charged species fraction evolution in time has been used. First, we assume that presence of ions and electrons does not significantly change thermal regime of premixed laminar flame and calculate spatial profiles of temperature and gas velocity in the flame using kinetic mechanism without charged species. Then, calculated spatial temperature profile is recalculated to time-dependent temperature profile. At final stage the time evolution of temperature change is used for integration of 0D chemical reactor using second chemical mechanism, which contains charged particles kinetics.

Fig. 1 shows the time evolution of charged species in premixed stoichiometric methane/air laminar flame at 10 atm pressure. It is seen that H_3O^+ ions and electrons are dominant species in flame front “located” right before 0.005 s. Then electrons concentration decreases a bit lower than CO_3^- ions concentration and NO_3^- ions appear in almost the same amount as H_3O^+ .

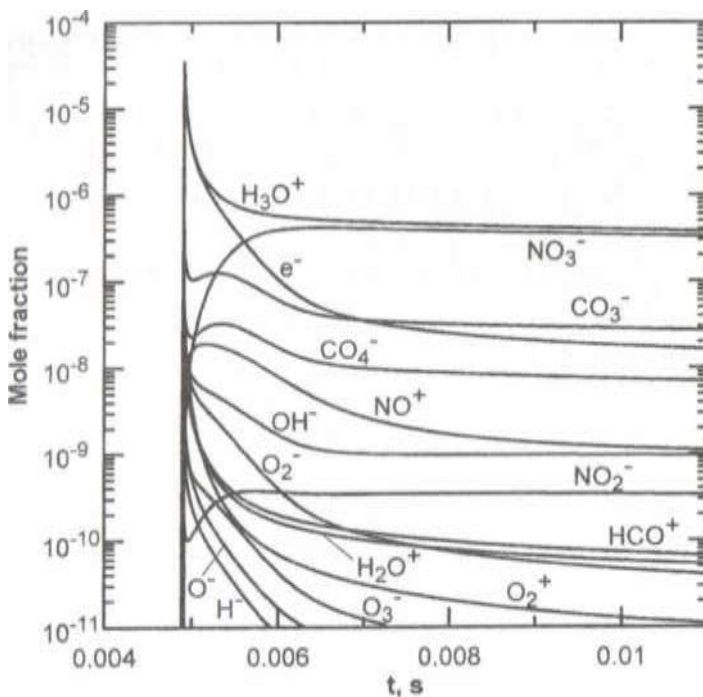


Fig. 1. Evolution of charged species mole fraction in time

One can conclude that H_3O^+ is the main positive ion in stoichiometric methane/air laminar flame at 10 atm pressure. Electrons dominate among negative species in flame front while NO_3^- - behind flame front.

Acknowledgements

This work has been partially supported by the INTAS Grant No.03-51-4736, KBN project 4 T10B 019 22 and Polish Academy of Sciences in frame of co-operation program between Poland and Belarus.

References

- Migoun A.N., Chemukho A.P., Labuda S.A., Genian A., Zhdanok S.A. *Numerical view on premixed methane/air flame diagnostics*, Proc. Int. School-Seminar "Nonequilibrium processes and their applications", Minsk, Belarus, HMTI. 2002. Dautov N.G., Starik A.M. *On the problem of choosing a kinetic scheme for the homogeneous reaction of methane with air*, Kinetics and Catalysis. 1997, Vol.38, No.2, pp.207-230.
- Starik A.M., Titova N.S. *Kinetics of Ion Formation in the Volumetric Reaction of Methane With Air*, Combustion, Explosion and Shock Waves. 2002, Vol.38, No.3, pp.253-268.
- Kee R.J., Rupley F.M., Miller J.A., Coltrin M.E., Grcar J.F., Meeks E., Moffat H.K., Lutz A.E., Dixon-Lewis G., Smooke M.D., Wamatz J., Evans G.H., Larson R.S., Mitchell R.E., Petzold L.R., Reynolds W.C., Caracotsios M., Stewart W.E.,
- Giarborg P., Wang C. and Adigun O. *CHEMKIN Collection, Release 3.6*, Reaction Design, Inc., San Diego, CA. 2000.
- Du H., Hessler J.P., Ogren P.J. *Recombination of methyl radicals. I. New data between 1175 and 1750 K in the falloff region* J. Phys. Chem. 1996, Vol. 100, pp.974-983.
- Gilbert R.G., Luther K., Troe J., *Ber. Bunsenges. Phys. Chem.* 1983, Vol.87, p.169.
- <http://cea.grc.nasa.gov/>
- <http://webbook.nist.gov/chemistry/>

SIMULATION OF MICROWAVE DISCHARGE IN NITROGEN AT ATMOSPHERIC PRESSURE

M.N. ROLIN¹, S.I. SHABUNIA¹, J.C. ROSTAING², J. PERRIN²

¹ A.V. Luikov Heat and Mass Transfer Institute of NAS of Belarus,
15, P. Brovka Str, Minsk, 220072, Belarus, rolin@itmo.by ²Air Liquide Recherche et Developpement, Boite
Postale 126 Les Loges-en-Josas,
78354 Jouy-en-Josas, France, jean-christophe.rostaing@airliquide.com

Description of steady microwave discharge in dielectric tube through-passing the waveguide is presented. Such discharges are applied at synthesis of ultra dispersed powders [1], clearing of noble gases [2] and neutralization of industrial wastes, which is in a focus of the present investigation. Therefore nitrogen of atmospheric pressure with small additives (O₂, SF₆) is considered as a working medium. To the present time the experimental researches of such discharges using spectroscopic methods of diagnostic [3] are conducted. It was shown, that the conditions in microwave discharge of atmospheric pressure essentially differ that were observed at underpressures. The discharge is essentially contracted to tube axis.

We don't know numerical investigations of steady microwave discharges of atmospheric pressure. In a fig. 1 the sketch of discharge device used at simulation is shown.

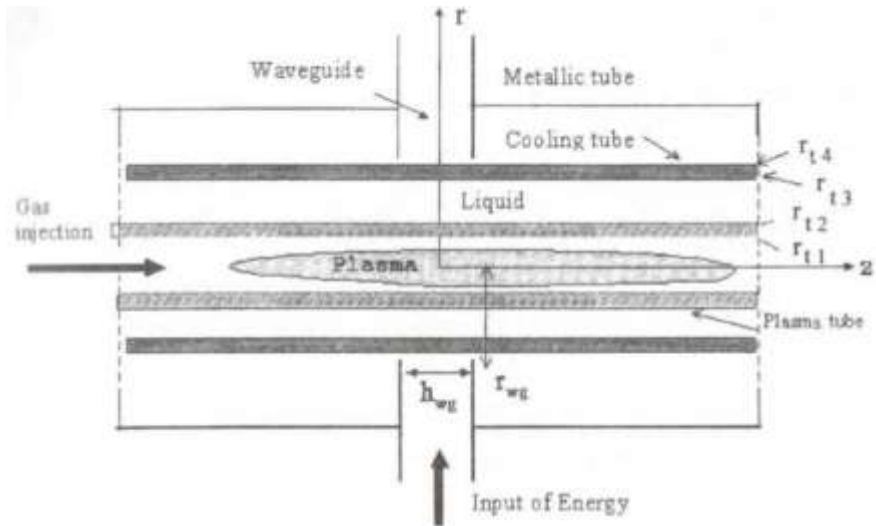


Fig. 1. Typical parameters of the device: $2r_{t1} = 8$ mm, $2r_{t2} = 12$ mm, $2r_{t3} = 16$ mm, $2r_{t4} = 18$ mm, $2r_{wg} = 20$ mm, $2r_{mt} = 52$ mm, $h_{wg} = 20$ mm, $\epsilon_{pl} = 9.5$, $\epsilon_{liq} = 2$, $\epsilon_{ct} = 3.6$

Formulation of the model

The actual field in the waveguide is a superposition of incident and reflected waves with a maximum electric field in the centre of the tube, such pattern has a definite symmetry (two planes). In order to simplify computational procedure the following assumptions in

model is assumed. Electromagnetic field in unit coupling the waveguide with plasma tube is azimuthal-symmetrical represented by superposition of concurrent and diverging cylindrical waves. Such field is described by wave equation:

$$\frac{\partial}{\partial r} \left[\frac{1}{\varepsilon r} \frac{\partial(rH)}{\partial r} \right] + \frac{\partial}{\partial z} \left(\frac{1}{\varepsilon} \frac{\partial H}{\partial z} \right) + \left(\frac{\omega}{c_0} \right)^2 H = 0, \quad (1)$$

$$\frac{1}{r} \frac{\partial(rH)}{\partial r} = i\varepsilon_0 \varepsilon \omega E_r, \quad \frac{\partial H}{\partial z} = i\varepsilon_0 \varepsilon \omega E_z, \quad (2)$$

where r and z are radial and axial coordinates accordingly, $H = H_\varphi$ is azimuthal component of magnetic density, $\omega = 2\pi f$ is circular frequency, c_0 is speed of light in vacuum, ε is complex index of relative inductivity.

The tangential components of an electrical field are equal to zero on metallic surfaces. On borders dielectric - dielectric the tangential components of electrical field are $E_{t1} = E_{t2}$, and normal are connected by condition $\varepsilon_1 E_{n1} = \varepsilon_2 E_{n2}$. The conditions of radiation absorption [4] are used on face planes to the right and to the left. Analytical solution of wave equation on large spacing intervals from axis is used as boundary conditions in the waveguide. The amplitude of such solution is set outgoing from fixed value of absorbed power.

The inductivity of plasma can be calculated using cumulative distribution function of electrons on energies $f(\epsilon)$ [5]

$$\varepsilon = 1 + \frac{2}{3} \frac{\omega_p^2}{\omega} \int_0^\infty \frac{\epsilon^{3/2}}{\omega - i\nu} \frac{d}{d\epsilon} \left[\frac{f(\epsilon)}{\sqrt{\epsilon}} \right] d\epsilon, \quad (3)$$

where ϵ is energy of electron, ω_p is plasma frequency, ν is collision frequency of electron with atoms and molecules.

The function $f(\epsilon)$ can be determined from the solution of Boltzman equation for electrons [6]. The values of collision cross-section of electrons with nitrogen molecule are similar to [7].

The calculations of the fields conducted using value of ε determined' by methods described above have shown, that the field intensity in discharge is insufficient to ensure effective reactions of ionization by collision. Due to high temperature the nitrogen in discharge is substantially dissociated and can effectively flow past reactions of associative ionization including of atoms of nitrogen and oxygen basically and exited metastable states. The list of reactions taken into account is shown in [8].

The conservation equation of energy is written as

$$\frac{\partial(\rho H)}{\partial t} + \operatorname{div}(\rho q) + \operatorname{div}(S^{MW}) - \lambda \operatorname{div}(\nabla T) - \sum_k h_k J_k = 0, \quad (5)$$

where H is enthalpy of specific volume of gas, q is density of heat flux due to heat conduction and diffusion, S^{MW} is energy flux due to microwave radiation, S^{rad} energy flux due to own radiation of plasma

where λ is thermal conductivity of gas, J_k is diffusive flows a component, $h_k(T)$ is enthalpy of a component recalculated for one particle.

Component conservation equation is written as

$$\frac{d(N_i V_i)}{dt} + \text{div}(J_i) = \omega_i, \quad (6)$$

where ω_i is total local generation of a component by all reactions, where this component is appeared or consumed.

Molecular transfer is occurred dominant in radial direction. However, it is necessary to take into account and molecular transfer in axial direction too, as such processes provide steady regime of discharge in the field of plasma generation. Nevertheless it is possible to neglect convective transfer in radial direction.

The diffusion of the components is calculated in approach of binary diffusion. Anibipolar approach is used for the description of diffusion of electrons and ions.

As the absorption of electromagnetic energy is possible only at a definite level of gas Ionisation, in a discharge tube with gas pumping there should be a physical mechanism of energy transfer and generation of ionization towards to flow. The analysis of diffusive mechanisms of transfer demonstrates, that they are too gentle and can give only small contribution to counter transfer of energy. In considered conditions most probably such energy transfer could be explained by radiation of plasma in vacuum area of a spectrum.

Generation of photons able to initiate photoionization and photodissociation can be caused by the following processes: 1) photorecombination of atomic and molecular ions with electrons; 2) radiation association of atoms; 3) radiation of molecules excited by electronic impact in the systems of singlet bands; 4) ruled radiation of atoms.

The rate of photochemical reaction $M + \text{Photon} \rightarrow \text{Products}$ is determined by the following expression

$$\omega_{\text{photon}} = N_M \int_{\epsilon_0}^{\infty} \sigma_{\text{photon}}^M(\epsilon) U_{\epsilon} d\epsilon, \quad (7)$$

where ϵ_0 is threshold energy, $\sigma_{\text{photon}}^M(\epsilon)$ is cross-section of the process. The value U_{ϵ}/c has physical meaning equal to number of photons in specific volume. The method of spherical harmonics [9] is used to calculate radiation field

Photoionization of molecules and oxygen atoms, monoxides of nitrogen and metastable atoms of nitrogen are taken into account among the processes of absorption in plasma. The cross-sections of these processes are taken from [9] - [11]. The most probable source of radiation is the transitions from high singlet levels of nitrogen molecule.

Simulation results

In the calculations conducted at low intensity of ultraviolet radiation of discharge, which is insufficient to increase an electron concentration in incident gas up to values required for its heating by microwave field, the "blowing-out of discharge" takes place, i.e. discharge quenching. In conditions of actual experiment there is no any quenching. It means, that there are the mechanisms of ionization stabilizing discharge.

Artificial source of radiation is used to obtain steady solution. The assumption about existence of some unknown process in spectral range $\delta = 12.1 \dots 15.6 \text{ eV}$ described by

reactions $N_2 + e \rightarrow N_2^+ + e + \text{photon}$ is made. Relation determining the rate constant of this

reaction has the following form $k = 1 \cdot 10^{-8} \exp(-T_a/T_e) \text{ cm}^3 / \text{s}$. Activation temperature T_a is

varied within the limits of 75000 - 100000 K. Besides it is assumed, that there is process

$N_2 + \text{photon} \rightarrow N_2^+ + \text{photon}$ bound with this radiation, i.e. fluorescence. The influence of a fluorescence

on radiation transfer results in increase of an effective path of quantum in a gas up to collision of this one with tube wall. The fluorescence results in increase of absorption

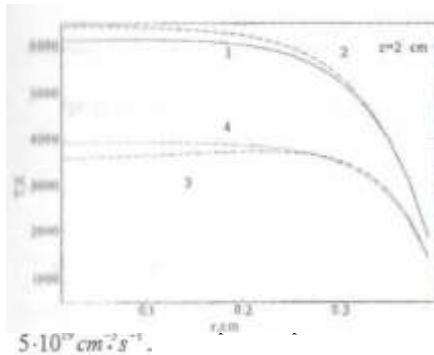


Fig. 6. Example of radial distribution of gas temperature in plasma tube.

value ref_{calc} remains permissible. Total amount of calculation is about 100 W that corresponds to 1 maximum power of radiation source is equal to

The estimations of probable mechanisms generating radiation are conducted. 1) Excitation by direct electronic impact; 2) Stepwise excitation by electron impact; 3) Populating of a level at a recombination of excited atoms; 4) Inverse of predissociation; 5) Populating by recombination + electron impact; 6) Three-body recombination ion - electron - neutral.

Unfortunately, all these mechanisms do not provide required level of ionizing radiation. Thus, the question about the nature of radiation ensuring stable regime of discharge remains open.

References

1. Batenin V.M. *SVCH-generatory plazmy (In Russian)*, M.: Energoizdat, 1988.
2. Rostaing J.C., Breselbout F., Moysan M., Parent J.C. *Acad. Sci. Ser. IV, Paris, T.1, P.99 (2000)*.
3. Kabouzi Y., Calzada M.D., Moisan M., Tran K.C., Trassy C. *J. of Appl. Phys.*, Vol. 91, P. 1008(2002).
4. Engquist B., Majda A. *Mathematics of Computation*, Vol. 31, P. 629 (1977).
5. Golant V.E. *Ultrahigh frequency methods for plasma investigation. (In Russian)* M., Nauka (1968).
6. Rockwood S.D., *Physical Review A*, V.8, P.2348 (1973).
7. Phelps A.V., Pitchford L.C., *Phys. Rev.* 31, P. 2932. (1985).
8. Rolin M.N., Shabunya S.I., Rostaing J.C., Perrin J. *IV International Conference Plasma Physics and Plasma Technology*. Vol. 1. P. 187, Minsk 2003.
9. Chetvertushkin B.N. *Mathematical modelling of radiative gas dynamics. (In Russian)* M. Nauka, 1985.
10. Cook G.R., Metzger P.H. *J. Chemical Physics*, Vol. 41, P. 321 (1964).
11. Biberman L.M. *Optical properties of hot air. (In Russian)*. M. Nauka, 1970.

Section 3. Nonequilibrium processes in combustion

TURBULENT FLAMES WITH REALISTICALLY LARGE DENSITY DROP AT THE FRONT

V. AKKERMAN^{1,2}, V. BYCHKOV¹

¹Institute of Physics, Umea University, S-901 87 Umea, Sweden tel. (46 90) 786 99 85, fax (46 90) 786 66 73, e-mail: slava.akkerman@physics.umu.se

²Nuclear Safety Institute (IBRAE) of the Russian Academy of Sciences,
B. Tulsckaya 52,113191 Moscow, Russia

Abstract

The increase in the velocity of premixed weakly turbulent flames of finite thickness with realistic thermal expansion is studied using the rigorous analytical theory. It is shown how the flame velocity depends on:

- 1) the flow parameters (the turbulent intensity, the turbulent spectrum, the length scale of the flow);
- 2) the thermal and chemical properties of the burning matter (thermal expansion, the Markstein and Prandtl numbers, the temperature dependence of transport coefficients).

It is demonstrated that influence of the finite flame thickness is especially strong close to the resonance point, when the wavelength of the turbulent harmonic is equal to the cut-off wavelength of the Darrius-Landau instability. The velocity increase is almost independent of the Prandtl number. On the contrary, the Markstein number, which characterises flame response to curvature and stretch, is one of the most important parameters controlling the velocity increase. The relative role of the external turbulence and the Darrius-Landau instability for the velocity increase is studied for different parameters of the flow and the burning matter. The velocity increase for turbulent flames in the methane and propane fuel mixtures is calculated for different values of the equivalence ratio. The present results are compared to the previous experiments on turbulent flames [1-3]. In order to perform the comparison, the theoretical results obtained are extrapolated to the case of a strongly corrugated flame front using the ideas of self-similar flame dynamics [4-6]. It is demonstrated that the theoretical results of the present work are in a good agreement with the experimental data.

References

1. Kobayashi H., Kawabata Y. and Maruta K., *27th International Symposium on Combustion (The Combustion Institute)*. 1998, p.941.
2. Lee T. W. and Lee S. J., *Combust. Flame*. 2003, Vol.132, p.492.
3. Klingmann J. and Johansson B., SAE paper 981050.1998.
4. Yakhot V., *Combust. Sci. Technol.* 1988, Vol.60, p.191.
5. Pocheau A., *Phys. Rev. E*. 1994, Vol.49, p.U09.
6. Bychkov V.V., *Phys. Rev. E*. 2003, Vol.68, p.66304.

ASPECTS OF REVERSE-PROCESS WITH GAS-PHASE REACTION FOR METHANE OXIDATION

V.S. BABKIN

Institute of Chemical Kinetics and Combustion SB RAS,
Novosibirsk, Russia

There is under certain conditions the phenomenon of spontaneous energy concentration in chemical reaction zone of travelling thermal waves with exothermic reaction under reaction gas mixture filtration in porous media. Technological process, based on this phenomenon, is named reverse-process. It allows specifically to utilize low-calorific fuels, for example, venting gases of coal mines with methane concentration 0.5-1%.

There are possible two principal schemes of reverse-process. The first one is with catalytic reaction and the other with homogeneous gas reaction. It is interesting in this connection to reveal advantages and disadvantages of these schemes, common and specific features of the processes. Marginal difference in equations, describing these related processes, allows us to assume the existence of some common features and, from the other hand, specifics in the schemes. Thus the conception of comparison of two schemes may be Informative and useful.

In this connection qualitative theory of hybrid thermal wave is developed, combining two types of wave processes - travelling thermal waves in catalytic bed and combustion waves with gas reaction in inert porous medium. The theory is developed as applied to reverse-process with operating parameters in transition region. In this region surface and volume reactions proceed simultaneously. The theory allows us to analyze an influence of controlling parameters on main characteristics of thermal wave, to predict regime transitions, to study unsteady-state effects. It is shown that theoretical and experimental results are in a good agreement.

Normal mode of reverse-process operating implies regular repetition of characteristics of temperature, concentration, and velocity fields. In other words, any disturbances, unsteady- state deviation in half-cycle of reverse-process have to be compensated in the following halfcycle. Otherwise one can expect failure of normal mode. In this connection the analysis of hydrodynamic, thermal-diffusion and gravitational flame instability has been done under filtration combustion with homogeneous gas reaction. There was shown the principal possibility of such types of instability in experiments. The analysis of parameters, determining flame front instability, has been carried out. It is assumed that in reverse-process some types of instability are compensated at changing of flow direction. As far as instability of wave front with catalytic reaction is concerned, there is not enough data on this question.

Optimal operating regimes of reverse-process depend on many factors. One of the most important among them is process thermal efficiency. It is determined by the value $\Delta T/\Delta T_{ad}$, were ΔT_{ad} is adiabatic heating-up. The theory of filtration combustion shows that thermal efficiency at equality of heat capacity fluxes of solid and gas phases tends to infinity. Of course this situation is not real, for example due to heat losses. It is darkly for the time present what is the reality at parameter values tending to the critical condition. Experiment shows that the combustion wave structure can change in these conditions.

In frame of conception of comparison of two reverse-process schemes it is interesting to compare global kinetic parameters for catalytic and homogeneous gas reactions. These parameters determine which of two schemes takes place in practice. The comparison of methane oxidation rates in catalytic and homogeneous gas reaction shows that rates are

comparable at temperature close to 1000 K. At the same time appreciable scatter of data on global kinetic parameters for homogeneous gas reaction was displayed in data of different authors. Data analysis shows that the scatter of data is due to not only by error of measurement, but mainly by changing of global kinetic parameters at reaction path changing. In particular if initial temperature changes proportional to the distance (the model of reverse- process), then ignition temperature increases and ignition delay decreases at temperature gradient rise. The same tendency is observed under increasing of gas mixture flow rate. In other words, methane oxidation rates, determined for the same methane oxidation mechanism, with different temperature increasing ways, are different.

Taking into account this circumstance, values of global kinetic parameters were selected from the array of literature data based on the principle of maximum variety of chemical reaction conditions. Among them are isothermal and nonisothermal (with temperature gradient) conditions, conditions close to reverse-process (inverse problem of propagation of filtration combustion wave), laminar and turbulent flame conditions and others. As a result of such selection there was obtained the following expression for methane oxidation rate in a range of methane concentration 0.5-1.5 % and temperature range 800-2000K:

$$W = 1.2 \cdot 10^{10} [\text{CH}_4] \exp(-50000/RT), \text{ (mol/cm}^2\text{s)}$$

The work was partially supported by EC Commission within the Programs INCO Copernicus - 2 (contract ICA-2-CT-2000-10035) and RFBR (Grant N 03.03.32357).

References

1. Babkin V.S., Wierzba I., Karim G.A. *The phenomenon of energy concentration in combustion waves and its applications*. Chem. Eng. J. 2003, Vol.91, pp.279-285.
2. Laevsky Yu.M., Babkin V.S. *On the theory of traveling hybrid wave*. Combust. Sci. and Tech. 2001, Vol.164, pp.129-144.
3. Babkin V.S., Laevsky Yu.M., Ismagilov Z.R. *Travelling waves offiltration combustion with homogeneous-heterogeneous reaction*. Proc. of the 1st Intern. Conf. on Application of Porous Media. Eds: R. Bennacer and A.A.Mohammad, Jerba, Tunisia. 2002, pp.643-654.
4. Babkin V.S., Bunev V.A., Gritzan V.I. *Problems of fire and explosion safety in context of sustainable development*. J. Phys. IV, France. 2002, Vol.12, pp.413-421.

CREATION OF THE ALTERNATIVE LIQUID FUEL FOR THE INTERNAL COMBUSTION ENGINE USING THE HYDRODYNAMIC CAVITATION

V.U. BONDARCHUK, S. KULIASHOU A.V. Luikov

Heat and Mass Transfer Institute of NAS of Belarus

Abstract

Fuel mixtures on the base of petrol and methanol are extensively used at present time. Such fuel has high knock-sensitive properties for internal-combustion engines. Fuel mixtures allow to decrease the content of harmful substances of vehicle exhaust gas. Because of low spirit combustion temperature per unit of consumed energy the volume of nitric oxide is decreased. The improvement of spirit mixtures combustion (combustion fullness) allows decreasing the ejection of CO and CH₄. The ejections of toxic aromatic hydrocarbons are reduced ten times more in comparison with using the traditional gasoline.

The theoretical and experimental studies of homogenization of liquid-liquid system (gasoline - methanol) are presented at this paper. This investigation is a very difficult task because a great many factors influencing on the homogenization process should be taken into account.

Stability of mixture fuels on the base of gasoline and methanol is determined by the component mixing quality to a considerable degree. Gasoline and methanol are unstable and segregate into the components during the time. Segregation rapidly varies depending on temperature and storage time. The mixture segregates into the gasoline and methanol under the typical mixing at positive temperature. For example the mixture segregates during a few days at +10 °C and a few hours at -20 °C.

The unintentional water additive is another important factor influencing on gasoline - methanol mixture stability. The unintentional water additive is inevitable under the vehicle exploitation.

Different chemical additives are added to the fuel mixture to increase the stability. Frequently these additives are injurious to the fuel quality and increase the engine wear.

However the fuel stability can be increased without introduction of additional chemical additives. The necessary methanol - gasoline fuel stability can be obtained by increasing the homogenization level. The component mixing intensification at the molecular level allows fulfilling this task. The mixing of gases at the molecular level is not difficult task at practice. A certain difficulty exists under the liquid mixing at the molecular level. It is very arduous to get the fine homogeneity of gasoline - methanol mixture because the spirit molecules combine into a robust system as a result of high polarity.

Experiment

The main idea of proposed method is the mixing of methanol and gasoline is conducted at steam and gas phases achieved at the hydrodynamic cavitation regime [1,2]. For this purpose the premix is accelerated to achieve the steam pressure.

The experimental equipment was built for mixing of gasoline and methanol. The experimental equipment consists of: the components and product (fuel mixture) tanks, high- pressure pump, cavitation module, controlling and monitoring system.

Cavitation module is the main assembly of experimental equipment. The mixture components transform to gas-vapour phase at the cavity pocket. The main gasoline and methanol mixing occurs at this cavity pocket. To intensify mixing it is necessary to increase

the mixing component residence time at the cavity pocket. The various hydrodynamic mixing regimes and geometrical forms of divergent part of cavitation module were studied experimentally. Various cavitation module behavior regimes are presented at Fig.1.

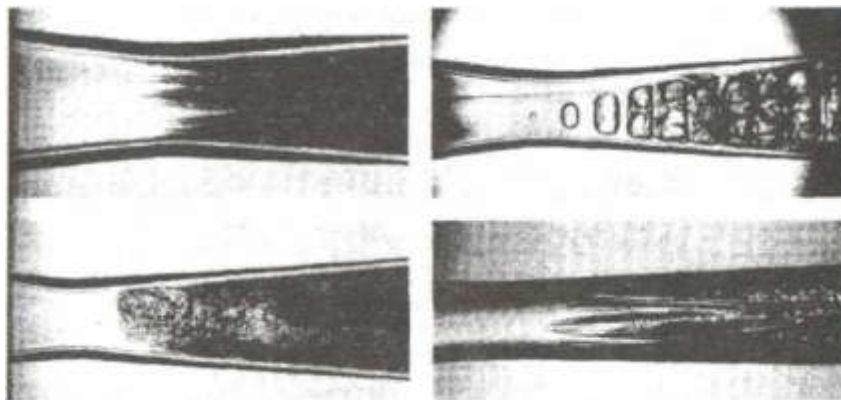


Fig. 1. Images of fluid flow in cavitation module channel

The high stability gasoline-methanol mixtures were obtained as a result of experimental study. The low-octane gasoline with methanol additives in volume terms from 15% to 20% was used for production of high-octane fuel. Premixing methanol and gasoline was delivered to cavitation module for single-stage treatment. The independent analysts shows the produced fuels are almost corresponding to the gasoline types of “regular” and “premium”.

Conclusion

The creation of cavitation regime is not difficult task. Thereto it is enough to accelerate the flow with a high velocity. The main problem is the detailed elaboration of cavitation module geometry in flow widening zone. It is very important to take into consideration the hydrodynamics properties of flow as well as physical properties of agitated liquids. The task is to organize and operate the cavitation pocket behavior.

Suggested technology allows to produce the high- homogeneous fuel mixtures which are able to keep the original homogeneity level and correspond to technical conditions during all the exploitation time.

References

1. Puris B.I., Baranova T. A., Bondarchuk V.U., *Experimental study of homogenization of liquid-liquid system, Heat and mass transfer -97*, Minsk, 34-37 (1997).
2. S.A. Kuliashou, *Intra-channel dispersion of intensive shear flows of low-viscosity fluids, Eng. Physical Journal*, V.54, 20-25 (1988).

CATALYTIC REACTOR FOR METHANE PARTIAL OXIDATION OF REVERSE-GAS FLOW OPERATING

S.A. ZHDANOK, V.V. GAVRILYUK, V.I. KALININ, I.F. BUYAKOV, A. DOD

A. V. Luikov Heat and Mass Transfer Institute of NAS of Belarus

The work is devoted to development of the original design of partial methane oxidation reactor, which operates in regime of periodical reverse-gas flow direction. The major task was to realize reactor's stable operation at atmospheric and higher pressures. Optimization of operation condition and parameters of the reactor was carried out to obtain maximal hydrogen yield.

Experimental setup

To perform experiments at normal and higher pressure, reaction mixture preparation system was equipped with TYLAN flow controllers, which allowed operating at the pressure till 10 bar. The scheme of the experimental setup is presented on Fig. 1. It is the last of three designs where the length of the casing was reduced to 250 mm to minimized free spaces between the porous operating medium of the reactor and inlet flanges. For comparison two previous generations of converters were 700 and 360 mm long. Size optimization allowed reducing length, to switch pressures over and to decrease the time of reactor heating, preserving same productivity. Improvement of the porous medium of the reactor was directed

to stabilize the location of heat generation zone on the edge of the catalytic layer. According to our estimates, under the conditions realized in the reactor the time of reactants' heating and products' hardening constitutes some hundredth fractions of a second even at 10 atm and does not exceed induction time of methane oxidation reaction. Heat released during surface methane combustion is quickly spent on catalytic methane-to-hydrogen conversion; therefore, the temperature all over the reactor does not exceed 900°C. Such relatively low temperatures do not make excessive requirements to structural materials and guarantee long-term reactor's service life.

According to thermodynamic calculations made in our laboratory, to obtain 95% methane-to-hydrogen conversion at atmospheric pressure, 750 °C is enough, whereas at 10 bar the required temperature approaches 1000°C. Such high temperature requires more heat-resistant nickel catalyst. All experiments describe below were made on the reactors with inert bed of quartz and a porous layer of nickel catalyst on alumina substrate.

Major results of experiments

Reactor's operation is defined by the properties and geometry of the working medium, reaction mixture flow rate and composition. The most important characteristic for the user is a yield of the target reaction product, i.e. hydrogen. The fact that the converter does not require external energy supply is an important feature and one of advantages of the design used. This ensures beneficial economical characteristics and quick regime setting. On the other hand, there is no opportunity to directly control working medium temperature distribution and, hence, methane conversion level. During operation, one may say, a self-consistent regime is set, what define hydrogen yield.

An experimentalist can obtain only those parameters that indirectly influence the efficiency of converter's operation. These parameters are specific flow rate of reaction

mixture, its composition and geometrical characteristics of the layers of reactor's working medium. The work aim is to study the effect of these parameters to obtain maximal hydrogen yield at stable operation modes not accompanied by soot deposition.

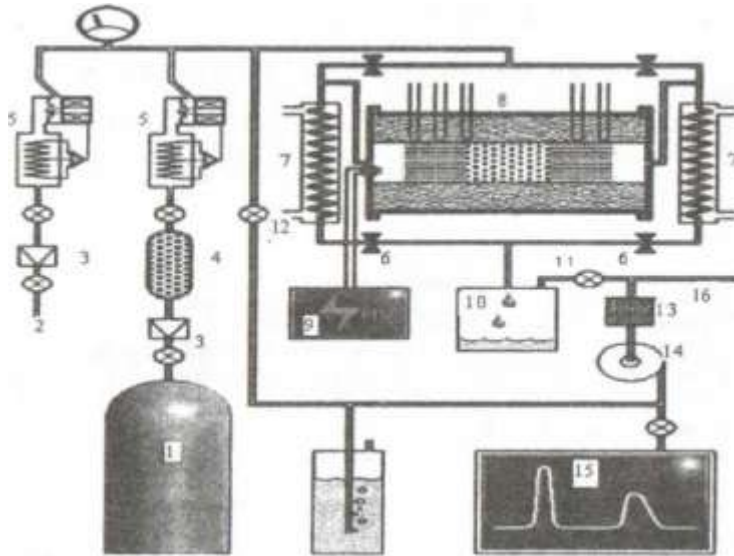


Fig. 1. Experimental setup: 1 - methane bottle, 2 - pressurized air from the line, 3 - gas pressure regulator with shutoff valve, 4 - sulfur absorbent, 5 - TYLAN 2900 series flow controllers, 6 - magnetic valve, 7 - water cooler, 8 - reactor, 9 - ignition unit, 10 - condensate collector, 11 - pressure control valve, 12 - bypass valve to supply input mixture to chromatograph, 13 - filter, 14 - membrane micro compressor, 15 - chromatograph, 16 - reaction product outlet

a) Selection of inert layer parameters

Conversion efficiency growth with the inert layer elongation is obvious. But, unfortunately, at the given specific flow rate there is a limitation for such temperature growth shown in Fig. 2.

The figure shows the sequence of the temperature profiles in the reactor with the inert layers of 80 mm, operating at 10 atm and $0.26 \text{ kg/m}^2\text{s}$ specific flow rate. The profiles are given starting from switching-over of reaction mixture flow direction with 10-second interval. The figure shows the formation of reaction zone in the inert layer. Temperature growth is possible only to the ignition temperature in noncatalytic layer.

b) Effect of specific flow rate of reaction mixture

Growth of specific power with the increase of the flow rate through the reactor similarly as inert layers' length growth augments process temperature and conversion degree

a. Effect of flow rate at 10 atm is shown in Fig. 3. Heat losses from the reactor's porous body increases with specific flow rate growth, but slower than specific power. Excessive flow rate

growth to $5 \text{ nm}^3/\text{hr}$, in case of our reactor, results in ignition temperature outside catalytic zone. Inadmissibility of this situation is mentioned above.

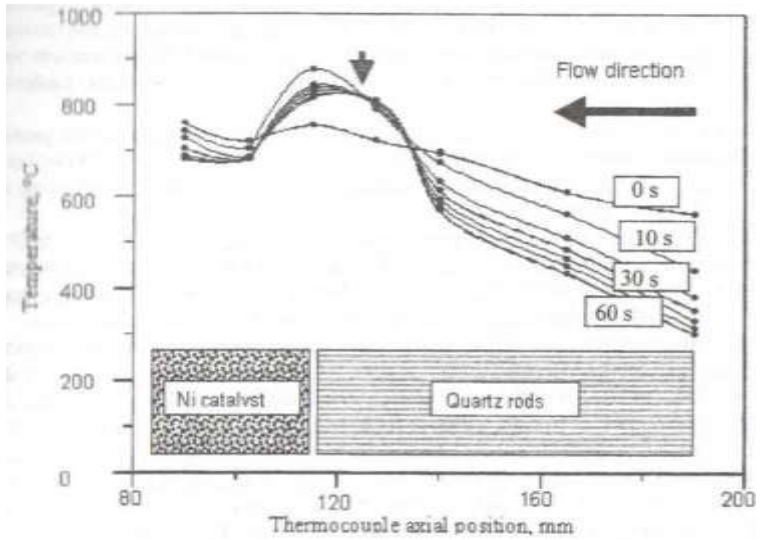


Fig. 2. Shift of the ignition point into inert layer. Ignition zone is marked by red arrow. Inert layer length - 80 mm, pressure - 10 bar, gas mixture flow rate - $3 \text{ m}^3/\text{hr}$

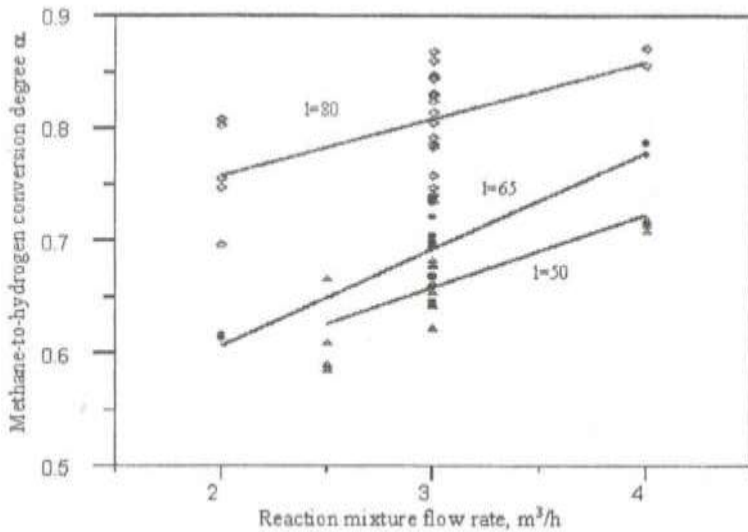


Fig. 3. Effect of reaction mixture flow rate on conversion degree for different thickness of inert layers

The most important result achieved at present is a stable hybrid reactor's operation at the pressure of 10 atm. And it is more important that methane-to-hydrogen conversion was not accompanied by prominent soot deposition, which was ensured by the reaction without reaction mixture overheating and high rate of reactants' heating and products' hardening in the used design of the reactor.

The mechanism proposed by the executors to stabilize the location of heat generation zone proved its efficiency due to fractional void volume jump at the boundary of two layers at simultaneous jump of the energy of surface reaction activation. This allowed achieving stable operation at the required operating pressure.

The temperature required to convert methane to hydrogen does not exceed 900°C for the given reactor. Such temperature is admissible for the available nickel catalyst on alumina substrate and does not represent a danger to available structural materials. Thus, long working capacity of methane converters designed, as hybrid reverse-flow reactor has no doubts.

Geometrical parameters of reactor's porous medium uniquely ensure optimal working mixture flow rate through the reactor. Thus, reactor's efficiency can be controlled only due to on-off time ratio of regularly discontinued flux of the reaction mixture. During temporary shutdown of the reactor its working medium cools with typical time of some hours. The time of setting temperature profiles is units of seconds. Thus, we believe that reactor's efficiency can be controlled during its supply with reaction mixture flux as a sequence of pulses with instantaneous flow rate equal to optimal one at the given reactor geometry. Simple set of electromagnetic valves will allow to alter average flow rate due to on-off time ratio and inevitable pulsations can be smoothed by using receiver of the required volume at the reactor's outlet.

THEORETICAL ANALYSIS OF COMBUSTION WAVES PROPAGATION WITHIN POROUS INERT MEDIA

V. BUBNOVICH, M. TOLEDO, C. ROSAS

Universidad de Santiago de Chile Departamento de Ingeniería Química B. O'Higgins
3363, Casilla 10233, Santiago, Chile E-mail: vbubnovi@lauca.usach.cl

Introduction

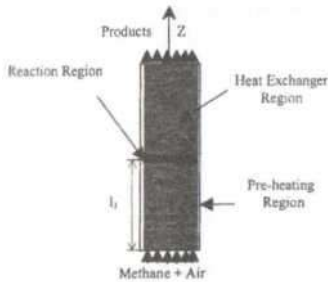


Fig.1. Scheme of the considered physical problem

The study of combustion waves during the filtration of lean methane - air mixtures in inert porous media is carried out using the two - temperature approximation in a semi - infinite canal. The analytical solution is built in three different regions, the pre - heating region, the reaction region and the region occupied by the combustion products. Analytical expressions predicting the temperature and methane mass fraction profiles in the wave, as well as the combustion wave velocity and the longitudinal extension of the reaction region, and the ignition temperature of the mixture in the porous media are derived. The results obtained are confirmed by numerical calculations.

Modeling of premixed combustion on inert porous media

The physical situation for which the mathematical model is built is the following (see

Fig. 1). It is assumed that:

- the semi-infinite porous canal is made up of 5.6 mm diameter alumina spheres forming an $e = 0.4$ porosity between particles. Other physical properties of the material are: specific heat $C_{p,s} = 1300 \text{ J/(kg}\cdot\text{K)}$, mass density $\rho_s = 2500 \text{ kg/m}^3$, the effective thermal conductivity $\lambda_{eff} = 1.3 \text{ W/(m}\cdot\text{K)}$ where the combined effects of gas and solid conductivity is considered.
- The previously pre-mixed methane-air gas enters through section $z = 0$ with excess air equal to ϕ (see eq.(5)) and initial temperature T_0 and gas speed u_0 . In addition, the mass density of the gas is $\rho_g = 1.13 \text{ kg/m}^3$ and the specific heat is $C_{p,g} = 1100 \text{ J/(kg}\cdot\text{K)}$. The thermal conductivity of the porous media is considered to be large relative to that of the gas mixture.
- The flow is one-dimensional; the gas is incompressible and obeys the perfect gas law. For the species diffusivity, we assume that the molecular Lewis number is unity:

$$\frac{\lambda_g}{\rho_g C_m D} = 1. \tag{1}$$

- The energy exchange between the solid and the gas is proportional to the local temperature difference. The fluid-to-solid volumetric convective heat transfer coefficient is expressed in the form suggested by Wakao and Kaguey:

$$a = \left(\frac{6\varepsilon}{d_p^2} \right) \lambda_g \left[2.0 + 1.1 \text{Pr}^{1/3} \left(\frac{\rho_g u_g d_p}{\mu} \right)^{0.6} \right] \quad (2)$$

- The heat transfer between the system and the environment occurs only through the porous media by natural convection and thermal radiation, and the effective coefficient for heat exchange with the surroundings β_e , $\text{W}/(\text{m}^2 \cdot \text{K})$ is found from the next energy balance applied to a cylindrical control volume of diameter D and length dx :

$$\left[h(T - T_a) + \varepsilon' \varepsilon'' \sigma (T^4 - T_a^4) \right] dx \pi D = \beta_e (T - T_a) dx \frac{\pi D^2}{4} \quad (3)$$

Then

$$\beta_e = \frac{4}{D} \left(h + \varepsilon' \varepsilon'' \sigma \frac{T^4 - T_a^4}{T - T_a} \right) \quad (4)$$

where $\varepsilon' = 0.45$ is an emissivity of the solid spheres, $\varepsilon'' = 0.38$ is a transmissivity factor for the quartz glass tube, $h = 10 \text{ W}/(\text{m}^2 \cdot \text{K})$ is heat transfer coefficient and σ is Stefan-Boltzmann constant.

- The combustion of the mixture is described by means of the global chemical reaction in a single step:



where φ represents the proportion of excess air in the reactant streams at the inlet to the system. The reaction rate is considered to obey the first-order Arrhenius equation with the activation energy $E_d/R_0 = 15643.8 \text{ K}$ and the pre-exponential factor $K = 2.6 \cdot 10^8 \text{ s}^{-1}$.

- The packed bed will be essentially an optically thick region around the high temperature zone and the radiation conductivity was included in the effective thermal conductivity of the porous media with the particle diameter d_p [1]:

$$k_{\text{eff}} = k_{\text{eff}} + \frac{3\lambda_g \varepsilon' \varepsilon'' \sigma T^3}{4(\beta_e - \varepsilon' \varepsilon'' \sigma T^3)} \quad (6)$$

- The reaction region thickness is defined here as the distance in the canal between the section where the temperature is equal to the ignition temperature and the section where the methane mass fraction equals 1/1000 of its maximum.

Using the preceding work assumptions, the energy equations for both the gas and particulate phases, as well as the continuity equations for the chemical species and the mixture are formulated, respectively, as

$$\rho_g \frac{dT_g}{dt} + \rho_g u_g \frac{dT_g}{dx} = -\rho_g (F_1 - F_2) + \rho_g h_c (T_p - T_g) \quad (7)$$

$$(\rho \cdot C_p)_g \frac{\partial T_g}{\partial t} = \frac{\partial}{\partial z} \left(\lambda_g \frac{\partial T_g}{\partial z} \right) + a(T_g - T_s) - \beta_v(T_g - T_0), \quad (8)$$

$$\frac{\partial w}{\partial t} + u_g \frac{\partial w}{\partial z} = \frac{\partial}{\partial z} \left(D \frac{\partial w}{\partial z} \right) - K w e^{-E/RT_g}, \quad (9)$$

$$\frac{\partial}{\partial z} (\rho u_g) = 0, \quad (10)$$

where T_g, T_s are the solid and gas temperatures, $(C_p)_g, (C_p)_s$ their heat capacities, u_g the gas velocity, a the interfacial heat exchange coefficient, β_v the effective coefficient for heat losses from the system, T_0 the ambient temperature, Δh_c the heat content of the reactive mixture, w the mass fraction of fuel, e the porosity. The density ρ was calculated for a mixture of perfect gas using the ideal - gas law:

$$\rho = \frac{PM}{RT_g}. \quad (11)$$

The following initial and boundary conditions are imposed on the solution:

$$t = 0: \quad T_g = T_s = T_0, w = w_0 = \frac{1}{(1 + 17.16 \cdot (1 + \varphi))}, \quad (12)$$

$$z = 0: \quad T_g = T_s = T_0, u_g = u_0, w = w_0, \quad (13)$$

$$z \rightarrow \infty: \quad \frac{\partial T_g}{\partial z} = \frac{\partial T_s}{\partial z} = \frac{\partial w}{\partial z} = 0. \quad (14)$$

In the paper there's the purpose of building the temperature $T(z)$ and methane gas mass fraction $w(z)$ profiles as well as the reaction zone movement speed values U_{FC} and the width of the reaction region, Δ .

Analytical method of solution

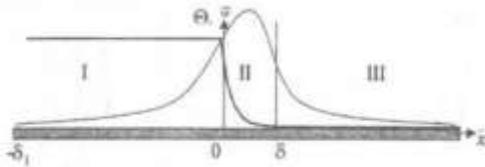


Fig. 2. Three representative regions of the system according to the work's hypothesis

In addition to the previous assumptions, the followings take place here. The thermodynamic pressure in the system is uniform and equals the reference pressure P_0 . All the physical properties of solid and gas are assumed to be homogeneous and constant. The radiative heat transport is neglected and the hydrodynamic velocity is uniform and equals the reference value u_0 .

Before integrating the three differential equations (7) - (9), there is a shift to the reference system which moves together with the combustion wave: $x = z - U_{FC} \cdot t$, $U_{FC} \ll u_0$. Then it is

assumed that the diffusion term in the equation (9) is considerable only in the small reaction region:
 $u_g w = -Kw \exp(-E/RT)$.

The results formulae are:

$$u_{FC} = \left(\frac{\rho_g C_{pg} u_g}{\rho_s C_{ps}} \right) \left[1 - \frac{1}{\frac{a\lambda_g}{(\rho_g C_{pg} u_g)^2} + \frac{4\beta_g (T_{ig} - T_0) e^{\frac{E}{R T_{ig}}}}{\rho_g w_0 \Delta h_c K}} \right] + \frac{K\lambda_g}{4u_g \rho_g C_{ps} e^{\frac{E}{R T_{ig}}}} \quad (15)$$

To obtain the analytical prediction for the dimensionless combustion wave velocity UFC from equation (15), the ignition temperature T_{ig} must be defined. The former may be estimated by considering the temperature evolution of a gas element moving through the heated porous media in a self-sustaining combustion wave. Assuming a moderate interfacial heat exchange coefficient and the reaction (fuel consumption) is almost completed in the distance of the order of the porous size the temperature increase for the gas element may be treated as a thermal explosion. Thus, one can directly apply the corresponding theory of Frank - Kamenetzki [2] with the correction for fuel consumption and derive an approximation for the ignition temperature T_{ig} in the following implicit form [3]:

$$\frac{e^{\frac{E}{R T_{ig}}} - 1}{(E/R T_{ig})^{7/3}} = \left(\frac{\Delta h_c^2 w_0^2 R_g^5}{2 \cdot \pi^2 C_{pg}^2 E_c^2} \right) \left(\frac{d_p \varepsilon T_g K}{u_g} \right) \quad (16)$$

Numerical solution

To support and to test the analytical solutions obtained here, a computational procedure was performed using a full set of the basic equations (1) - (14). These were calculated using the implicit finite difference solution of the equations (7)-(9) and the Tree-Diagonal Matrix Algorithm (TDMA). The time step $\Delta t = 0.01$ s and 800 grid points are used for numerical calculations.

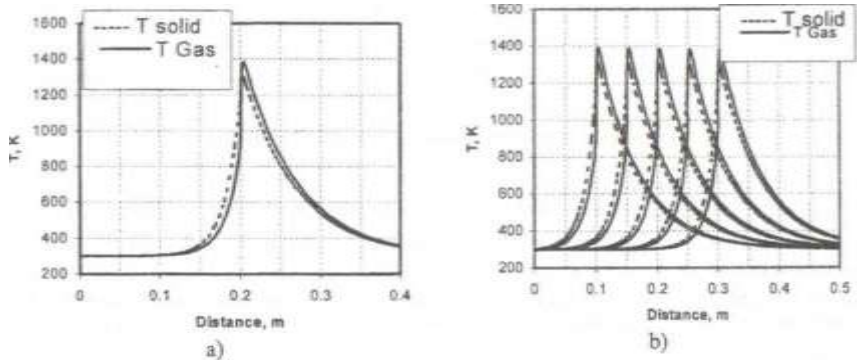


Fig. 3. a) Temperature profiles of the two-temperature analytical solution: $cp=4.88$, $u_g=0.43$ m/s, $T_{ig}=1150$ K, $U_{fc}=1.5E-04$ m/s. b) Temperature profiles of the two-temperature numerical solution: $\phi=4.88$, $u_g=0.43$ m/s, $T_{ig}=1150$ K, time interval 5 min between adjacent peaks

With respect to the strongly nonlinear source terms in the governing equations, one must careful attention to dealing with these terms in the numerical computations; otherwise, numerical computation may lead to unreasonable results. In this work, the nonlinear terms in the energy and species equations were linearized by means of a development in series of Taylor. To invoke combustion of the fuel, the artificial ignition temperature calculated by means of the equation (16) and few centimeters in length was set in the solid phase of the first region for the first one or two time steps. In figures 3 and 4 the analytical solution obtained in this paper is compared to the numerical solution built in same paper. Many coincidences between the compared cases are observed in the figures. Apart from that, the maximum temperatures reached at the combustion front according to our solution are found within the maximum temperature values of the gas and solid in numerical solution.

Conclusions

The theoretical study of gas combustion in inert porous media concluded with the analytical construction of a series of simple algebraic formulas, which represents the methane mass fraction and temperature profiles in a semi-infinite inert porous media. Also, simple formulas were built, which allow the prediction of the combustion wave velocity in the system and the thickness of the reaction region. Six dimensionless parameters define heat and mass transport in mathematical model. The analytical solution satisfactorily coincides with numerical solution in finite difference of the complete model (1)-(14). In the study it is shown that the reaction region is not infinitely thin, as it is usually considered. It is developed an analytical formula, which predicts the thickness of combustion region. Consequently, the results of this research can be used in the analysis of combustion waves in porous media for technical applications.

Acknowledgments

The results reported herein were obtained during an investigation supported by the CONICYT-Chile, project FONDECYT 1010354 and by Academia Politecnica Aeronautica de FACH, Chile. Their support is gratefully acknowledged.

References

1. Dobrego K.V., Zhdanok S.A., Khanevich E.I., *Analytical and experimental investigation of the transition from low - velocity to high - velocity regime of filtration combustion*, Experimental Thermal and Fluid Science, Vol. 21, PP.9-16, (2000).
2. Frank-Kamenetzki D.A., *Diffusion and heat transfer in chemical kinetic. (In Russian)*, Nauka, Moscow, (1987).
3. Foutko S.I., Shabunya S.I., Zhdanok S.A., Kennedy L.A., *Superadiabatic combustion wave in a diluted methane - air mixture under filtration in a packed bed*. Proceeding of Twenty - Sixth Symposium (International) on Combustion // The Combustion Institute, Naply, Vol.2, PP. 1556 - 1565 (1996).

PROPERTIES OF FILTRATION COMBUSTION WAVES OF RICH AIR-METHANE MIXTURES

YU.M. DMITRENKO, R.A. KLEVAN, V.G. MINKINA, S.A. ZDANOK A.V. Luikov Heat and Mass Transfer Institute of NAS of Belarus

Introduction

A need for compact and efficient hydrogen production technologies for fuel cell power plants stimulates studies in hydrocarbon reforming. Natural gas or methane is attractive primary fuel of choice for fuel cells [1]. Among currently available methods of converting natural gas into hydrogen are catalytic or non-catalytic steam reforming, pyrolysis and partial oxidation. In the case of partial oxidation of methane the main conversion products are hydrogen, carbon monoxide, carbon dioxide, methane and water:



The product composition is strongly dependent on process conditions, the temperature being the first. Though the process of partial methane oxidation is exothermic, the thermal effect of reaction is insufficient for self-sustained non-catalytic process. In large-scale industrial plants external heating of reaction zone up to 1500°C is used. The main drawbacks of existing industrial technologies for partial oxidation are intensive soot formation and low conversion efficiency. Recent studies [2-7] demonstrate, that filtration combustion wave propagating in inert porous media can provide reasonably high conversion of gas fuel into hydrogen without external heating and soot formation. In this approach the so-called "super adiabatic effect" of filtration combustion wave is used. This property is due to the internally self-organized process of heat recuperation between incoming fuel gas mixture and solid porous media.

Our previous studies [3-5] of methane to hydrogen conversion were made only for a fixed equivalence ratio of fuel mixture $\gamma=4$. It was found that at fixed γ the maximal wave temperature increases with specific flow rate of air-methane mixture g (g is a flow rate per unit of cross section area). Maximal wave temperature strongly effects on methane conversion efficiency. Unfortunately, the rate of temperature growth gradually drops as g increases. In our earlier experiments maximal temperature was about 1350 °C. Further temperature increase can be achieved by lowering of equivalence ratio.

The main goal of present study is to extend the range of equivalence ratio and specific flow rate to explore optimal operating mode for methane to hydrogen conversion by its partial oxidation in filtration combustion wave propagating in inert porous media. Another goal is to improve the model of numerical simulation of combustion wave using experimental data. Now we have enough evidence to suspect that well known kinetic patterns of A.Konnov, GRI, Miller-Bowman, Frenklach, Wamatz are not quite adequate in the case of partial oxidation. It was demonstrated by our earlier experiments were a considerable discrepancy of experimental and predicted data both on maximum temperature, and on conversion products composition was found. One of the probable reasons of this discrepancy is effect of heterogeneous reactions on a surface of packed bed particles.

Experimental setup

The experimental setup consists of porous media combustion reactor, reactor preheat unit, gas flow rate control equipment, temperature measurement system, gas chromatograph and data acquisition systems. A scheme of experimental setup is shown in Fig.1.

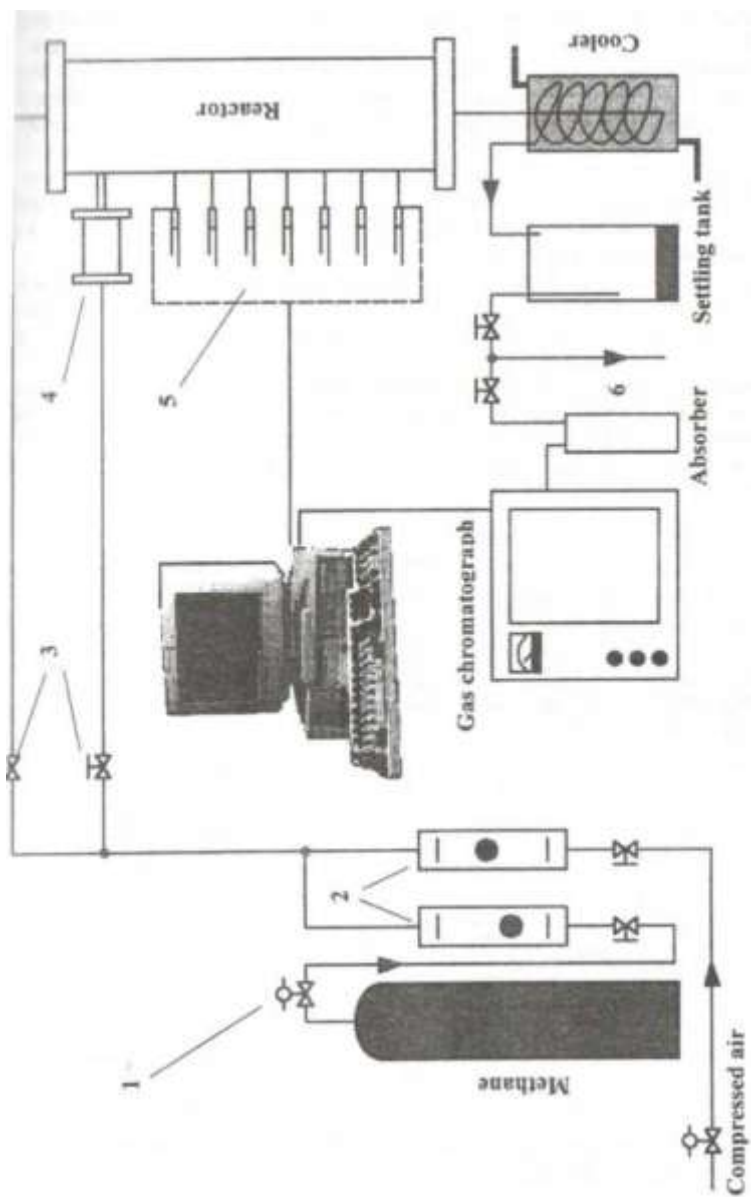


Fig.1. Experimental setup: 1 - reducer, 2 - flow controllers, 3 - flow controllers, 4 - reactor, 5 - gas chromatograph, 6 - exhaust

The reactor case is a flanged stainless steel tube with 140 mm outer diameter and 6- mm wall thickness. The reaction zone is filled with randomly packed bed of 5-6 mm alumina spheres. The space around packed bed is filled with pressed Kaowool insulation. Gas filtration through insulation layer is negligible due to its extremely low permeability. Preheat burner is used to preheat the porous medium prior to start the combustion of air-methane mixture. The unit is a small porous media burner using methane/air mixture as a fuel and ignited by a spark plug.

The air is taken from the high-pressure line, while methane was taken from the standard 50-liter high-pressure cylinder. Flow rates of fuel components are controlled by needle valves and measured by mass flow controllers. Laboratory ventilation system is used to remove the exhaust gas out of the room.

The axial temperature distribution in the porous medium reactor is measured with an array of six S-type (Pt-10%Rh/ Pt) thermocouples in ceramic shell with exposed junction. A PC based data acquisition system was employed to read and record the temperatures at regular intervals.

Chemical composition of reaction products was measured using modified Chrom-4 Gas Chromatograph. Digital signal processing was performed with A/D Converter based on Analog Devices AD7289 chip. The best component separation were achieved with two 3m long 1/8” in diameter columns filled with molecular sieve CaA and Poropack Q. Argon was used carrier gas.

Results

Present study show that efficiency of methane to hydrogen conversion in superadiabatic combustion wave is directly related with maximal reactor temperature. This temperature is a function of specific flow rate g and equivalence ratio γ and is given in Fig. 2. For all values of γ a tendency of T_{ra} growth with g is clearly seen, especially for $g < 0.6$. This tendency completely agrees with our previous experimental and numerical simulation results for $\gamma = 4$ [3].

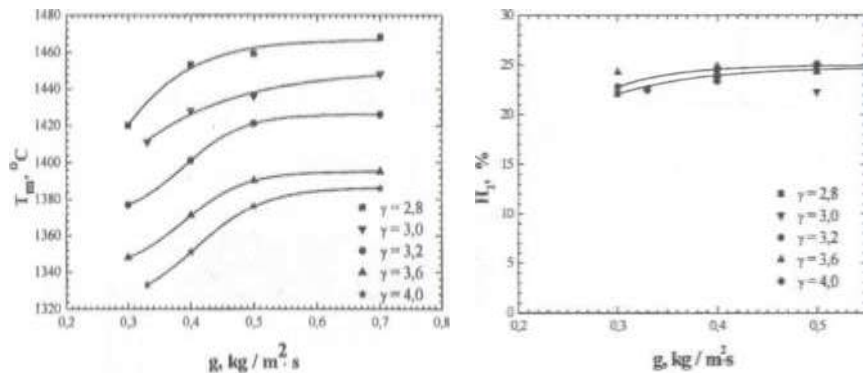


Fig. 2. The effect of equivalence ratio and mass flow rate on maximal temperature

Output concentrations of hydrogen also increases with g as shown in Fig. 3. However, this growth is insignificant. The most sensitive parameters of conversion efficiency are concentration of residual methane in reaction products and methane-to-hydrogen conversion

where C_{H_2} and C_{CH_4} - hydrogen and nitrogen output concentrations,

C_{N_2} and C_{CH_4} - nitrogen and methane input concentrations. These parameters are given in Fig. 4 and 5 respectively. As maximal reactor temperature increases, residual methane concentration while methane-to-hydrogen conversion ratio increases.

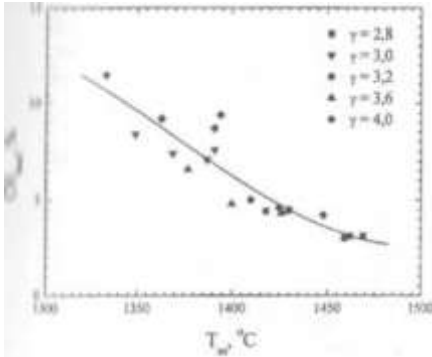


Fig. 4. CH₄ concentration in products

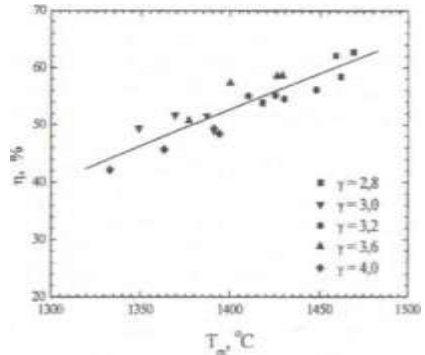


Fig. 5. CH₄ to H₂ conversion efficiency

Conclusion

Partial oxidation of methane can be performed in filtration combustion wave propagating in inert porous medium. The most efficient conversion process seems to be for $\gamma=2.8 - 3$. The maximal methane to hydrogen conversion efficiency is about 63%. No evidence of soot formation was observed. This is one of the most attractive features of the process.

References

1. Dicks A.L. *Journal of Power resources*. 1996, Vol.61.
2. Drayton M.K., Saveliev A.V., Kennedy L.A., Fridman A.A., Li Y. *Twenty-Seventh Symposium on Combustion, The Combustion Institute*. 1998, pp. 1361-1367.
3. Dmitrenko Yu.M., Gavriluk V.V., Minkina V.G., Shabunya S.I., Zhdanok S.A. *Proc. of IV Int. School-Seminar "Non Equilibrium Processes and their Applications"*. Minsk, HMTI. 1998, pp.170-173.
4. Gavriluk V.V., Dmitrenko Yu.M., Zdanok S.A., Minkina V.G., Shabunya S.I., Yadrevskaya N.L., Yakimovich A.D. *Theoretical fundamentals of chemical technology (in Russian)*. 2001, Vol.35, N6, pp.627-635.
5. Gavriluk V.V., Dmitrenko Yu.M., Zdanok S.A., Minkina V.G., Shabunya S.I., Yadrevskaya N.L., Yakimovich A.D. *Proc. of IV Int. Forum on Heat and Mass Transfer MIF-2000*. Minsk, HMTI. 2000, Vol.4. pp.21-31.
6. Kennedy L.A., Bingué J.P., Saveliev A.V., Fridman A.A., Foutko S. *Proceedings of Combustion Institute*. 2000, Vol.28. pp.1431-1438.
7. Bingué J.P., Saveliev A.V., Fridman A. A., Kennedy L.A. *International Journal of Hydrogen Energy*. 2002, Vol.27, pp.643-649.

NUMERICAL MODELING OF DETONATION PROCESSES IN HYDROGEN-AIR MIXTURES

V.YU. GIDASPOV, I.E. IVANOV, I.A. KRYUKOV, V.YU. STRELTSOV

Moscow aviation institute (State technical university)

Study of burning waves and detonation distribution in reacting media is of significant interest from the point of view of explosion safety for industrial buildings, experimental installations, starting complexes, etc. Inflammable mixture, and in particular hydrogen-air, can appear as a result of hydrogen leak in reactor chamber of the atomic power station, in the rocket and aviation engines using hydrogen as fuel and many other cases.

In the paper three problems are considered:

- study of unsteady reacting flows of hydrogen-oxygen gas mixture in a nozzle - limited supersonic jet - Hartman resonator configuration;
- numerical simulation of interaction of gas dynamic structures formed by spherical explosion in reacting gas mixtures with a conic cavity;
- investigation of dispersed water droplets effect on ignition and detonation of hydrogen- air mixture.

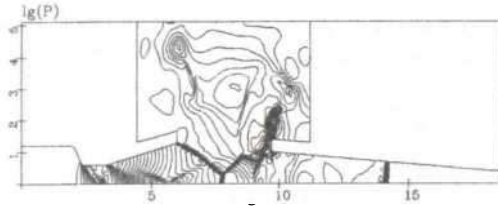
As mathematical model system of Euler equations for chemically reacting gas mixture is used (for the first two problems - 2D non-steady gas dynamics equations, for the third one

- ID non-steady equations). In order to close the corresponding system of equations, the submodels of thermodynamics and gaseous chemical kinetics are used. For the case of two- phase flows the submodels of droplet drag and heat and mass transfer [1,2] are used in addition. Corresponding initial and boundary conditions are used as well [3-5].

2D non-steady Euler's equations were solved with the help of quasimonotonic Godunov's conservative high order scheme [4]. For ID non-stationary equations solution the grid method of characteristic with obvious allocation of strong and weak discontinuities was used [1]. The equations of chemical kinetics and droplet drag and heat and mass transfer were solved with the aid of original numerical method specially developed for the solution of rigid systems [3].

For modeling chemical transformations of gaseous components, the detailed kinetic mechanism describing burning of hydrogen in air was used, which consisted of 19 reversible reactions and included 9 components [6].

In Fig. 1, 2, the calculation results of reacting gas flow in a system "nozzle - limited supersonic jet - Hartman resonator" (Fig. 1) are presented. Calculation began from a "nozzle start", as a result of which a shock wave was formed moving along an axis to the open end of resonator and further along the resonator up to a close end. The reflected from a close end shock wave moves through an open end and leaves resonator, thus forming an underpressure wave. Periodic movement of shock waves and underpressure waves along a resonator path defines an oscillatory mode of flow in a system "nozzle - Hartman resonator" that is accompanied under some conditions by heating of an inactive gas layer near a close end. In Fig. 2, one can see the readings of a temperature numerical gauge located in the middle of a resonator close end, for two cases: without chemical reactions and for nonequilibrium process.



In the assumption that no chemical reactions occur, the mixture composition remains constant, and averaged by the period temperature in resonator quickly grows, reaching values higher than 1700 K. Then “a heat failure” occurs [2] and an average temperature stabilizes (Fig. 2a). If chemical reactions occur in a gas mixture, heating gas behind a front of the reflected from a close end of the resonator shock wave up to the temperature of hydrogen- oxygen mixture ignition yields to the ignition of this mixtures (Fig. 2b).

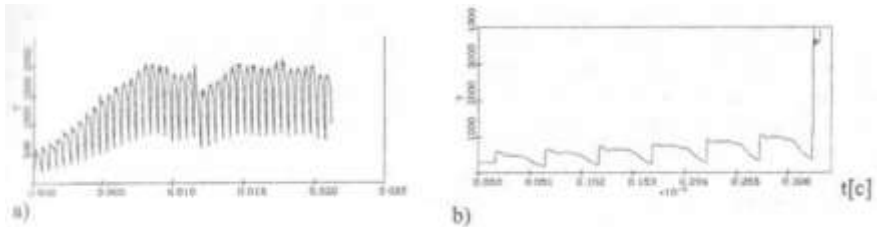


Fig. 2. Time dependence of gas temperature at a close end of the resonator
 a) Flow without taking into account chemical transformations, b) nonequilibrium flow

Fig. 3 shows the initial distribution of spherical explosions in the hydrogen-oxygen mixture. Shock wave structure of the flow at some time instant to consists of a head shock wave (SW Fig. 3), the secondary, reflected from the coordinate center, shock wave (SW2), the contact discontinuity separating gaseous combustion products of solid explosive from products of combustion of hydrogen-oxygen mixture (CD), and the front of burning, which divides an area of high-temperature combustion products from an area of non-reacted hydrogen-oxygen mixture (FB). Inside the area it is placed a slightly truncated hollow cone equipped with pressure gauges P1, P2, P3, P4, P5, P6.

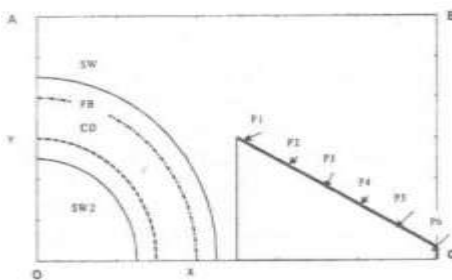


Fig. 3

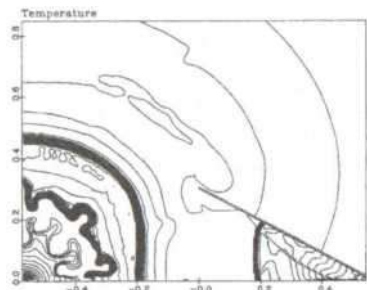


Fig. 4

Fig. 4 shows temperature isolines corresponding to the time instant when the head shock wave has reflected from a close end of a tube, and the wave of burning is near to an inlet of conic cavity.

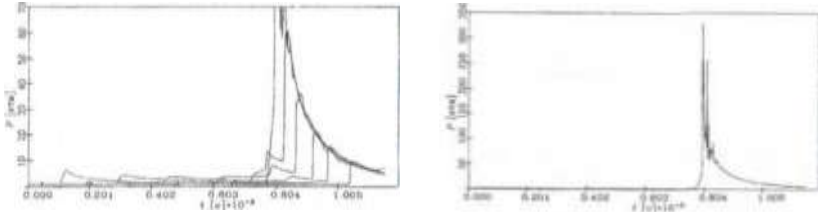


Fig. 5

In Fig. 5, time readings of numerical pressure gauges in points P1, P2, P3, P4, P5 (a) and in top of the cone P6 (b) are presented.

Fig. 6 represents the time development of flow, which arises after an arrival of shock wave to the boundary of air - a hydrogen-air mixture with the sprayed droplets of water, p. (0,0). Dependence of gas mixture ignition on a mass fraction of water particles and initial diameter of droplets has been studied. Various modes of flow have been found: formation of non-fading wave of burning; suppression of a wave of burning; non-formation of a wave of burning. Fig. 7 represents the influence of a mass fraction and diameter of water droplets on a wave of burning formation. An ordinates axis presents time delay of ignition (the moment of drastic temperature growth near to the contact break).

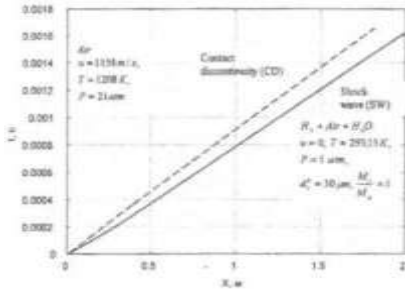


Fig. 6

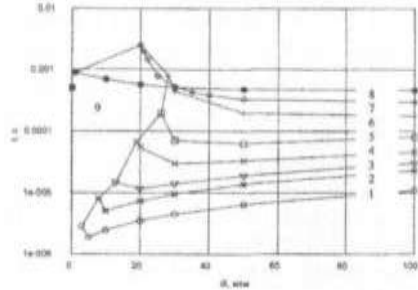


Fig. 7

Lines with different markers correspond to a various initial mass fraction of water in a gas mixture (1-0.005, 2- 0.01, 3 - 0.1, 4 - 0.2, 5- 0.3, 6- 0.4, 7- 0.5, 8- 1.0). At a mass fraction of droplets within 1.0 to 0.005, there was a limiting value of particles (the last left marker) at which ignition took place. At a mass fraction of injected particles within 1.0 to 0.2, time delay of ignition was less than in case of a pure gas (designated as 9). The effect is connected with local temperature rise near a contact break because of velocity difference of gas and of particles behind a shock wave. It should be noted that questions of steady burning wave formation after ignition were not considered within the given study.

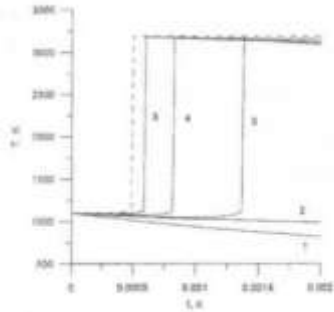


Fig. 8

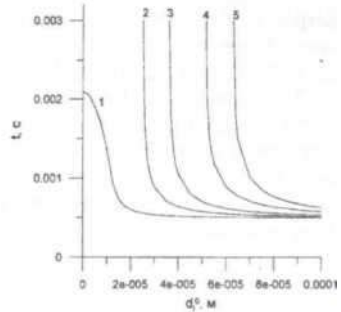


Fig. 9

In order to eliminate the influence of high-speed backlog of particles on ignition, the study of ignition in a bomb of constant volume has been performed. Fig. 8 contains gas temperature dependences on time in a bomb of constant volume at various initial water droplets diameters (1 - 40 μm , 2-57 μm , 3 - 60 μm , 4-70 μm , 5-100 μm). The weight of injected water was $M_l/M_g = 0.5$, initial gas pressure in stoichiometric hydrogen-air mixture was equal to 1.8 MPa. The dashed line corresponds to ignition of a gas mixture without water droplets. At injection of droplets of less than 57 μm in diameter ignition does not occur.

In Fig. 9, dependences of time delay of ignition on initial diameter of water droplets in a mixture are represented for various fractions of injection M_l/M_g (1 - 0.02, 2 - 0.1, 3 - 0.2, 4 - 0.4, 5 - 0.6).

Comparison of calculation results shows that ignition in the two considered statements proceeds differently in quality. In a shock tube, with presence of water droplets the delay in ignition decreases in comparison to a case of pure gas mixture, (Fig. 7), and in a bomb of constant volume - grows (Fig. 9). Thus, numerical modeling shows that water spraying in hydrogen-air mixtures can result both in suppression of ignition and detonation, and to acceleration of ignition. The important role is played by a mass fraction of injected water and initial diameter of droplets.

This study was supported by grant of Russian Foundation for Basic Research (№ 03 - 01-00866).

References

1. Volkov V.A., Gidaspov V.Yu. *Numerical simulation of initiating detonation with the help of strong shock waves* // Proc. of the 2nd Japan-Soviet Union joint symposium on computational fluid dynamics.- Tsucuba: University of Tsucuba, 1991, Vol. 2, pp. 80-88.
2. Volkov V.A., Gidaspov V.Yu., Pirumov U.G., Streltsov V.Yu. *Numerical Simulation o Flows of Reacting Gas-Droplet and Gas Mixtures in Methanol Ignition Experiments* // High Temperature, Vol. 36, № 3. 1998, pp. 401-411.
3. Volkov V.A., Musin V.R., Pirumov U.G., Prohorov M.B., Streltsov V.Yu. *Numerical Modeling of Carbon Monoxide Neutralization by Metered Water Indaction into a High- Temperature Mixture of Combustion Products* // Translated from Proceedings of the Russian Academy of Sciences, Mechanics of liquid and gas, № 6. pp. 96-106, November- December, 1993.

1. Gidasov V.Yu., Ivanov I.E., Krukov I.A. Streltsov V.Yu. *Investigation of nonstationary nonequilibrium processes in acoustic Gartman resonator* Mathematical modeling (In Russian) 2003. Vol.15, № 6, pp.41-47.
2. Dohi T., Hayashi A.K., Ogawa S. *Numerical simulations of layered detonation using a detailed hydrogen chemistry // 21st International Symposium on Shock Waves*, Great Keppel Island, Australia, July 20-25, 1997. Paper 2660.
3. Ivanov I.E., Krukov I.A. *High precision quasimonotonous method for calculation of internal and jet flows of nonviscous gas* Mathematical modeling (In Russian). 1996, Vol. 8, № 6, pp.47-55.

SPECTROSCOPY OF PROPANE-BUTANE/AIR FLAMES

G. GRIGORIAN¹, A. CENIAN², M. SAWCZAK², G. SLIWINSKI²

¹ VA.Fock Institute of Physics, St.Petersburg University, St.Petersburg, 198504, Russia

²The Szwedzki Institute of Fluid-flow Machinery., Polish Academy of Sciences,
80-952 Gdansk, Fiszerska 14; Poland, cenian@imp.gda.pl

Introduction

The physical and chemical processes in hydrocarbon flames have been extensively studied during the last century. However, several aspects of these investigations are still far from being clarified, particularly the mechanisms leading to the appearance of various charge particles in a flame front. The adequate description of the combustion chemistry can be very complicated, due to the fact that the concentrations of species formed in a flame depend on numerous processes, which mechanisms are often not known in all details, even more so, when non-stationary (and non-equilibrium) flame-fronts are considered. Therefore, a monitoring of relative concentrations of stable and transient species formed in a flame front may improve our understanding of combustion chemistry. Furthermore, the high concentrations of excited particles in a flame front may give raise to effective chemi- ionization. Therefore, a new data on the excited species concentrations can improve our understanding of ionization mechanisms in various flames.

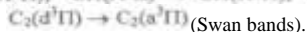
The main objective of our work was to investigate LPG/air flames using emission spectroscopy. The LPG gas consisting of propane-butane (-50:50) mixture is more and more popular used in EU as a fuel for internal combustion engines. The goal of the study was to obtain more information about the energy distributions of various molecules and atomic species. First of all we wanted to establish, to what extent the electronic excitation of species in LPG flame might be ascribed to non-thermal excitation processes and how this excitation depends on the experimental conditions. This paper presents preliminary results of a qualitative and quantitative analysis of the excited species. The vibrational and rotational temperatures of molecular species were determined from an analysis of band spectra intensities. The rotational temperatures were derived by comparing measured and simulated molecular spectra.

Description of the experimental conditions

A scheme of the experimental setup is shown in Fig.1. Emission spectra of flame were observed in the wide spectral range between 260 and 1000 nm. The LPG/air stoichiometric mixture was combusted in a simple Bunsen type burner in open air. The flame was positioned vertically in front of the entrance slit of the scanning spectrometer.

In order to discern the processes taking place along the flame "symmetry axis" a simple optical system consisting a lens ($f = 5$ cm) and an iris with the 2 mm hole was applied. The spectra were recorded at three different positions: (i) the lowest one at $L = 0.5$ cm above the burner exit, (ii) the middle one at $L = 1$ cm above the exit and (iii) the upper position at $L = 1.5$ cm above the exit.

Investigations confirmed that the emission spectra of LPG-air flames consist of a large number of molecular bands and several atomic lines. The highest intensities were observed for the bands of electronically excited molecules CH, OH, and C₂, corresponding to the transitions:



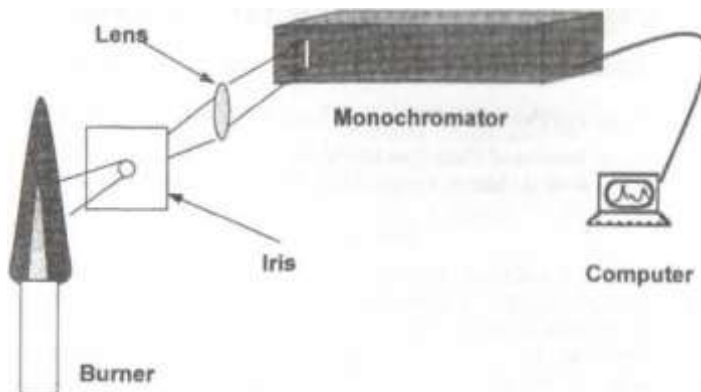


Fig. 1. Scheme of the experimental set-up

Results and discussion

The excitation energies of the respective excited states are as follows: $E[\text{OH}(A^2\Sigma)] = 5.2 \text{ eV}$, $E[\text{CH}(A^2\Delta)] = 3.8 \text{ eV}$, $E[\text{CH}(B^2\Sigma)] = 4.6 \text{ eV}$, $E[\text{C}_2(d^3\Pi)] = 2.6 \text{ eV}$. Besides the molecular bands, the atomic lines of excited oxygen and hydrogen were detected. The observed hydrogen lines (H_{α} , $\lambda=656 \text{ nm}$, H_{β} , $\lambda=486 \text{ nm}$, H_{γ} , $\lambda=434 \text{ nm}$) corresponds to the emission from the excited electronic states with energy of 12.09, 12.75 and 13.05 eV, respectively. The intensities of these lines were very low in the whole examined range of fuel content in the flame. Contrary, the intensities of oxygen lines were quite high. The spectral lines $\text{O}(3p^3P) \rightarrow \text{O}(3s^2S_1)$, $\lambda=777 \text{ nm}$, $\text{O}(3p^3P) \rightarrow \text{O}(3s^2S_1)$, $\lambda=844 \text{ nm}$ and $\text{O}(5d^3D^0) \rightarrow \text{O}(3p^3P)$, $\lambda=844 \text{ nm}$ originates from electronic states with $E = 10.74, 10.99$ and 13.07 eV , respectively. Large concentrations of highly excited species evidently point out to an existence of non-thermal mechanisms of their formation, most probably related to the excitation in various chemical reactions. Besides electronically excited species discussed above, we detected also significant concentrations of vibrationally excited hydroxyl molecules $\text{OH}(v)$.

The (0-0) Swan band of the C_2 molecule (centered around 515 nm) was used to estimate the rotational temperature. The registered band had a quite high resolution of the rotational lines. By comparing the experimental band profile with the simulated spectrum, the rotational temperature, $T_R(\text{C}_2(d^3\Pi)) = 2500 \pm 200 \text{ K}$, was determined. When mixture with a lower content of air was used, $T_R(\text{C}_2(d^3\Pi)) = 2200 \pm 300 \text{ K}$.

The emission of the 0-0 and 1-0 sequences of the $\text{C}_2(d^3\Pi) \rightarrow (\text{C}_2(a^1\Pi)$ transition (centered around 515 and 470 nm) were used for an estimation of the effective $\text{C}_2(d^3\Pi)$ vibrational temperature. The emission spectrum of the 0-1 sequence (around 560 nm) were taken to allow an independent estimation of the vibrational excitation. The temperatures were measured in the central part of the flame contour, $L = 0.5$ and 1 cm above the burner exit - see the Table 1. The determined values of the rotational and vibrational temperatures for the $\text{C}_2(d^3\Pi)$ excited state point out again to the non-thermal character of its excitation in the studied flame.

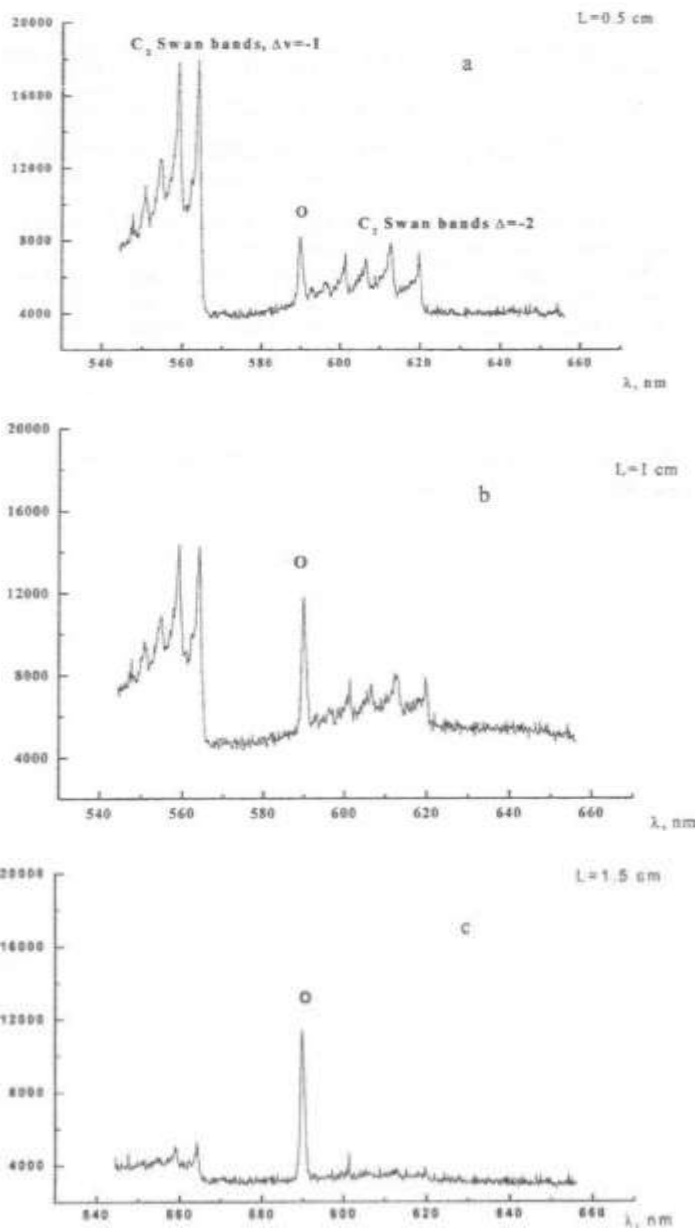


Fig. 2. Intensity of oxygen line and C₂ molecule bands in different regions of flame

Table 1

L. [cm]	$T_{10}^{(00)}$ [K]	$T_{10}^{(01)}$ [K]	$T_{10}^{(10)}$ [K]	$T_{21}^{(01)}$ [K]	$T_{21}^{(10)}$ [K]
0.5	8500±500	9300±500	9100±500	11000±700	10500±700
1	8000±500	9000±500	9300±500	12000±700	11500±700

Fig. 2 shows the intensity of C₂ Swan bands and $O(3p^1P \rightarrow 3d^1D)$ spectral line measured at three different positions above the burner exit, L = 0.5, 1 and 1.5 cm. One may see that the concentration of C₂(d³IT) molecules sharply decreases but concentration of O(3p³P) atoms markedly increases as the distance from the burner exit increases. The similar increase was registered for the concentrations of the O(3s³S°) atoms and the OH(v) molecules.

Acknowledgments

We acknowledge a financial support from the 4T10B 01922 Project of Polish Committee for Scientific Researches.

A NONEQUILIBRIUM APPROACH FOR TURBULENCE MODELLING

I.I.KOVALEV

A.V. Luikov Heat and Mass Transfer Institute of NAS of Belarus,
15, P. Brovka Str, Minsk, 220072, Belarus

Turbulent flows are the subject of intensive investigations for more than hundred years. The reason is its numerous applications in fluids and gas dynamics, hydraulics, combustion, technical devices and technological processes. Literature on this subject is extensive and we'll not analyze here existing models of turbulence. Instead, the paper aimed at discussing of common- in-use turbulence concepts and presenting a new approach for turbulence modeling which seems to be promising. The presented results are only preliminary and further investigations in this direction are needed, of course.

The classic approach for description of turbulence movement is based as a rule on Navier-Stokes equations, moment description, similarity theory and dimensional analysis.

As usual one considers the developed turbulence to be characterized with irregular velocity variations in time at any point of space. All turbulent flow parameters are considered as fluctuating ones with the scale of fluctuations being varying from external scale, corresponding to characteristic flow size, to small scale where the viscous dissipation dominates.

The absence of the better model forces one to suppose that turbulent movement is described by the same governing equations (Navier-Stokes equations) as laminar. This means that turbulence originates as flow non-stability or, mathematically, as instability of Navier- Stokes model at large Reynolds numbers. This assumption results in a number of contradictions. Indeed, none turbulent solution of the Navier-Stokes equations known so far. Moreover we don't even know if such a solution exists at all. Also it is a common practice to suppose that Navier-Stokes model govern each realization of turbulent field in time and space. If Navier-Stokes equations govern particular realizations of turbulent field then they must interact each other but this interaction is not represented in the model.

The description of turbulence as averaged and fluctuating movement gave Reynolds [1] the reason to introduce the procedure of implicit splitting of velocity and pressure fields in Navier-Stokes model on averaged and fluctuating components with averaging on a time interval. Neither time averaging, introduced by Reynolds, nor averaging on mass of liquid volumes, introduced subsequently by Favre [2], leads to closed turbulence model. Moreover the classic Navier-Stokes equations are not written in actual turbulent values and the formal Reynolds' procedure therefore is physically incorrect [3, 4]. The laws of physics and fluid mechanics don't describe directly turbulent flows without imposing additional hypothesis.

Most essential results in turbulence were obtained by Prandtl and Karman who studied experimental data of Nikuradse. Last experimental studies also contribute a lot to the development of turbulence theory. Today it's quite clear that turbulent flows differ from laminar ones by momentum and energy transfer due to molecular groups or clusters, rather than separate molecules. This is why the Prandtl's mean mixing path theory for molecular group l proved to be so fruitful instead of molecule free path X .

Thus, when constructing a turbulence theory one should proceed from the complicated movement of molecular groups in turbulent flows. In 1872 Boltzmann [5] developed kinetic gas theory for description of molecules movement and showed that Navier-Stokes equations can be obtained as a sequence from the theory. Prigogine in [6] showed that Navier-Stokes model corresponds to thermodynamics of weakly nonequilibrium processes. Therefore there

arc not reasons to use it for prediction of strongly nonequilibrium and nonhomogeneous turbulent flows.

In [4] the initial value problem for Boltzman's equation was studied and showed that the equation leads to Navier-Stokes model just with molecular viscosity rather than turbulent one. Also it was shown that at large Reynolds numbers role of molecular viscosity decreases and substantial non-homogeneities appear due to the presence of molecules groups. Therefore the classical kinetic gas theory with molecular viscosity corresponds to weakly nonequilibrium processes and can't describe turbulent flows.

In this paper for the sake of simplicity we only consider a flow of incompressible viscous fluid. In turbulence velocity fluctuations result in mass fluctuations at given space point. We postulate that continuity equation for turbulent flows reads:

$$\operatorname{div}(\vec{V}) = J \neq 0, \tag{1}$$

where J is a non-zero indefinite quantity to be calculated. Equation (1) is completed by the momentum equation:

$$\begin{aligned} \frac{\partial u}{\partial t} + \frac{\partial(uu)}{\partial x} + \frac{\partial(uv)}{\partial y} + \frac{\partial(vu)}{\partial z} &= -\frac{1}{\rho} \frac{\partial p}{\partial x} + \frac{1}{\rho} \frac{\partial}{\partial x} \left[\mu \left(2 \frac{\partial u}{\partial x} - \frac{2}{3} \operatorname{div} \vec{V} \right) \right] + \frac{1}{\rho} \frac{\partial}{\partial y} \left[\mu \left(\frac{\partial u}{\partial y} + \frac{\partial v}{\partial x} \right) \right] + \frac{1}{\rho} \frac{\partial}{\partial z} \left[\mu \left(\frac{\partial w}{\partial z} + \frac{\partial u}{\partial z} \right) \right], \\ \frac{\partial v}{\partial t} + \frac{\partial(vu)}{\partial x} + \frac{\partial(vv)}{\partial y} + \frac{\partial(vw)}{\partial z} &= -\frac{1}{\rho} \frac{\partial p}{\partial y} + \frac{1}{\rho} \frac{\partial}{\partial x} \left[\mu \left(\frac{\partial u}{\partial y} + \frac{\partial v}{\partial x} \right) \right] + \frac{1}{\rho} \frac{\partial}{\partial y} \left[\mu \left(2 \frac{\partial v}{\partial y} - \frac{2}{3} \operatorname{div} \vec{V} \right) \right] + \frac{1}{\rho} \frac{\partial}{\partial z} \left[\mu \left(\frac{\partial v}{\partial z} + \frac{\partial v}{\partial y} \right) \right], \\ \frac{\partial w}{\partial t} + \frac{\partial(wu)}{\partial x} + \frac{\partial(wv)}{\partial y} + \frac{\partial(ww)}{\partial z} &= -\frac{1}{\rho} \frac{\partial p}{\partial z} + \frac{1}{\rho} \frac{\partial}{\partial x} \left[\mu \left(\frac{\partial w}{\partial z} + \frac{\partial u}{\partial z} \right) \right] + \frac{1}{\rho} \frac{\partial}{\partial y} \left[\mu \left(\frac{\partial v}{\partial z} + \frac{\partial v}{\partial y} \right) \right] + \frac{1}{\rho} \frac{\partial}{\partial z} \left[\mu \left(2 \frac{\partial w}{\partial z} - \frac{2}{3} \operatorname{div} \vec{V} \right) \right], \end{aligned} \tag{2}$$

where $\operatorname{div} \vec{V} \neq 0$ according to (1).

In order to determine J we expand the quantity $\operatorname{div} \vec{V} \neq 0$ into the time-spatial Taylor's series:

$$\operatorname{div} \vec{V} \Big|_{\tau=0} = \operatorname{div} \vec{V} \Big|_{\tau=0} - \tau \left(\frac{\partial}{\partial t} + u \frac{\partial}{\partial x} + v \frac{\partial}{\partial y} + w \frac{\partial}{\partial z} \right) \operatorname{div} \vec{V} + O(\tau^2), \tag{3}$$

where τ is the relaxation time, $f = \operatorname{div} \vec{V}$ and operator D/Dt is the substantial time derivative. According to adopted assumption we treat $\operatorname{div} \vec{V} = 0$ as corresponding to laminar flow state (equilibrium) and $\operatorname{div} \vec{V} = J$ corresponding to turbulent flow state (nonequilibrium) one:

To calculate quantity $\frac{\partial}{\partial x}(\dots), \frac{\partial}{\partial y}(\dots), \frac{\partial}{\partial z}(\dots)$ we apply the operators $\left(\frac{\partial}{\partial t} + u \frac{\partial}{\partial x} + v \frac{\partial}{\partial y} + w \frac{\partial}{\partial z} \right) \operatorname{div} \vec{V}$ to the first, second and third equations in (2) (supposing hereinafter $\mu = \text{const}$).

Then calculating (3) at $x=0$ with taking into account $\operatorname{div} \vec{V} \Big|_{\tau=0} = 0$ we finally obtain:

$$\operatorname{div} \vec{V} = \tau \left[\frac{1}{\rho} \left(\frac{\partial^2 p}{\partial x^2} + \frac{\partial^2 p}{\partial y^2} + \frac{\partial^2 p}{\partial z^2} \right) + \frac{\partial u}{\partial x} \frac{\partial u}{\partial x} + \frac{\partial v}{\partial y} \frac{\partial v}{\partial y} + \frac{\partial w}{\partial z} \frac{\partial w}{\partial z} + 2 \frac{\partial v}{\partial x} \frac{\partial u}{\partial y} + 2 \frac{\partial w}{\partial x} \frac{\partial u}{\partial z} + 2 \frac{\partial w}{\partial y} \frac{\partial v}{\partial z} \right]. \quad (4)$$

For practical use one should resolve equation (4) relatively pressure p in the form

$$\frac{1}{\rho} \left(\frac{\partial^2 p}{\partial x^2} + \frac{\partial^2 p}{\partial y^2} + \frac{\partial^2 p}{\partial z^2} \right) = \frac{1}{\tau} \operatorname{div} \vec{V} - \frac{\partial u}{\partial x} \frac{\partial u}{\partial x} - \frac{\partial v}{\partial y} \frac{\partial v}{\partial y} - \frac{\partial w}{\partial z} \frac{\partial w}{\partial z} - 2 \frac{\partial v}{\partial x} \frac{\partial u}{\partial y} - 2 \frac{\partial w}{\partial x} \frac{\partial u}{\partial z} - 2 \frac{\partial w}{\partial y} \frac{\partial v}{\partial z} \quad (5)$$

and rewrite (2) in the form

$$\begin{aligned} \frac{\partial u}{\partial t} + \frac{\partial(uu)}{\partial x} + \frac{\partial(uv)}{\partial y} + \frac{\partial(uw)}{\partial z} &= -\frac{1}{\rho} \frac{\partial p}{\partial x} + \nu \left[\left(\frac{\partial^2 u}{\partial x^2} + \frac{\partial^2 u}{\partial y^2} + \frac{\partial^2 u}{\partial z^2} \right) \right] + \frac{1}{3} \nu \frac{\partial}{\partial x} (\operatorname{div} \vec{V}), \\ \frac{\partial v}{\partial t} + \frac{\partial(vu)}{\partial x} + \frac{\partial(vv)}{\partial y} + \frac{\partial(vw)}{\partial z} &= -\frac{1}{\rho} \frac{\partial p}{\partial y} + \nu \left[\left(\frac{\partial^2 v}{\partial x^2} + \frac{\partial^2 v}{\partial y^2} + \frac{\partial^2 v}{\partial z^2} \right) \right] + \frac{1}{3} \nu \frac{\partial}{\partial y} (\operatorname{div} \vec{V}), \\ \frac{\partial w}{\partial t} + \frac{\partial(wu)}{\partial x} + \frac{\partial(wv)}{\partial y} + \frac{\partial(ww)}{\partial z} &= -\frac{1}{\rho} \frac{\partial p}{\partial z} + \nu \left[\left(\frac{\partial^2 w}{\partial x^2} + \frac{\partial^2 w}{\partial y^2} + \frac{\partial^2 w}{\partial z^2} \right) \right] + \frac{1}{3} \nu \frac{\partial}{\partial z} (\operatorname{div} \vec{V}). \end{aligned} \quad (6)$$

The parameter τ in (5) left undefined so far. To determine the value of τ one should obey the following requirements: on the one hand τ must be small enough to fulfill (3), on the other hand it must be a universal quantity, preferable constant.

We express dimensional time parameter τ through the nondimensional parameter τ^* as following, $\tau^* = \tau L_0^{-2} V_0$, where L_0 and V_0 are some characteristic length and velocity scales used to bring the governing equations to the nondimensional form. For the further discourse it is convenient to associate the turbulent relaxation time τ to a turbulence scale l . Note, that the nondimensional product τv is a square of length. Then we introduce a turbulence length scale l , $l^2 = \tau v$ and rewrite τ^* as

$$\tau^* = l^2 L_0^{-2} Re, \quad (7)$$

where $Re = V_0 L_0 / \nu$ and the scale l is unknown in advance. To determine the value of l we refer to the [7]. Universal turbulence spectrum (hence, the length scale structure) is observed only at large wave numbers corresponding to the Kolmogorov dissipative microscale of length $\eta = (\nu/\epsilon)^{1/4}$, where ϵ is the dissipation rate per unit mass ($m^2 \text{sec}^{-3}$). Therefore we choose l/L_0 as $\eta/L_0 \sim Re^{-3/4}$ [8] we can rewrite (7) as follows

$$\tau^* = l^2 L_0^{-2} Re = (\eta/L_0)^2 Re = (Re)^{-6/4} Re = Re^{-1/2}. \quad (8)$$

Equations (7)-(9) constitute the closed mathematical model for predicting of both laminar and turbulent flows. When utilizing (5)-(8) one should replace $\nu \rightarrow 1/Re$, $\tau \rightarrow \alpha/Re^{1/2}$, where α must be adjusted from comparison with available experimental data.

We apply the model above for the solution of the 2D lid-driven cavity problem. Driven cavity problem is widely used as a benchmark for comparison of numerical codes. The agreement between different codes is within 1% or better. Published 2D Navier-Stokes solutions can qualitatively describe the flow structure, the number and location of vortexes and their size, but show poor agreement with the experimentally measured velocity profiles by Koseff and Street for $Re = 3200$ and $Re = 10^4$ [9]. Results obtained by Ghia et al. [10] on a fine mesh (256x256) for Reynolds number up to $Re = 10^4$ are only the stationary solutions while the actual fluid flow is essentially transient. A 3D Navier-Stokes solution still can not

improve this discrepancy, and known 3D results differ significantly [11], One may suppose that the flow turbulence is a reason for a disagreement.

We solved the lid-driven problem by transient method using the equations (7), (8), (10). We perform calculations of the problem for different Reynolds numbers. At low Reynolds numbers (≤ 1000) solutions obtained differ insignificantly from those obtained with the Navier-Stokes model. Results of calculations for $Re=3200$ and $Re=10000$ are presented in Fig. 1-4.

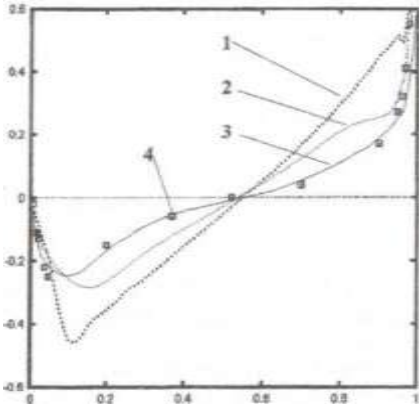


Fig. 1. Variation of U along vertical centerline of the cavity at $Re=3200$: 1 - Navier-Stokes model, 2 - $k-\epsilon$ model, 3 - present model, 4 - experiment [9]

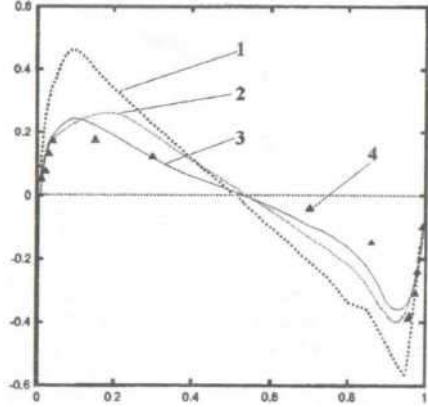


Fig. 2. Variation of V along horizontal centerline of the cavity at $Re=3200$: 1 - Navier-Stokes model, 2 - $k-\epsilon$ model, 3 - present model, 4 - experiment [9]

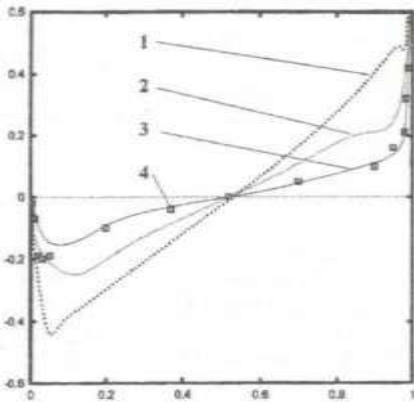


Fig. 3. Variation of U along vertical centerline of the cavity at $Re=10000$: 1 - Navier-Stokes model, 2 - $k-\epsilon$ model, 3 - present model, 4 - experiment [9]

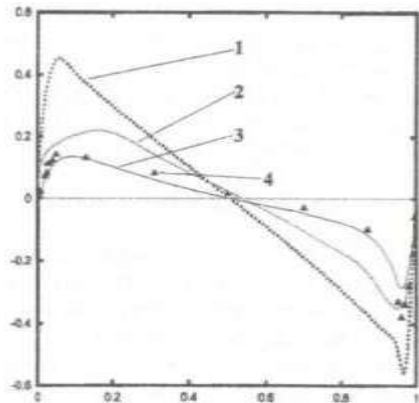


Fig. 4. Variation of V along horizontal centerline of the cavity at $Re=10000$: 1 - Navier-Stokes model, 2 - $k-\epsilon$ model, 3 - present model, 4 - experiment [9]

We used 100x100 grid for numerical calculations. The equations (7), (8), (10) were solved by finite-differences implicit method of the first order in time and the second order in space. The value for τ^* was chosen as $\tau^* = 0.2 \text{Re}^{-1/2}$

Nomenclature

p - density, $\text{Re}\lambda$ - turbulent Reynolds number, μ - dynamic viscosity, ν - kinematic viscosity. Subscripts: *eq* - equilibrium.

References

1. Reynolds O. *Philos. Trans. R. Soc.* 176, 123 (1894).
2. Favre A.I. *Studies in turbulence*, 324 (1992).
3. Alekseev B.V. *Physical principles of the generalized Boltzman kinetic theory* (in Russian), Successes of physical sciences, Vol. 170, N. 6, 649-679 (2000).
4. Struminskii V.V. *Kinetic theory of turbulent flows* (in Russian), Problems of turbulent flows, 14-32 (1987)
5. Boltzmann L. *Sitzungsber. Kaiser. Akad. Wiss.* 66 (2), 275 (1872)
6. Prigogine I. *Le domaine de validite del shermodynamique des phenomenes irreversibles*, Physica, XV, No1, 272-284 (1949).
7. Belotserkovskii O.M., Oparin A.M. *Numerical experiment on the turbulence: from order to chaos* (in Russian), (2000)
8. Tennekes H., J.L. Lumley *A first course in turbulence*, (1972)
9. Koseff K.R., Street R.L.. *The Lid-Driven Cavity Flow: A Synthesis of Qualitative and Quantitative Observations*, Trans. ASME/Journal of Fluids Engineering, 106, 390-398 (1984)
10. Ghia U., Ghia K.N., Shin C. T.. *Solution of Incompressible Navier-Stokes Equations by Strongly Implicit Multi-Grid Method*, J. Comp. Phys., 48, 387 (1982).
11. Deville M., Le T.-H., Morchois Yv. (Editors), *Numerical Simulation of 3-D Incompressible Unsteady Laminar Flows*, A GAMM Workshop, Notes on Numerical Fluid Mechanics, 36, (1992).

SIMULATION OF HETEROGENEOUS CHEMICAL PROCESSES UNDER COAL
GASIFICATION USING GENERALIZED VOLUME-AVERAGED MODEL OF FILTRATION COMBUSTION

K.V. DOBREGO, I.A. KOZNACHEEV

A.V. Luikov Heat and Mass Transfer Institute of NAS of Belarus P. Brovka Street 15, Minsk 220072,
Belarus, e-mail: kdob@itmo.by

Gasification problem is actual for Belarus and many other countries. It is related to utilization of a city and industrial wastes as well as low quality brown coals. State policy in this area stipulates rise of wastes conversion level by inculcation of new conversion technologies. One of the technologies capable to reduce conversion expenses and increase conversion quality is gasification - thermochemical conversion of solid fuels to gaseous fuels. Gasification allows both wastes and specific fuels (biomass, peat, black oil, wood) processing. Since oil and natural gas resources deteriorate, significance of alternative fuels utilization will grow. Besides coals gasification may be performed at the place of extraction or even at the underground site (*in situ*). Concept of thermochemical coal conversion *in situ*, called underground coal gasification, was proposed in the work of D.I. Mendeleev (1888). This process may be cost effective for Belarus taking into account that belarussian resources of coal consist mainly of low-quality brown coals, direct extraction of which is disadvantageous both from economical and ecological points of view.

In present work coal gasification process was investigated with numerical methods. Generalized volume-averaged model of filtration combustion was used. The special attention was paid to heterogeneous chemical reactions taking place under gasification process.

Mathematical model

Mathematical formulation of generalized volume-averaged model is based on consideration and consistent averaging of acting forces, mass, energy, species and momentum flows. For simplification of mathematical formulation it was suggested that there is only one chemically active solid phase component. Equations of the model in case of sufficiently general consideration of heterogeneous chemistry (without chemical kinetics specification) look as follows:

$$\frac{\partial(\varepsilon\rho_g)}{\partial t} = -\bar{\nabla} \cdot (\varepsilon\rho_g \bar{u}) + \varepsilon \sum_i R_i, \text{ continuity equation,}$$

$$\rho_g \frac{\partial \bar{u}}{\partial t} = -\rho_g (\bar{u} \cdot \bar{\nabla}) \bar{u} - \bar{\nabla} p + \bar{j}_{visc}, \text{ motion equation,}$$

$$\varepsilon\rho_g \frac{\partial c_i}{\partial t} = -\varepsilon\rho_g \bar{u} \cdot \bar{\nabla} c_i - \bar{\nabla} \cdot (\varepsilon \bar{J}_i) + \varepsilon R_i, \text{ gas-phase species transport equation,}$$

$$\varepsilon\rho_g c_p \frac{\partial T_g}{\partial t} + \varepsilon\rho_g c_p \bar{u} \cdot \bar{\nabla} T_g = -\bar{\nabla} \cdot (\varepsilon \bar{J}_q) + \alpha (T_s - T_g) - \varepsilon \sum_i h_i R_i, \text{ heat conductivity equation in}$$

gas phase,

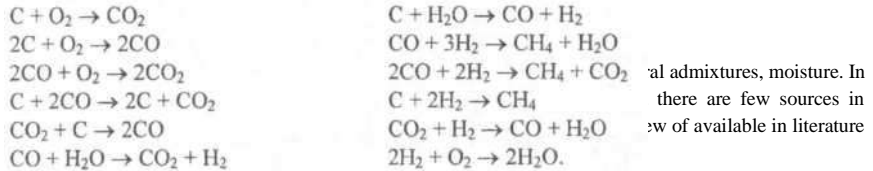
$$\rho_s \frac{\partial [(1-\varepsilon) E_s]}{\partial t} = \bar{\nabla} \cdot (\lambda \bar{\nabla} T_s) + \alpha (T_s - T_g), \text{ energy transport equation in solid phase,}$$

equation, solid phase mass balance

Direct averaging of acting viscous forces was not carried out, Dupuit-Forscheimer flow model as averaged force was used.

In these equations: ϵ - porosity, ρ_g - density of gaseous mixture, u - gaseous mixture mass-averaged velocity, R_i - formation rate of i -th gas mixture component, p - gas pressure, $f = -\frac{1}{k_0} u - \frac{1}{k_1} |u| u$ - averaged viscous friction force (Dupuit-Forscheimer mass

flow model), μ - viscosity coefficient, k_0, k_1 - Forscheimer's coefficients, c_i - mass fraction of i -th component, $J_i = -\rho_g D_i \nabla c_i$ - diffusive flow density of i -th component, D_i - tensor of diffusivity, c_p - specific heat capacity of gas mixture, T_g - gas phase temperature, $\vec{J}_q = -\Lambda \nabla T_g$ - heat flow density in gas phase, Λ - tensor of heat conductivity in gas phase, T_s - solid phase temperature, a - interfacial heat exchange coefficient, h_i - specific enthalpy of i -th gaseous mixture component, ρ_s - solid phase material density, E_s - specific intrinsic energy of solid phase, A - effective heat conductivity of solid phase.



Kinetic parameters of air gasification reactions are given in works [1,2].

Problem statement

Depending on fuel type used in gasification, fuel peculiarities, gasification technique etc. different types of gasifiers may be used. These types differ by gas and fuel feed direction and organization, fuel motion manner, (fixed bed, fluidized (boiling) bed, spouted bed, entrained bed and others) etc. One of the most widely used types of gasifier is direct scheme gasifier (Fig. 1).

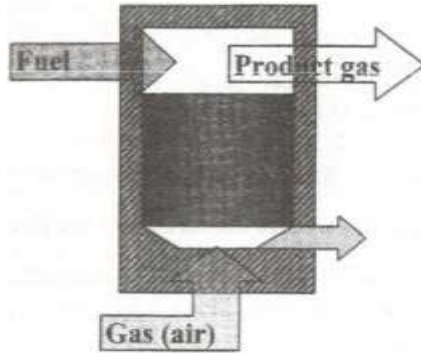


Fig. 1. Schematic model of direct scheme gasifier

In present work direct scheme gasifier with fixed bed was considered. Initial inhomogeneities of different characters and sizes were used. Height and diameter of gasification chamber were equal 0.5 m. Schematic drawing of filling porosity isolines for two types of inhomogeneous packing are presented in Fig. 2.

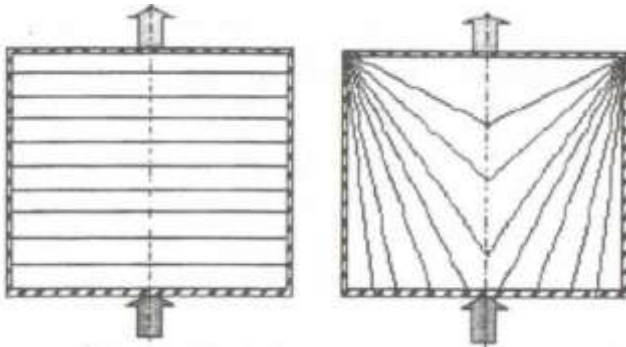


Fig. 2. Configuration of gasifier filing inhomogeneity: Porosity isolines

Monotonic coordinate dependencies of porosity were used in calculations. Porosity values were varied in the range from 0.2 to 0.5, that corresponded to filling mass about 100 kg under filling material density equal 1500 kg/m^3 . Initial typical size (effective diameter) of filling particles was $d_0 = 2 \text{ cm}$. Due to burnout effective diameter was decreased in calculations in order to preserve particles total number. Authors had no reliable information about kinetic parameters for gasification reactions, which have hydrogen-containing species involved. That's why calculations for air gasification were performed. Computations were carried out in the range of air draft consumption G varied from 1 to $10 \text{ Nm}^3/\text{h}$. As initial and boundary conditions the following were used: initial filling temperature was equal T_{burn} (values in the range from 700 to 1500 K); gasification chamber was initially filled with porous filling and nitrogen; air draft temperature was T_0 ; chamber walls temperature was equal T_w (values in the range from 300 to 1400 K were used).

The most important characteristics of gasifier performance are: quasi-steady regime establishing time, gasification mass rate, product gas composition. Computations of the above characteristics were performed for two different kinetic mechanisms of coal gasification. [1,2]. Calculations indicated that quasi-steady regime establishing time of the considered reactor is about 0.5-2 hours depending on flow rate. Mass gasification rate is directly proportional to draft consumption. Mass gasification rate is strongly depend on temperature. The dependence on initial filling inhomogeneity character and size is comparatively weak. Computations showed that product gas consists mainly of two components: nitrogen and one of carbon oxide (monoxide CO and dioxide CO₂). Under low temperatures (lower than 1000 K) CO₂ dominates in product gas composition, under high temperatures (higher than 1300 K) CO dominates in product gas composition. These results are in concord with experimental data of other investigators concerning air gasification of coal.

Resume

Computations showed that generalized volume-averaged model can be used for qualitative and quantitative studies of gasification process in gasifier. Utilization of developed software let one (if reliable experimental data are available) to conduct kinetic parameters fitting and verification for water vapor and vapor-air gasification. For simulation of more complex processes such as underground coal gasification it is necessary to include additional sub-models of porous bed structure transformation at gasification process.

References

1. Predvodiltelev A.S., Hitrin L.Ya., Tsuhanova O.A. et al. *Carbon combustion*. Moscow: Publishing house of Academy of Sciences of USSR, 1949, P.407. (in Russian).
2. Becker A.V., Polianchik E.V., Volkova N.N., Manelis G.B. *Filtration combustion of carbon*/ Theoretical foundations of chemical technology. 24 p. (In print).

QUASI-DETONATION IN POROUS MEDIA: ON PROPOGATION MECHANISM AND ON TRANSMISSION INTO CONFINED VOLUME

P.N. KRIVOSHEYEV, O.G. PENYAZKOV, S.A. ZHDANOK

A.V. Luikov Heat and Mass Transfer Institute of NAS of Belarus,
15, P. Brovka Str., Minsk, 220072, Belarus

Abstract

The propagation of quasi-detonations in a porous packed bed and subsequent transmission into smooth tube were studied. It was established that a necessary quasidetonation velocity required for re-ignition of detonation downstream of the porous bed is approximately equal to the isobaric sound speed of combustion products. The relative influence of a normal shock wave reflection mechanism on ignition and propagation of quasidetonations near the limit were investigated in details.

Introduction

The propagation of quasi-detonations in porous media is characterized by existence and interaction of distinct ignition mechanisms being responsible for sustaining the supersonic combustion mode under filtration conditions [1-3]. These are in the broad sense the local shock adiabatic compression resulting in auto-ignitions of the mixture [4] and ignition of unburnt products at elevated thermodynamic conditions in surroundings of the burnt material, usually referred as turbulent mixing mechanism [5]. In the case of adiabatic compression, hot spots in porous media can be formed via single or multiple reflections of the leading shock front, shock wave diffractions resulting in focusing phenomena inside a porous matrix, and interactions of shock headed transient gas jets from the adjacent pores.

Usually in a given porous bed, the velocity of quasi-detonation decreases from the maximal value at the most sensitive mixture to $V/V_{cj} \approx 0.3$ at the limits [5, 6]. Transmissions of such high-speed deflagrations are often accompanied by the flow acceleration and formation of a leading shock wave, which is strongly coupled with a flame front. The interaction and propagation of transverse shock waves caused by individual hot jets across the random flow stream of an porous bed can create hot spots in a fresh mixture by means of shock wave focusing and diffraction on flow inhomogeneities. In addition, the motion of transverse waves enhances the mixing and deforms the turbulent interface between reacted and unreacted products, thus increasing local reaction rates. Both mechanisms can lead to the formation of localized explosions in unburnt materials, which are capable of sustaining the leading shock during its expansion into the large volume, and can significantly promote the transition or re-initiation of a detonation wave [6, 7].

For some applications the evaluation of the parameters required for successful transition to detonation is of vital importance. Moreover, the development of engineering approaches for estimation of these parameters is necessary. The aim of these studies was also to investigate the transmission of quasi-detonations from a regular porous bed into smooth tube of same diameter, to determine the critical conditions required for detonation initiations and to elaborate the tools for their estimations.

Experimental Setup

Experiments were conducted in a square (35 x 35 mm) tube of 80 cm long attached to the smooth test part (40 cm long) of the same cross-section (Fig. 1). A normal combustion wave formed in a small pre-chamber initiated the propagation of quasi-detonation in a porous bed. A spark plug was used for ignition of the mixtures. The ignition energy was $E = 0.8$ mJ.

Experiments were made in a stoichiometric oxy-acetylene mixture $C_2H_2 + 2.5(O_2 + \beta N_2)$, with different degrees of nitrogen dilution and at initial pressures varying from 0.02 to 0.3 MPa.

Commercial grade acetylene, oxygen and nitrogen of 99.9 % purity were used for mixture preparations. All mixtures were prepared by the method of partial pressures and kept for two days before use. Prior to each experiment, the tube was pumped out to the pressure of $\sim 10^{-2}$ mm Hg. A pressure meter controlled the initial pressure of the mixture in the tube with an accuracy of ± 0.4 mm Hg. A porous filling comprised of 5.5-mm steel balls was used in all tests.

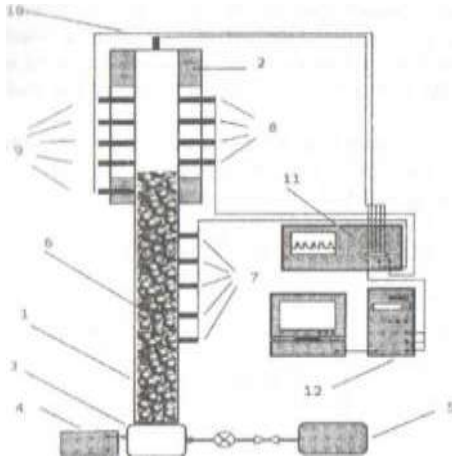


Fig. 1. Experimental setup. 1 - detonation tube; 2 - test section; 3 - ignition chamber; 4 - ignition unit; 5 - vacuum pump; 6 - porous filling; 7, 8 - ion gauges; 9, 10 - pressure sensors; 11 - digital oscilloscopes; 12 - PC

transmission into smooth sections of the tubes. Pressure transducers and ion sensors have controlled the arrival times of shock and combustion waves at different locations along smooth tubes. The deflagration to detonation transition run-up distance along the smooth tube was defined as the distance between the exit plane of the porous filling and the locations of pressure and ion gauges, at which the detonation velocity of transmitted deflagrations was attained.

Ion gauges and pressure transducers measured the velocity, and pressure of shock and reaction fronts. Ion sensors provided preliminary measurements of a high-speed deflagration velocity in a porous medium before

Results

Two different transition scenarios in a smooth tube were observed in the experiments (Fig. 2). At initial pressure higher than the critical one, the transmission of quasi-detonations led to the direct initiation of detonation downstream of the porous medium. At lower pressures, the leading shock wave decoupled from the reaction front and propagated with a continuously decreasing velocity to the reflecting wall

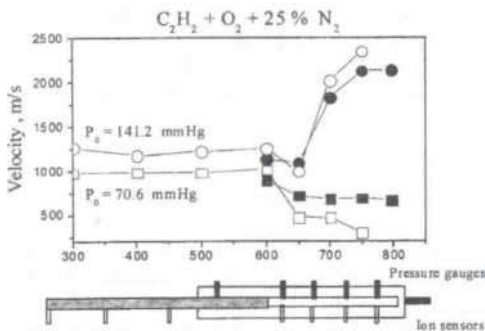


Fig. 2. Propagation velocities of shock and reaction fronts along a porous bed and a smooth tube for supercritical and subcritical transmissions

of the test section. The flame behind the shock wave decelerated more rapidly and this resulted in an increasing detachment zone between them. Figure 2 presents velocity histories of the leading shock reaction waves along the smooth tube for sub- and supercritical transmissions. Experiments showed that a venting of spatial distributed flame jets formed in a porous bed into a smooth section of the tube facilitates significantly the onset of detonations. The deflagration to detonation transition run-up distance downstream of the porous medium was less than one diameter of the tube within a wide range of compositions and initial pressures of the mixture.

Special attention was paid in the experiments to critical parameters of the venting gas flow, which result in the detonation onset behind the porous bed. Figure 3 shows the propagation velocities of reaction front in porous bed and shock front in smooth test section in stoichiometric oxyacetylene mixtures with 25% and 50% nitrogen dilutions. As is seen in the figure, the velocities of quasi-detonation in a porous bed required for successful detonation

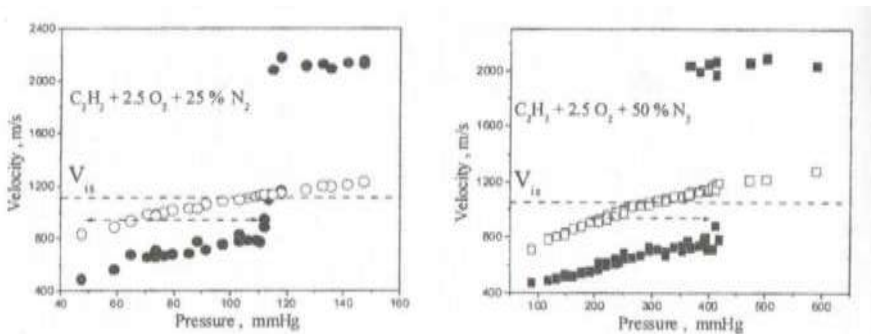


Fig. 3. Propagation velocities of shock (dark symbols) and reaction fronts (hollow symbols)

initiations correlate well (with accuracy ± 40 m/s) with the isobaric sound speed of the combustion products calculated for critical initial pressures in both mixtures from thermochemical equilibrium codes. This critical venting speed generates the necessary conditions to trigger the onset of detonation downstream of the flow. For subsonic outflows, the leading shock wave decouples from the reaction front and detonation occurs after reflection of the shock wave from the end flange of the tube (Fig. 2).

Thus, using results of previous works [5, 6] we may formulate the necessary requirements for direct detonation initiation behind a regular porous bed comprised of spherical particles

$$V_{ia} < V_{C2} [1 - 0.33 \log (d_c / d_p)], \quad (1)$$

where V_{ia} is an adiabatic sound velocity estimated for the critical initial pressure of the mixture.

The pressure transducer installed at the reflecting wall (Fig. 1) was used to determine the chemical induction time of the mixtures. The induction period was measured as the time interval between the beginning of a normal reflection of incident SW and the second pressure spike, initiated by the self-ignition of a shock-compressed gaseous mixture in a detachment zone. Figure 4 present the induction time measured for the conditions of normal shock wave reflection. The induction zone length was defined by using a simple relation $L_{ind} = \tau_{ind} \cdot V$, where, τ_{ind} is the chemical induction time corresponding to stagnation temperature and

pressure of the gas flow behind the leading shock front, V is a shock velocity. Figure 5 shows the induction length versus velocity of the transmitted shock wave. The normal reflection of incident shock wave produces the induction zone of $\approx 20\text{--}40$ mm for different mixtures in smooth section (Fig.5). The experiments demonstrate that at 3 times higher initial pressure of the mixture in the hollow tube than in a porous bed at the same SW velocities (Fig.3). The extrapolation of value of induction zone length to corresponding post-shock conditions of quasi-detonation using the pressure dependence of ignition time gives the induction length of $L_{ind} \approx 40\text{--}150$ mm in the porous body (Fig.5). It means that during the time between initial shock compression and auto-ignition of the mixture in porous bed the leading shock front should travel the distance approximately equal to 1-4 channel widths, or 80 pore sizes.

At the same time, pressure and ion current profiles of quasi-detonations show that the

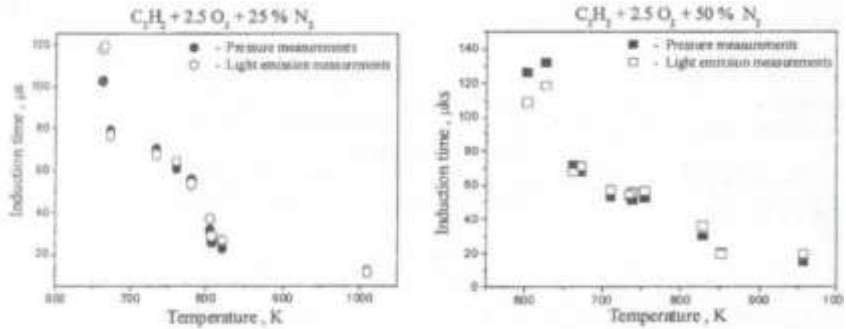


Fig. 4. Induction time on temperature for the conditions of normal reflection

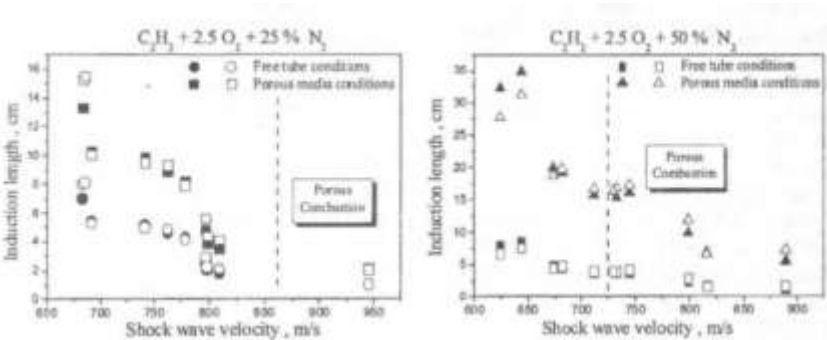


Fig. 5. Induction length for the conditions of normal shock wave reflection

length between shock and reaction fronts does not exceed the value of 1.5 - 3 mm, i.e. 1 - 2 pore sizes, within the scatter of experimental data. Thus, it evidences that the normal reflection of leading shock wave itself is not sufficient to ensure propagation mechanism of quasi-detonation at low velocities, and 3-D interactions of shock waves and transient flows in porous matrix should be taken into account to achieve the necessary level of thermal excitation of the mixture, create hot spots, and switch on the self-sustained mechanism of quasi-detonation propagations.

Conclusions

The propagation of quasi-detonations in a porous packed bed, comprised of 5.5-mm steel balls, and a subsequent transmission into smooth tubes has been studied experimentally.

Experiments revealed that venting of spatially distributed hot jets formed in a porous bed into a smooth section of the tube facilitates the onset of detonations. The deflagration to detonation transition run-up, downstream of the porous medium, was less than one tube diameter within a wide range of compositions and initial pressures of the mixture. It was established that a necessary quasi-detonation velocity required for re-ignition of detonation downstream of the porous bed is equal to the adiabatic sound speed of combustion products with an accuracy ± 40 m/sec. The necessary requirements for direct detonation initiation behind a regular porous bed comprised of spherical particles was

$$V_a < V_{CJ} [1 - 0.33 \log(d_c / d_p)],$$

where V_a is an isobaric sound speed of combustion products estimated for the critical initial pressure of the mixture.

It was established that the normal shock reflection mechanism itself cannot produce the successive auto-ignition of the mixture at real length scale in a porous bed and ensure the self-sustained propagation of quasi-detonation in a porous bed near the limits.

Acknowledgements

State Scientific Program of Republic of Belarus «Energy 18» and «Hydrogen8» and Found of Fundamental Studies of Republic of Belarus (grant T04M-015) sponsored these works.

Nomenclature

V_{CJ} - Chapman-Jouguet velocity of ideal detonation; d_c - critical tube diameter; d_p - pore size; τ_{ind} - chemical induction time; L_{ind} - induction zone length.

References

1. Kauffman C. W., Chuanjun Yan, Nicholls J. A. *Gaseous detonation in porous media* Nineteenth Symposium (International) on Combustion, Pittsburg, The Combustion Institute. 1982. pp. 591-597.
2. Pinaev A.V., Lyamin G.A.. *Fundamental laws governing subsonic and detonating gas combustion in inert porous media*. Combustion Explosion Shock Waves. 1989, Vol.25, pp.75-85.
3. Babkin V. S., Korzhavin A. A., Bunev V. A. *Propagation of premixed gaseous explosion flames in porous media* Combustion and Flame. 1991, Vol. 87, N.2. pp. 182-190.
4. Zel'dovich, Ya.B. *Theory of Combustion and Detonation in Gases*. Moscow- Leningrad, Russia: Izd. Acad. Nauk SSSR. 1944, p.71.
5. Makris A., Shafique H., Lee J. H. S, Knystautas R. *Influence of mixture sensitivity and pore size on detonation velocities in porous media* Shock Waves, 1995, Vol.4, N.1-2, pp.89-95.
6. Achasov O.V., Krivosheyev P.N., Penyazkov O.G, Sevruc K.L, Zhdanok S.A. *Ignition of an explosive gas mixture by a detonation wave formed in a porous medium*. Advances in Confined Detonations. Eds. G. Roy, S. Frolov, R. Santoro, S. Tsyganov. Moscow, Russia. 2002, pp. 109-112.
7. Achasov O.V., Krivosheyev P.N., Penyazkov O.G, Zhdanok S.A. *Flame-jets initiation of detonation in large volumes*. Proceedings of 19th International Colloquium on Dynamics of Explosions and Reactive Systems, July 27 - August 1, 2003 Hakone, Japan, paper 1.

DIGITAL SPECKLE PHOTOGRAPHY APPLICATION TO VORTICES MONITORING IN COMPLEX TURBULENT FLOWS

N.A. FOMIN, A.V. KRAUKLIS, E.I. LA VINSKAYA

A.V. Luikov Heat and Mass Transfer Institute of NAS of Belarus,
15, P. Brovka Str., Minsk, 220072, Belarus

Digital speckle photography (DSP) based on the computer aided acquisition and evaluation of time evolution of dynamic speckle patterns recorded by digital CCD cameras allows the instantaneous quantitative derivation of a 2D map of deflection angles and retardation of the light passing through the flow under study. Even for 3D flows, recent advances in digital optical data storage and analysis make it possible to extract quantitative data from line-of-sight flow visualization techniques [1,2]. Among the most important advantages of DSP are its high spatial resolution and the possibility to collect a great amount of experimental information from a single speckle-pattern record. In principle, the resolution can be as high as the diffraction limit of line-of-sight measurements (about 0.2-0.3 mm) [2]. For 2D flows, the maps of the deflection angles so obtained can be easily transformed into 2D density (temperature) gradient maps using simple calculations and without any calibration. In addition, precise digital multi-projection measurements allow the reconstructing of a 3D vortices structure using computerized tomography approach as below.

The first step of digital specklegram processing is similar to PIV and is performed by evaluation of statistical functions (cross-correlation or structural functions) of the recorded dynamic speckle fields. The record of the whole field is scanned by moving a $N \times M$ pixels window across the field. The pattern of the window in a frame 1 taken from the first exposure specklegram is cross-correlated with the pattern of the respective window at the same position in a frame 2 from the second exposure specklegram. Finally, the speckles displacement attributed to the area covered by the window is found from determining the maximum peak of the correlation in quasi-real time operation, see [2,3].

The general way to obtain interior flow information is to use multidirectional, line-of-sight measurements and to reconstruct 3D data using computer assisted tomography (CAT). For a given test object, the quality of the tomographic reconstruction depends on the number of projections taken, the covered total angular range of viewing directions, and the amount of information available from each projection. The integral Radon transformation can be used for data obtained from either laminar or turbulent flow, but an exact determination of the interior flow parameter distributions would need an infinite number of projections. The high data density is particularly advantageous for analyzing complex 3D turbulent flows. For direct recording of the light ray deflection angles, as in DSP, the integral Radon transformation simplifies and the optical disturbance (refractive index distribution) can be predicted from the transformation

$$f(x, y, z) = \int_{-\infty}^{\infty} \int_{-\infty}^{\infty} \int_{-\infty}^{\infty} \dots \int_{-\infty}^{\infty} f(x, y, z) \delta(x-x_0) \delta(y-y_0) \delta(z-z_0) \dots \delta(x-x_0) \delta(y-y_0) \delta(z-z_0) \dots$$

Because of the finite number of projection measurements available the application of the Radon transformation becomes an ill-posed mathematical problem. In practice this means that a small inaccuracy in the experimental data can lead to significantly large errors in the final flow parameter determination and that a finite number of flow structures can be reconstructed using a finite number of projections. So, only the large structures in turbulent

flows will be reconstructed here using the Radon integral transform, whereas the microstructure of turbulence will be further analyzed using statistical specklegram treatment. Several mathematical algorithms are available for reconstructing the 3D field from the information recorded in the various projections with the convolution back projection method being the most widely used. In the present paper an iteration technique has been adopted for the calculation of the Radon integral. This approach has been refined to accommodate information about the sought distribution as the first approximation. The noise in the experimental data has been smoothed by a cubic spline technique. This smoothing procedure improves the reconstruction quality, but removes the low-scale variation of the refractive index distribution from the reconstructed field.

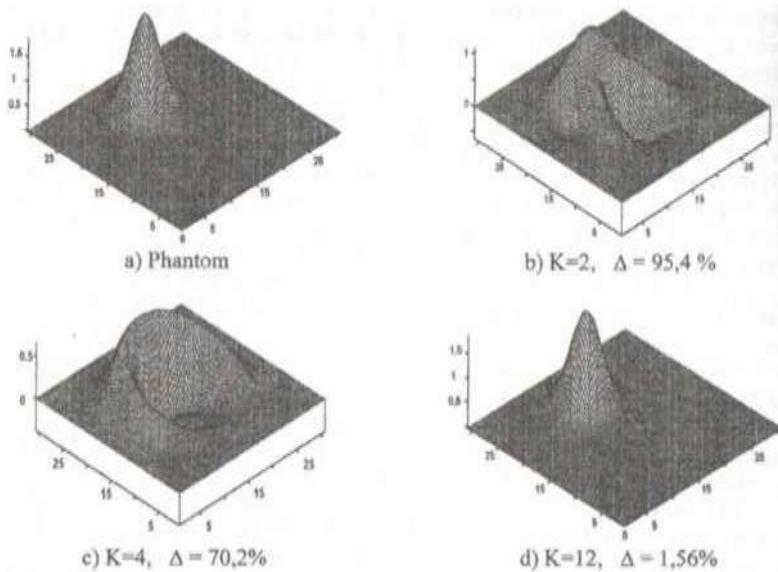


Fig. 1. Simulation results for 2, 4, and 12 - projectional speckle tomography: reconstructed phantom asymmetric function with one maximum

The mathematical procedure of tomographic reconstruction in turbulent flows was verified using numerical simulation with a "phantom" distribution of the refractive index. For each possible propagation direction in the flow simulation, the deflection angles of the light rays, $\epsilon(a, p)$, were determined from the refractive index distribution $n(x, y, z)$. An estimated measurement error was added randomly. This added noise simulates the influence of low length scale vorticity as well as random experimental errors. The deflection data were then used to estimate the refractive index distribution using the Radon transformation. Fig. 1 shows the simulation results for 2, 4, and 12 - projectional speckle tomography: reconstructed phantom asymmetric function with one maximum. Analyses of these and a number of similar simulation results for this scheme of speckle tomography revealed the following:

- By increasing the number of probing directions, it is possible to reconstruct the parameters to a prescribed accuracy in a flow of any complexity. This establishes the possibility of using the integral Radon inversion for diagnostics of turbulent flows.
- Imposing a random rms error of order 10% on the simulated functions does not significantly affect the net results when there are sufficient readings in the various directions. In this case the field-averaged rms error of reconstruction increases by less than 10%.
- When the number of directions of view is small, only the centre flow region with single-peak structure can be reconstructed to an acceptable accuracy.

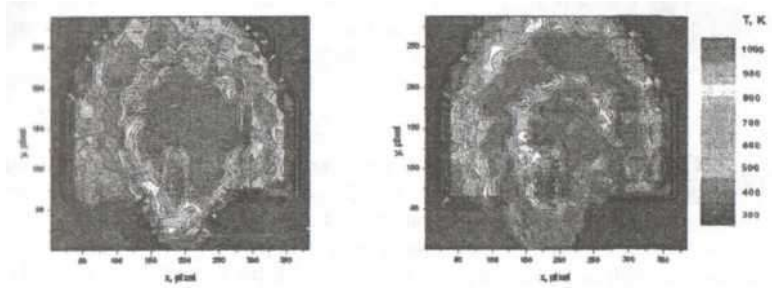


Fig. 2. Instantaneous temperature fields in combustion zone reconstructed using speckle photography data

Fig. 2 shows an example of quasi-real time reconstruction of the local parameters in an open turbulent flame from the digital speckle records taken in two directions.

The microscale turbulence structures are determined by using the 3-D density correlation functions evaluated with Erbeck-Merzkirch integral transforms. Using the relation between deflection angle and fluid density,

$$\epsilon_q(p, q) = K \int_0^L \frac{\partial \rho(p, q, s)}{\partial q} ds. \quad (2)$$

Erbeck and Merzkirch [4] has received a connection between density and deflection angle correlation functions

$$R_{\epsilon q}(\xi, \eta) = -K^2 \int_0^L \int_0^L \frac{\partial^2}{\partial \eta^2} R_\rho(\xi, \eta, \zeta) dz' dz''. \quad (3)$$

For the case of isotropic turbulence, this equation can be inverted with respect to density correlation functions:

$$R_\rho(r) = \frac{1}{\pi L K^2} \int_r^L \frac{1}{\sqrt{\tau^2 - r^2}} \left\{ \int_0^\tau R_\epsilon(\tau') d\tau' \right\} d\tau \quad (4)$$

and

$$R_\rho(r) = \frac{1}{\pi L K^2} \int_r^L \frac{\tau}{\sqrt{\tau^2 - r^2}} R_{\epsilon\perp}(\tau) d\tau. \quad (5)$$

It should be noted that the inversion of these functions to the original one, $R_p(r)$, is ill posed mathematical problem and care must be taken performing such calculations. As we can see, the inversion integrals are Abel type integrals, therefore the great experience of solving this equation may be used. Fig. 3 contains an example of correlation functions reconstructed by using a computer-simulated specklegram. The density correlation function here was reconstructed with the help of inverse integral transformation using about 200 readings at each phantom specklegram line. So, the quality of this reconstruction for a small-scale vorticity is

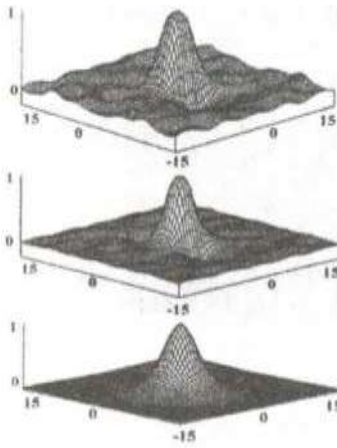


Fig. 3. Correlation functions reconstructed from a computer simulated specklegram

rather good with grids of about 200^2 . The discrepancy between initial correlation function constructed using the results of the direct numerical simulation and the function constructed using the deflection angle map increases with increasing the vorticity scale.

Using these data, both macro- and micro-scales of turbulence can be determined. Thus, the Erbeck-Merzkirch integral transform is an effective tool for local turbulence parameter determination using digital line-of-sight data. Both macro and micro spatial structures of the turbulent scalar (density) field in compressible flow can be visualized and quantitatively characterized with the applied multi-projectional DSP technique. It should be noted that the inversion of these functions to the original one, $R_p(r)$, is ill posed mathematical problem and care must be taken performing such calculations. As we can see, the inversion integrals are Abel type integrals, therefore the great experience of solving this equation may be used. The quality of this reconstruction for a small-scale vorticity is rather good with grids of about 200^2 .

Acknowledgements

The research described in this publication was supported by the Belarusian Fund for Basic Research (grant N Ф04P-063), Belarusian State programs “Hydrogen” and “Nanotex” and by INTAS (INTAS Projects N 00- 0135 and N 03-51-3332).

References

1. Merzkirch W. *Flow Visualization. Second edition*, Academic Press, Orlando (1987).
2. Fomin N. *Speckle Photography for Fluid Mechanics Measurements*. Springer Verlag, Berlin (1998).
3. Fomin N., Lavinskaja E., Merzkirch W., Vitkin D. *Turbulence microscale variations due to interaction with a shock wave*. Shock Waves, 10, 345-349 (2000).
4. Erbeck R., Merzkirch W.. *Speckle photographic measurements of turbulence in air stream with fluctuating temperature*. Proc. of the 1st Symposium on Turbulence, University of Missouri-Rolla University Pres, (1986).

HIGH-TEMPERATURE IGNITIONS OF HEAVY HYDROCARBONS

O.G. PENYAZKOV. K.L. SEVRUK

A.V. Luikov Heat and Mass Transfer Institute of NAS of Belarus,
15, P. Brovka Str., Minsk, 220072, Belarus

Introduction

In scramjets and detonation engines, rapid spontaneous ignition and reaction of the fuel-air mixtures are required to achieve the efficient functioning at supersonic combustion modes. Usually, the liquid hydrocarbons are considered as potential candidate fuel for supersonic propulsion because of their high energy density and storage capacity. For supersonic combustion, the high-temperature kinetics of ignition of large hydrocarbons determines a performance of the apparatus as a whole. At the same time, there is not so much information on auto-ignition of heavy hydrocarbon fuels at high temperatures and pressures [1-4]. Shock tube techniques are an ideal tool for studying auto-ignition phenomena for a number of reasons: post-shock conditions of fuel-air mixtures, covering the gas parameters in scramjets and pulsed detonation engines, can be readily and repeatedly attained behind the reflected shock wave; the flow conditions and ignition can be quantified and characterized by modern diagnostic methods. The shock-tube studies described in this report produce fundamental information on reaction kinetics of heavy hydrocarbon-air mixtures resulting in different initiation modes in a wide range of post-shock conditions behind reflected shock waves. The aim of these studies was to obtain reference data on ignition of Benzene, n-Hexane, and n-Decane at high temperatures.

Experimental set-up

The heated shock tube has been applied for these studies. Stainless steel shock tube of 76 mm in diameter equipped with pressure transducers and optical window for ignition delay time measurements was used in experiments. The length of the tube was 5.5 m. Four current circuits provided the independent heating of four parts of the shock tube to ensure the uniform temperature distributions along the tube length with accuracy of $\pm 1^\circ \text{C}$. Four thermocouples have registered the temperature along the device. Two of them have measured the metal temperature, another two - the gas temperature inside the shock tube. For all experimental runs presented in this report, the initial temperature of studied mixtures was 75 - 100⁰ C. The 18-liter stainless steel mixing cylinder heated up to the boiling temperature of hydrocarbon fuels 150 - 165⁰ C was used for mixture preparations. Two thermocouples measured the metal and gas temperature inside the cylinder. The heat insulation of the mixing assembly was the same as that of the shock tube. To evaporate the kerosene and stir the mixture, a stainless steel ball of 80 mm in diameter was inserted into the mixing cylinder. The ball rolled along the tank from one side to another, thus providing the mixing of the gas and accelerating the kerosene evaporation. The stirring time was 3-4 hour in all cases.

The initial temperatures in mixing vessel and shock tube were varied in accordance with vapor pressures of used fuel. Chemically pure n-Decane $\text{C}_{10}\text{H}_{22}$ (99.8 %), n-Hexane C_6H_{14} (99.55 %), and Benzene C_6H_6 (99.8%) liquid samples have been used for mixture preparation. To ensure a good evaporation of fuel samples at ambient pressure, the stirring temperature in mixing vessel was 174⁰ C in all experiments. The initial temperature of

resulting mixture in a shock tube was about of 75° C. Prior to the experiment, the shock tube was pumped out twice to the pressure of $\sim 10^{-2}$ mm Hg. After, the tube was filled with the mixture prepared in the mixing cylinder. Electronic pressure meter determined initial pressures of the mixture in a shock tube with an accuracy of ± 0.2 mm Hg.

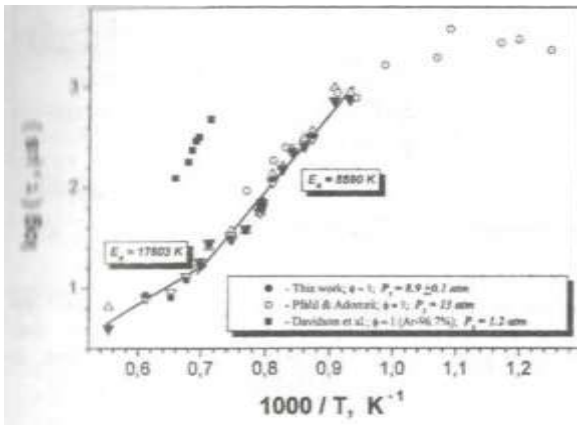
Pressure variations at different cross-sections of the shock tube were measured by high-frequency PCB pressure sensors Model 113A24 with rise time less than 1.5 μ s and with a 1.5-mm spatial resolution. Stainless steel test section for ignition delay time measurements are mated to the end flanges of shock tubes. Experimental signals were recorded and processed by an automatic 10-bit data acquisition system and a central computer.

To provide optical observations of fuel auto-ignition behind reflected shock waves, the quartz window of 45 mm in diameter has been mounted into reflecting end wall of the shock tube. The PCB pressure sensor installed near the quartz window measured the reflection time and pressure history behind reflected shock waves. To fix the instant at which the luminosity commences, a thin gas column ($\varnothing 5$ mm) along the tube axis is focused on photomultiplier cathodes. The beam-splitter divides output flame spectrum in two optical paths to ensure the simultaneous observations at two spectral bands. Monochromatic interference filters transmitted only the desired portion of emission spectrum of the gas mixture. The luminosity from C_2 ($\lambda=516.5$ nm; $\Delta \lambda = 5$ nm) radicals and integral emission from spectral band of 380 - 480 nm were employed to measure auto-ignition of the mixture. In the present work, ignition delay time was defined as the time difference between shock arrival at the end wall and the onset of emissions at required intensity levels from the measuring gas column along the tube axis. The flame emission in selected spectral band was registered by means of the photomultiplier having the maximal sensitivity in the selected spectrum.

Comparing velocities reflected shock wave and pressures at different locations from the reflecting wall identified auto-ignition modes of the mixture (strong transient and weak). The reflected wave velocity in the end part of the tube was defined as $V = V_5 + u$, where V_5 is visible propagation velocity of reflected shock wave, and u is flow velocity of incoming flow behind ISW (incident shock wave). Visible velocity was calculated by processing shock- arrival times at pressure sensors along the tube.

Auto-ignitions of Decane, Hexane and Benzene behind reflected shock waves

Fig. 1 illustrates the comparison of our data with results of Pfahl and Adomeit [5] and Davidson et al. [6] obtained behind reflected shock waves. Measurements of Pfahl and Adomeit [5] in stoichiometric n-Decane/Air mixture at postshock pressure of 13 atm correlate well with our observations. Longer ignition times in their study can be explained by the differences in experimental methods and ignition delay time definitions. Pfahl and Adomeit defined the onset of ignition from the rapid pressure rise measurements. So, they have obtained the longer ignition times. In contrary, we have used the initial pressure rise criterion for ignition delay time definition. Data points of Davidson et al. have been obtained in a mixture with a high argon dilution and at low pressures. Although, the measured ignition times follows the Arrhenius law, the significant decrease of activation energy has been observed in our experiments at high temperatures $T_5 > 1400$ K. Where, the approximate value of activation energy was $E_A = 8890$ K. At low temperatures $T_5 < 1400$ K, the second value for activation energy was deduced from our experimental data $E_A = 17603$ K. Fig. 1 indicates this behaviour. The measured critical post-shock temperature required for direct initiation of detonation in n-Decane was $T_5 = 1260$ K. No weak ignition has been observed in these tests in studied range of post-shock conditions. It should be noted the extremely high level of peak pressures in a shock-compressed mixture near reflecting wall have been developed at transient



Mg. 1. Shock tube ignition delay data vs. reciprocal temperature in a stoichiometric n-Decane / Air mixture

Hexane in comparison with n-Decane at equivalent post-shock conditions. As is seen in the figure, n-Hexane exhibits longer ignition times than n-Decane at temperatures of $T_5 < 1500$ K and lower activation energy of $E_a = 16280$ K. Ignition times in n-Hexane/Air mixture follow the Arrhenius law in all studied range of postshock temperatures 1100 - 1715 K. It should be pointed that the n-Hexane activation energy of $E_a = 16280$ K derived from these tests should be considered as approximate value, since the linear correlation of experimental points does not take into account variation of species concentrations with temperature at a constant post-shock pressure.

Fig. 3 presents the temperature dependence of reflected shock wave velocity in n-Hexane/n-Decane/Air mixtures at different distances from the end wall. The critical postshock temperature required for direct initiation of detonation in n-Hexane is $T_5 = 1300$ K (Fig. 3). The corresponding value for n-Decane is equal to $T_5 = 1260$ K.

To obtain the reference data on Aromatics oxidation at high temperatures measurements have been performed in stoichiometric Benzene/Air mixtures. To ensure a good evaporation of Benzene sample at ambient pressure, the stirring temperature in mixing vessel was 80°C in all tests. The initial temperature of resulting mixture in a shock tube was about 72°C .

Fig. 4 presents the temperature dependencies of ignition times in stoichiometric mixture obtained in this work and results of Burcat et al [8] for lower post-shock pressures. As is seen in the graph, ignition times in Benzene /Air mixture follow the Arrhenius law in all studied range of temperatures 1020 - 1660 K. As for n-Hexane/Air mixture, activation energy for Benzene $E_a = 16430$ K derived from these tests should be considered as an approximate value, since the linear correlation of experimental points does not take into account the temperature dependence of species concentrations at a constant post-shock pressure. The slope of ignition delay curve is in a good correlation with Burcat data points. The gap between results is explained by significant differences in post-shock pressures. As is seen in the Fig. 4, Benzene exhibits longer ignition times than n-Decane in all studied range of conditions. Ignition properties of Benzene are very similar to n-Hexane/Air mixture (Fig. 2).

regimes. These peak pressures almost twice exceed the pressure level for strong ignition mode.

According to chromatographic analysis, n-Hexane is the lightest from n-alkanes, which was in a significant amount (0.33 % by volume) in liquid aviation kerosene. The volatility of n-Hexane is extremely high as compared with heavy alkanes. So, in many case, the pre-ignition of n-Hexane can affect very strongly on combustion of kerosene sprays and non-premixed mixtures [7], Fig. 2 shows ignition delays in n-

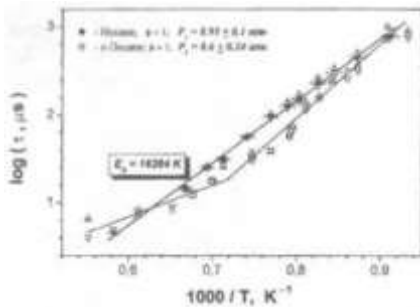


Fig. 2. Ignition delay time vs. reciprocal temperature in stoichiometric n-Hexane and n-Decane /Air mixtures at equivalent postshock conditions

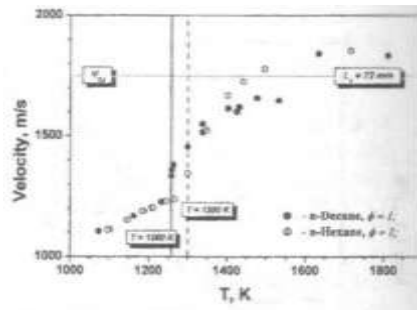


Fig. 3. Velocity of reflected shock wave and positions of the strong ignition limit vs. postshock temperature in stoichiometric n-Hexane and n-Decane/Air mixtures

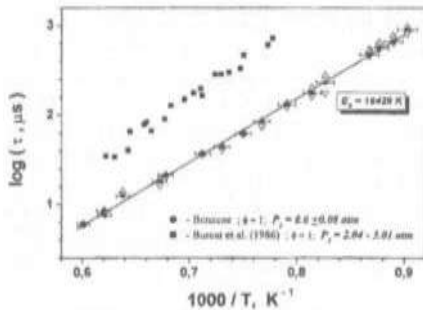


Fig. 4. Shock tube ignition delay data vs. reciprocal temperature in a stoichiometric Benzene / Air mixture

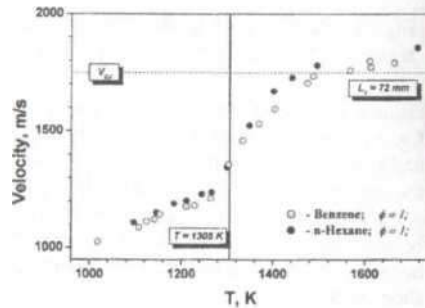


Fig. 5. Velocity of reflected shock wave and positions of the strong ignition limit vs. postshock temperature in stoichiometric n-Hexane and Benzene/Air mixtures

Fig. 5 presents the temperature dependence of reflected shock wave velocity in Benzene/n-Hexane/Air mixtures at different distances from the end wall. These graphs indicate that both ignition times and auto-ignition behavior in Benzene/Air mixture are practically the same as for n-Hexane. The critical post-shock temperature required for direct initiation of detonation in both mixtures was $T_5 = 1305$ K (Fig. 5). The corresponding value for n-Decane is equal to $T_5 = 1260$ K, respectively. Final C-J velocities are nearly the same in Benzene and n-Hexane mixtures.

Conclusions

Studies of Benzene, n-Hexane, n-Decane fuels representing kinetics and auto-ignition properties of aromatics and n-alkanes compounds of aviation kerosene have been performed using a heated shock tube. The mutual influence of each component on ignition delay time and dynamics of reflected shock wave propagation has been investigated in details.

Pure stoichiometric ($\phi = 1$) Benzene and n-Hexane/Air mixtures exhibit the same temperature dependencies for ignition times and reflected SW velocities at temperatures of

1100-1700 K and pressures of 8.6 - 8.9 atm. Approximate activation energies derived from our data were $E_a = 16429$ K and $E_A = 16284$ K for Benzene and n-Hexane, respectively. The critical postshock temperature required for direct detonation initiations in both fuels was $T = 1300$ K, which corresponds to ISW Mach numbers of $M = 2.94$ and $M = 3.0$, respectively.

Ignition delay times and auto-ignition regimes have been studied in stoichiometric n-Decane/Air mixture within temperature range of 1070 - 1630 K and pressure of 8.9 ± 0.2 atm. It was shown that n-Decane exhibits the best ignition properties in comparison with the other studied mixtures. The critical post-shock temperature required for direct initiation of detonation in n-Decane was $T_5 = 1260$ K.

Acknowledgements

These works were sponsored by State Scientific Programs «Energy 18» and "Hydrogen 36» (Republic of Belarus).

References

1. Lindstedt R. P., Maurice L. Q., *Surrogate mixtures to represent complex aviation and rocket fuels*, Journal of Propulsion and Power, Vol. 17, 2, P. 461-466, 2001.
2. Gueret C., Cathonnet M., Boettner J-C, Gaillard F., *Experimental study and modeling of kerosene oxidation in a jet-stirred flow reactor*, 23rd Symp. (Int.) on Combustion, The Combustion Institute, P. 211-216, 1990.
3. Moriue O., Eigenbrod C., Rath H.J., Sato J., Okai K., Tsue M., Kono M., *Effects of dilution by aromatic hydrocarbons on staged ignition behavior of n-Decane droplets*, Proceeding of the Combustion Institute, Vol. 28, P.969-975, 2000.
4. Eigenbrod C., Moriue O., Weilmunster P., Rath H.J., *Development of a simple model fuel for kerosene droplet ignition*, Proceeding of the Combustion Institute, Vol. 29, 2002.
5. Pfahl U., Adomeit G., *Twenty-First International Symposium on Shock Waves*, P. 273-278, 1997.
6. Davidson D.F., Herbon J.T., Hoving D.C., Hanson R.K., *OH concentration time histories in n-alkane oxidation*. Int. J. Chem. Kinet. 2001, Vol.33, P.775-783.
7. Burcat A., Olchanski E., Sokolinski C., *Kinetics of hexane combustion in a shock tube*. Israel J. Chem. 1996; Vol.36, P. 313-320.
8. Burcat A., Snyder C., Brabbs T. *Ignition delay times of benzene and toluene with oxygen in argon mixtures*, NASA Technical Memorandum 87312 (1986).

high temperature OF HYDROGEN-AIR MIXTURE AT HIGH PRESSURES BEHIND REFLECTED SHOCK WAVE

V.V. MARTYNENKO, O.G. PENYAZKOV, K.A. RAGOTNER, S.I. SHABUNYA A.V. Luikov Heat and Mass Transfer Institute of NAS of Belarus

Delay and characteristics of stoichiometric hydrogen-air mixture ignition behind reflected shock wave were carried out for temperature range 830-1450 K and pressures 2-21 atm. Experimental results were compared to based on well known hydrogen combustion kinetic scheme numeric calculations. Comparison has shown, that A.Konnov kinetic mechanism (version 4.0) and GRI mechanism (version 3.0) appears good quality accordance with the functional pressure dependence of hydrogen ignition delay at temperatures $T > 1200 K$. However, they need to be more accurately defined for better quantitative correlation with experimental results.

Influence of reflected shock wave interaction effects with dynamic boundary layer on ignition process and results of shock tube induction time measurement were studied. It is shown, that bifurcation of reflected shock essentially influenced on results of induction time measurement and hydrogen-air ignition regime changing at mixture temperature $T < 1100K$, which become stronger with gas pressure and density growth behind reflected shock wave.

It was determined that interaction with turbulent boundary layer leads to attenuation of temperature induction time dependency and stabilization of ignition process behind reflected shock wave.

Acknowledgements

This work has been partially supported by the belarussian goverment program of oriented fundamental research "Hydrogen".

THE MODEL OF FILTRATION COMBUSTION OF SOLID FUEL

E.A. SALGANSKY, E.V. POLIANCHIK, G.B. MANELIS.

Institute of Problems of Chemical Physics RAS,
142432 Chemogolovka, Moscow region, Russia

At filtration combustion (FC) the waves spreading of exothermal conversion in porous environment at gas filtration is understood [1-4]. Mechanism of reaction zone spreading in such system usually includes heating of initial materials before front and local chemical interaction of reagents with calorification of big enough amount of heat. The specific element determining the particularity of this systems class is gas filtration, which is not only the participant of chemical reaction, but also the heat-carrier forming the thermal structure of combustion wave. The wave spreading of exothermal conversion in mixture of condensed fuel with inert component at oxidant filtration through it leads to so-called "superadiabatic heating-up" [5, 6]. They arise because the releasing heat does not remove with reaction products but concentrates in combustion zone that allows raising greatly the temperature in it. The simplicity of "superadiabatic heating-up" realization advantageously distinguishes FC process from other combustion processes, so the spectrum of its using is very wide. The principle of FC occurs in natural (underground flames, smoldering), technological (coal gasification, SHS) and industrial (ore agglomeration, waste incineration) processes. However, It is necessary to note that in spite of growing interest to FC this process is not completely explored both from theoretical, and practical sides.

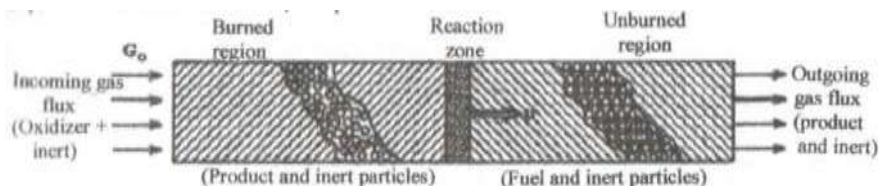
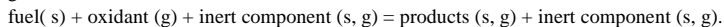


Fig. 1. Sketch of the colloid (forward) FC process

The principle scheme of filtration combustion is presented in Fig.1. Whereas practically any fuel initially contains chemical inert impurities (for example, ash), the porous medium before reaction zone presents itself in general case the mixture of condensed fuel with inert material. The porous residue containing the inert component and condensed combustion products remains after the combustion front. Heat releasing in the reaction is carried to initial layers of material with lower temperature and initiates in it its own heat release, that is why the process of wave propagation is self-sustaining. Both condensed, and gaseous products can be formed as a result of heterogeneous interaction of solid combustible with gaseous oxidant in FC wave. The scheme of the reactions is:



Here inert component denotes gases and condensed materials which is not participate in oxidation and gasification reactions. It is possible to refer air nitrogen, ash of solid fuel etc. to them.

For study of FC of solid fuel one-dimensional non-stationary two-temperature mathematical model has been suggested. It takes into account the kinetics of running reactions, the dependency of phases heat capacity on temperature and reagents composition, the reactor final sizes. This model is the development of thermodynamic mode! [7,8].

The model is built following suggestions. Heat losses through the lateral reactor wall are absent (the ideal adiabatic reactor). Pressure drop is small and is defined by assigned flow. Filling porosity remains constant. The coordinate system is connected with combustion limit.

The system consists of the following equations: conservation of each component mass of gaseous and solid media; conservation of energy; equation of state; characteristics of mass and heat exchange. Equation system was approximates on implicit scheme. Obtained difference equations were solved by Newton method.

The combustion (gasification) of mixture carbon - inert material in counterflow with gaseous oxidant has been considered. It has been supposed that the solid phase consists of two parts: incombustible part (the inert component) and burning part (fuel). At calculations the thermal physics characteristics of inert component are assumed as graphite or Al_2O_3 (corundum) has. It is possible to neglect CH_4 formation at carbon gasification since it is of importance, basically, at gasification at pressure above atmospheric [9].

Chemical scheme includes the following gross-reactions:

1. $C + 0.5 O_2 = CO$
2. $CO + 0.5 O_2 = CO_2$
3. $C + CO_2 = 2CO$
4. $C + O_2 = CO_2$
5. $C + H_2O = CO + H_2$
6. $CO + H_2O = CO_2 + H_2$
7. $H_2 + 0.5 O_2 = H_2O$

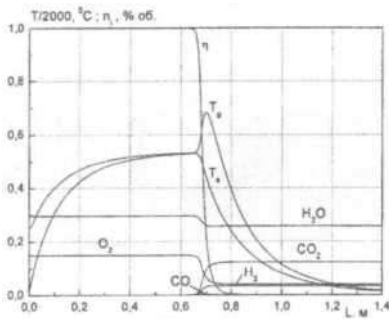


Fig. 2. Normal wave structure

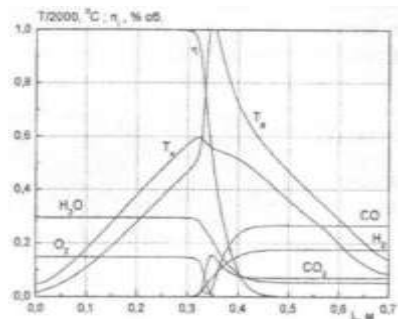


Fig. 3. Transition wave structure

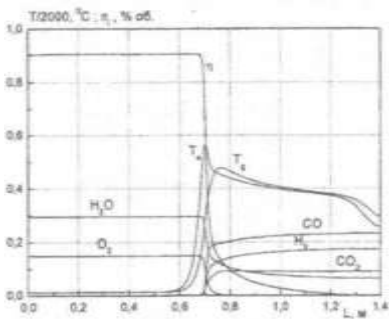


Fig. 4. Inversed wave structure

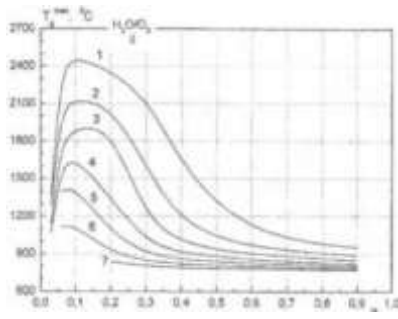


Fig. 5. Dependence of gas temperature on combustible part

Thermal and concentration fields typical for normal, transition and inversed waves are presented Fig. 2-4 [7, 8]. At normal wave structure a heat from the reactor is removed with solid products, at inversed wave structure a heat is removed with gaseous reaction product but at transition - both with solid, and gaseous products. The essential difference of phase temperatures in reaction zone is observed for temperature profiles (this effect denominates in transition waves field). Moreover, either gas or solid phase can be overheated, depending on general heat releases occurred in either gaseous or heterogeneous reactions. The kinetic combustion modes (modes with incomplete consumption of reactants) are presented on Mg. 2, 4. In case of normal wave oxygen skip behind the combustion front has been observed, but in case of inversed wave - incomplete burning-out of solid fuel. Stoichiometric mode is presented on Fig. 3 - both reagents are consumed completely.

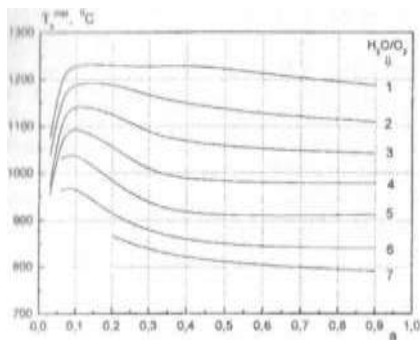


Fig. 6. Dependence of solid temperature on combustible part

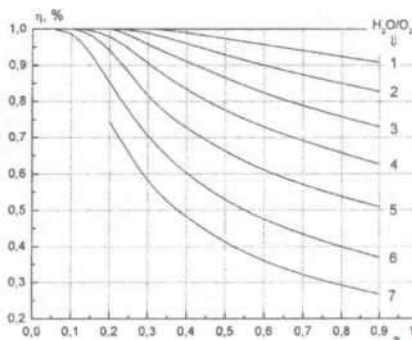


Fig. 7. Dependence of fuel conversion on combustible part

The dependencies of phases temperature on combustible part in initial mixture at different values of supplied vapor with gaseous oxidant are presented on Fig. 5, 6 (on graphs the curves corresponding to different ratio H_2O (vapor)/ O_2 , mol/mol have been presented). With increasing of supplied vapor high-temperature area in gas phase (Fig. 5) decreases, and its maximum shifts to smaller values of combustible part while the temperature changing of solid phase remains within 10% (at any values of parameter H_2O/O_2) in all interval of part of combustible component. Relative temperature insensitivity of solid phase to fuel part in initial mixture is explained by that after initiation of the combustion process heterogeneous reactions of gaseous oxidant with solid fuel take place in system first (in gas phase there are neither combustible gases (typifying for normal wave), nor the high enough temperature for their reactions (typifying for inversed waves)). At heterogeneous reactions the combustible gases (CO , H_2) are arises and mixture temperature increases. During interphase heat transfer the gas phase temperature increases, and if there are both reagents in gas (oxidant and combustible) gas-phase reactions begin to dominate over heterogeneous (the case of normal and transition waves). If oxidant was practically consumed in heterogeneous reactions (the case of inversed waves), gas reactions do not make the essential contribution to heat release process and the solid phase remains overheated.

The dependency of conversion degree of solid fuel on combustible part in initial mixture at different amount of supplied vapor with gaseous oxidant is shown on Fig. 7. Conversion degree is practically falls linearly with increasing of combustible part. Vapor

increasing leads to heat capacity increasing of gas phase flow, in this case the system is adjusted in such a way that ratio of heat capacity of flows has not changed. This is obtained by reduction of amount of consumed fuel and consequently by increasing of linear rate of solid phase (heat capacity of phase flow is equal to product of heat capacity multiplied by density and linear rate of phase).

The comparison of calculation results with experimental data is presented on Fig. 8. The calculations were carried out on the base of present model and on base of thermodynamic model [7, 8]. Experiments were conducted in quartz batch reactor. The internal reactor diameter was 46 mm, wall thickness - 2 mm. The mixture of reactor graphite with inert component (corundum) was as the initial filling. The wall of reactor was screened by aluminum foil for reduction of lateral heat losses. We shall remind that the lateral heat losses are not taken into account in the model while for present experimental installation they are 20-30 % from general power of heat release. The studied process is self-adjusted on temperature. This effect is in the following. Heat losses lead to temperature reduction so balance CO/CO₂ in combustion zone shifts to CO₂ for compensating of their influence (since oxidation up to CO₂ proceeds with bigger thermal effect than up to CO). The kinetics account of running reactions gives the more identical picture of process. The thermodynamic calculation overstates the combustion temperature at small vapor content in initial oxidant and understates it at higher contents of supplied vapor. The kinetic dependencies of reaction rate on the temperature "freeze" the corresponding reactions if the temperature is not enough for their running.

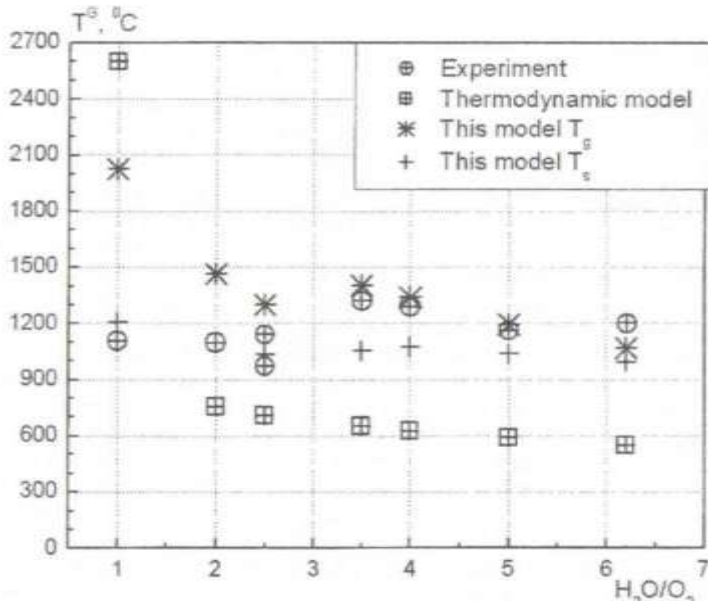


Fig. 8. Comparison with experimental data

As a result of conducted calculations the characteristics of filtration combustion wave of carbon been received. The kinetics account of running reactions allows to describe the modes incomplete reagents consumption, gives the more real picture on combustion temperature and composition of gaseous combustion products. In reaction zone there is the essential temperature difference of gas and solid phases; either gas or solid phase can be overheated depending on the general heat release occurred in either gaseous or heterogeneous reactions.

Nomenclature

Where T - temperature, v - gas rate, P - pressure, G - material inflow - outflow, Q - heat release of the chemical reactions, C - heat capacity, u - linear rate of initial mixture, F - specific surface of particles, a - fuel part in initial mixture, n - gaseous component part in gaseous phase, D - diffusion coefficient, R - universal gas constant, H - enthalpy, E_a - activation energy, k_0 - preexponent, x - current coordinate, ρ - density, α - heat transfer coefficient, θ - porosity, ε - heat part from heterogeneous reactions to solid phase, λ - thermal conductivity coefficient, γ - stoichiometric coefficients, η - conversion degree of fuel, μ - dynamic viscosity. Indexes; g - gaseous phase, s - solid, c - combustible, i - inert component, j - number, 0 - initial conditions.

References

1. Aldushin A.P., Seplyarsky B.S. *The spreading of exothermic reaction wave in porous bed at gas filtration (in Russian)*. Dokl. AS USSR, 1978, Vol. 241, №1, P. 72-75.
2. Aldushin A.P., Seplyarsky B.S. *The inversing of the combustion wave structure in porous media at gas filtration (in Russian)*. Dokl. AS USSR, 1979, Vol. 249, X^o3, P. 585-589.
3. Rabinovich O.S., Gurevich I.G. *Engineering physical journal, (in Russian)*. 1983, Vol.44, №1, P.75-80.
4. Babkin V.S., Vezhba I, Karim G.A. *Physics of combustion and explosion, (in Russian)*. 2002, Vol.38, №1, P. 3-11.
5. Aldushin A.P., Merzhanov A.G. *The theory of the filtration combustion: general information and state of research (in Russian)*. Thermal wave spreading in heterogeneous media. Novosibirsk: Nauka, 1998, P. 9-52.
6. Manelis G.B. *Superadiabatics (in Russian)*. Nature, 1996, .Ns3-4, P. 43.
7. Manelis G.B., Salgansky E.A., Fursov V.P., Glazov S.V., Salganskaya M.V. *Numerical study of carbon gasification in filtration combustion wave (in Russian)*. Science to Industry, 2001, .№8, P. 28-32.
8. Salgansky E.A., Fursov V.P., Glazov S.V., Salganskaya M.V., Manelis G.B. *The model of air gasification of solid fuel at filtration mode (in Russian)* Physics of combustion and explosion, 2003, Vol. 39, №1, P. 44-500.
9. Kantorovich B.V. *Introduction to combustion theory and solid fuel gasification (in Russian)*. M.: Metallurgizdat, 1960.
10. Glushko V.P. *Thermodynamics properties of the individual material (in Russian)*. M.: Nauka, 1978.

IGNITIONS OF PROPANE/AIR MIXTURE AT SHOCK WAVE FOCUSING IN TWO- AND THREE-DIMENSIONAL DUCTS

O.G. PENYAZKOV, K.L. SEVRUK A.V. Luikov Heat and Mass Transfer Institute of NAS of Belarus

Introduction

Functioning of propulsion devices based on supersonic combustion modes is usually accompanied by the formation and propagation of shock waves, which produce the necessary level of thermal excitation of the mixture to maintain high rate of energy release in the system. In many cases, PDE's design can be considered as a single self-consistent device in which interactions of shock waves with confinement walls and inner flow structure sustain the propagation of fast deflagrations and detonations along a certain trajectory. Under such approach, the confinement geometry can facilitate substantially the mixture re-ignition inside combustion chamber due to the effects of shock focusing [1-5]. This work addresses to systematic experimental and numerical investigations of auto-ignition phenomena at shock wave interaction with reflecting ducts of different geometry in propane/air mixtures, which are used as a model fuel for many studies of detonations.

Results

Experiments were carried in shock tube of 76 mm in diameter equipped with pressure transducers, ion gauges, and optical window for ignition delay time measurements (Fig. 1). Two-dimensional wedge, parabola, and corresponding axisymmetric ducts were used as the focusing elements. We have categorized four different regimes of the self-ignition at focusing conditions in the following terms: no ignition, weak ignition (deflagration), transient ignition resulting in DDT upstream the reflector and strong ignition (detonation) [4, 5]. The runs were performed at mean postshock pressure of 14.2 ± 2 atm and compared with auto-ignition tests

behind normally reflected shock wave and experiments that were performed at mean postshock pressure of 3 ± 0.5 atm. Particular attention has been paid to determining the critical ISW intensity required for initiation of different self-ignition modes. The absolute velocity of reflected shock wave in a frame of reference attached to gas flow moving behind incident shock and pressures at different locations from the reflecting wall identified the autoignition modes of the gas mixture (strong, transient and weak) The reflected wave velocity in this part of the tube was defined as $V = W + u$, where W is the visible velocity of reflected shock wave propagation outside the reflector, and u is the flow velocity behind ISW. Visible velocity was calculated by processing shock-arrival times at pressure sensors along the tube. If experimentally defined reflected shock wave velocities are compared with the calculated C-J velocity for temperature and pressure behind ISW, the direct detonation initiation occurs at shock wave focusing conditions.

The measured values of ignition delays vs. mean postshock temperature are plotted in the Fig. 2. As is seen in the figure, the shock wave focusing in two-dimensional and axisymmetric profiles significantly decreases the ignition thresholds of stoichiometric propane/air mixture as compared with the case of the normal reflection. The focusing results in a substantial decrease of ignition times in a wide range of postshock temperatures. For selfignition of the mixture, 3D axisymmetric reflectors are much more efficient than two- dimensional ones.

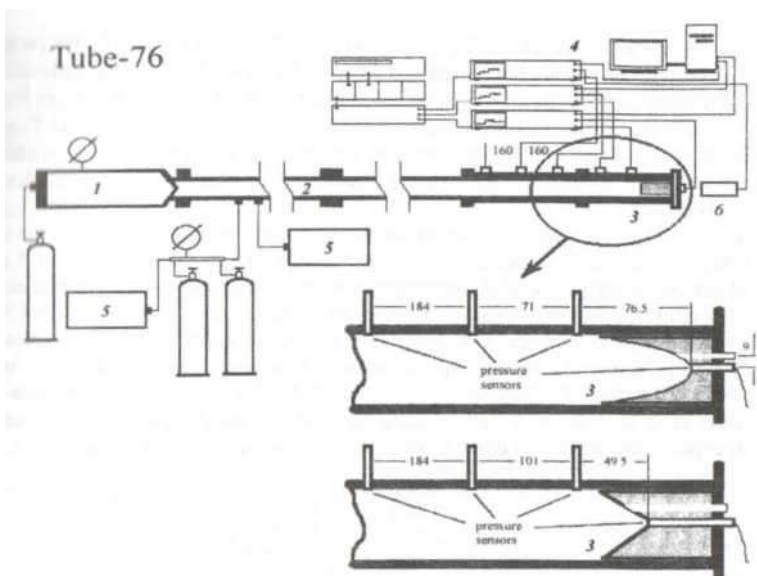


Fig. 1. Shock tube schematic diagram for ignition delay time measurements.
 1 - diaphragm-free high pressure chamber; 2 - low pressure chamber; 3 - test section; 4-1 Obit data acquisition system; 5-vacuum pump; 6-photomultiplier

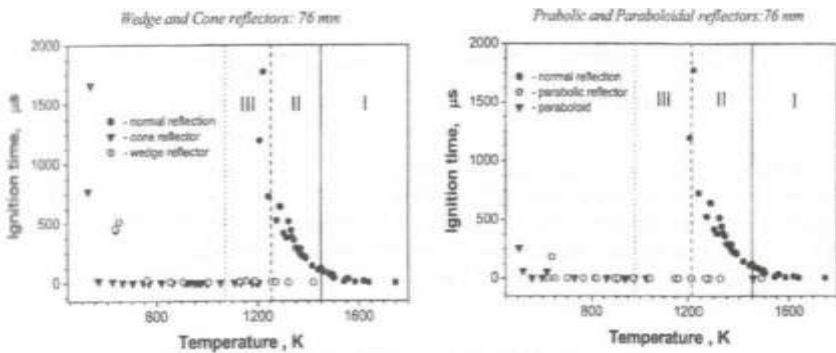


Fig. 2. Ignition time vs. mean postshock temperature at shock wave reflections from a plane wall, two-dimensional, and axisymmetric profiles. Domain I is strong ignition limit for normal reflection. Domain II is strong ignition limit in two-dimensional reflectors. Domain III is strong ignition limit in axisymmetric reflectors. Mean postshock pressure is

$$3.1 \pm 0.5 \text{ atm}$$

Figure 2 also illustrates the strong ignition domains responsible for direct initiation of detonations in studied geometries. The strong ignition domains for two-dimensional wedge and parabolic reflectors and corresponding axisymmetric profiles are approximately the same. The mean temperatures

$T_5 \approx 1240$ K for axisymmetric and two-dimensional profiles, respectively. The temperature $T_5 \approx 1400$ K corresponds to the strong ignition limit in the case of the normal reflection at equivalent postshock conditions. When the mean postshock pressure is about 5 times higher the mean temperatures required for direct initiation of detonations are $T_5 \approx 700$ K and $T_5 \approx 900$ K for axisymmetric and two-dimensional profiles, respectively. The temperature $T_5 \approx 1400$ K corresponds to the strong ignition limit in the case of the normal reflection at equivalent postshock conditions.

Figure 3 shows absolute velocities of the reflected wave at different parts of the tube from the reflector apex vs. ISW intensity, when the mean postshock pressure is about 3 atm. The critical Mach numbers required for direct initiation in the cone and paraboloidal reflectors are 2.76 and 2.69, respectively. For paraboloidal reflector, the transient regimes have not been observed experimentally, and as the ISW intensity decreasing, the weak ignition immediately follows the strong ignition mode. For cone reflector, the transient domain extends to lower Mach numbers and occurs at critical shock strengths of $M > 2.36$. So, one can conclude that cone reflectors with apex angle of 90° are more efficient than paraboloidal ones to generate the gaseous explosions via DDT or direct initiation at a studied range of conditions.

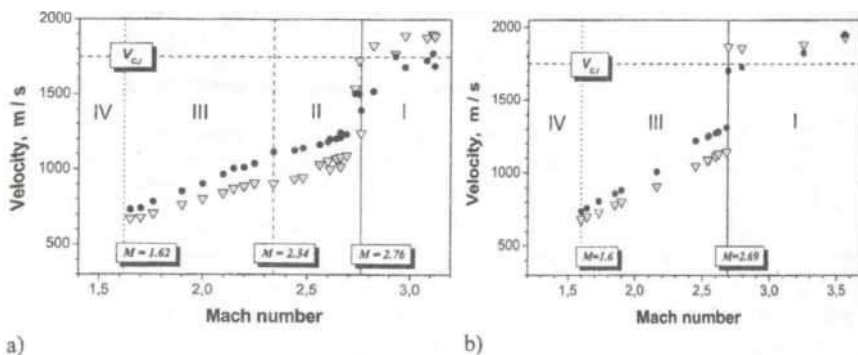


Fig. 3. Absolute velocity of reflected shock wave at different bases along the tube vs. ISW Mach number in cone (a) and paraboloidal (b) reflectors. Domain I - strong ignition limit. Domain II - transient ignition limit. Domain III - weak ignition limit. Domain VI - no ignition. Graph a: circles - the distance of 49.5 mm from the apex; triangles - the distance of 101 mm from the apex. Graph b: circles - the distance of 76.5 mm from the apex; triangles - the distance of 147.5 mm from the apex

Figure 4 shows absolute velocities of the reflected wave at different parts of the tube from the reflector apex vs. ISW intensity, when the mean postshock pressure is about 15 atm. The critical Mach numbers required for direct initiation in the cone and paraboloidal reflectors are 2.47 and 2.05, respectively. At these postshock conditions, the transient regimes have not been observed experimentally not only for the paraboloidal reflector but also for the cone reflector and with decreasing the ISW intensity, the weak ignition follows immediately the strong ignition mode.

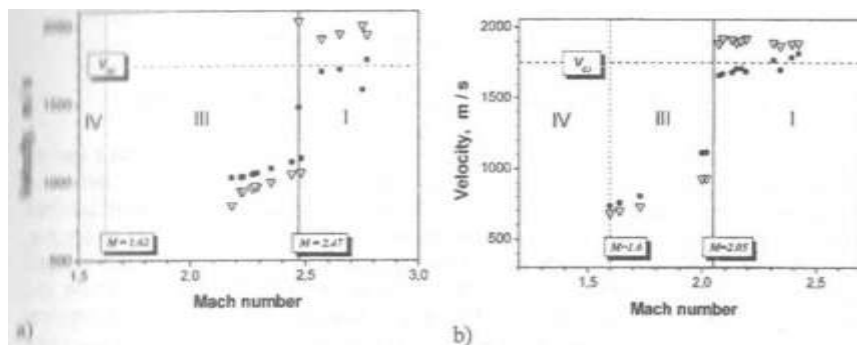


Fig. 4. Absolute velocity of reflected shock wave at different bases along the tube vs. ISW Mach number in cone (a) and paraboloidal (b) reflectors. Domain I - strong ignition limit. Domain III - weak ignition limit. Domain VI - no ignition. Graph a: circles - the distance of 49.5 mm from the apex; triangles - the distance of 101 mm from the apex. Graph b; circles - the distance of 76.5 mm from the apex; triangles - the distance of 147.5 mm from the apex

Conclusions

Auto-ignition domains in stoichiometric propane-air mixtures at post shock pressures of $P_5=3-15$ atm were determined at shock wave focusing in cone reflector with apex angles of 90° , and paraboloidal reflector. The critical Mach numbers required for direct initiation of detonations were 2.47 and 2.05 in cone and paraboloidal reflectors at high pressures, respectively.

Acknowledgements

These works were sponsored by State Scientific Programs («Energy 18» and «Hydrogen 18» (Republic of Belarus).

References

1. Borisov A.A., Gelfand B.E., Skatchkov G.L. et al. *Ignition of gaseous combustible mixtures in focused shock waves*. Sov. J. Chemicheskaya Phys. 1988, Vol.7, N12, p.387.
2. Chan C.K., Lau D., Tibault P., Penrose J.D. *Ignition and detonation initiation by shock focusing*. AIP Conf. Proc. 1990, Vol.208, p. 161.
3. Achasov O.V., Labuda S.A., Penyazkov O.G., Pushkin R.M. and Tarasov A.I. *Shock wave initiation of detonation in a semiclosed cavity*. Journal of Chemical Physics. 1993, Vol.12, N5, pp.714 -716 (in Russian).
4. Achasov O.V., Labuda S.A., Penyazkov O.G. and Ragozin D.S. *Shock wave and jets initiation of gaseous detonation*. Archivum Combustionis. 1995, Vol.15, N3-4, pp.253- 274.
5. Medvedev S.P., Gelfand B.E., Khomik S.V., Gronig H., Olivier H. *Shock tube study of hydrogen-air detonation induced by shock focusing*, Paper presented at Int. Workshop on Detonation under Geometrical Constraints, RWTH Aachen, December 15-17,1998.

DETONATION INITIATION IN DISPERSED FUEL-AIR MIXTURES

N.N. SMIRNOV, V.F. NIKITIN, J. KHADEM Moscow M.V. Lomonosov State University, Moscow

119899, Russia

Investigations of deflagration to detonation transition in gases and pulverized fuel-air mixtures were carried out for pulse detonating devices. The control of detonation onset is of major importance in pulse detonating devices. The advantages of detonation over constant pressure combustion bring to the necessity of promoting the DDT and shortening the pre- detonation length. Most of fuel-air mixtures being heterogeneous the problem of liquid droplet interaction with surrounding gas flow with account of heat and mass transfer and atomization becomes of key interest. The paper contains the results of theoretical investigations of detonation onset peculiarities in polydispersed hydrocarbon-air mixtures. The problem of shock wave initiation of combustible dispersed mixtures is discussed. Mathematical model for liquid droplet interaction with the gas flow is developed with account of non-equilibrium evaporation and atomization. Extensive numerical simulations of droplet thermal and mechanical relaxation in gas flows with account of evaporation and atomization were undertaken and summarized.

FLAME DYNAMICS AND FLOW FIELD CHARACTER AT COMBUSTION IN THIN SEMICLOSED TUBES

I.M. KOZLOV, K.V. DOBREGO, V.V. VASILIEV

A.V. Luikov Heat and Mass Transfer Institute of NAS of Belarus

Introduction

In this work the results of the detailed 2D numerical simulation of non-steady methane-air flame propagation in semi-closed tubes after ignition near the closed end are presented. It is shown that several characteristic regimes of flame propagation may take place in the system depending on tube diameter: close to normal laminar flames, non-steady accelerating flames and so called plough-type regime characterized with fuel incomplete combustion.

Problem statement

Non-steady gas dynamics of chemically reacting gas can be described by set of equations: continuity, Navier-Stokes, mass conservation for gas components and energy conservation.

$$\frac{d\rho}{dt} = -\rho \nabla \mathbf{u} \cdot \mathbf{e}_i \quad (1)$$

$$\rho \frac{d\mathbf{u}}{dt} = -\nabla p + \nabla \sigma' \quad (2)$$

$$\rho \frac{dc_i}{dt} = \dot{\rho}_i + \nabla \cdot (\rho D \nabla c_i), \quad i = \overline{1, N}, \quad (3)$$

here $\dot{\rho}_i$ - i -th component mass generating rate due to chemical reactions,

$$\sum_i \dot{\rho}_i = 0; \quad D -$$

diffusivity. Energy conservation equation is written in form of enthalpy conservation with regard to diffusion and heat conductivity processes

$$\rho \frac{dH}{dt} = \nabla \cdot \left(\rho \sum_i h_i D \nabla c_i + \Lambda \nabla T \right), \quad (4)$$

where h_i - mass enthalpy of i -th gaseous component, Λ - heat conductivity coefficient. Speed of sound is assumed to be infinitely high.

State of gas in arbitrary point is defined by pressure p , temperature T , gas velocity \mathbf{u} , gas components concentrations C_i (molar) or c_i (mass) together with gas state equations

$$\rho = \frac{pM}{RT} \quad \text{and} \quad H(T, c_1, \dots, c_N) = \sum_i c_i h_i(T). \quad \text{Mean molar mass of the gas } M \text{ is expressed via}$$

$$\text{component concentrations} \quad \frac{1}{M} = \sum_i \frac{c_i}{M_i}$$

Combustion gas dynamics in semi-closed tubes was simulated in the case of ignition near the closed end of the tube. Stoichiometric methane - air mixture was taken as a combustible. The length of the simulated tube was 4 cm and diameter of the channel varied in the range from ~ 0.7 to 5 mm. The space step of the mesh was $\Delta x = 0.01-0.02$ mm which guaranteed spatial resolution of concentration fields, temperature front and boundary layers. Combustion ignition was simulated with temperature step at the 0.5 mm length domain near the closed end of the tube at the initial instant. The gas composition and temperature of the

preheated domain corresponded to equilibrium at adiabatic combustion temperature T_{ikl} , Combustion front position was defined as a line of the 0.5 level of the initial concentration of methane, $\xi_{CH_4} = 0.5$. The velocity of the bow point of the front relatively to the walls $S_{f, mu}$ was considered as main characteristic of the flame front propagation dynamics.

Simulation results

According to calculations, flame dynamics, temperature and gas velocity fields substantially depend on tube diameter. Dependences of the flame velocity $S_{f,max}$ on the propagation distance for the tubes of different diameters are presented on the Fig. 1. The cases of the constant temperature of the tube walls (conductive heat losses) and adiabatic walls are presented on left and right graphs correspondingly.

Flame velocity at the distance of 3 cm from the closed end as a function of the tube diameter is presented on the Fig. 2. The curve corresponding to the adiabatic conditions lays higher than the curve calculated in the case of constant temperature walls. It is seen from the graphs that in the adiabatic conditions flame propagation is possible in very narrow tubes. In conditions of non-adiabatic walls flame propagation is impossible for the tubes diameters less than critical diameter d_{cr} . For stoichiometric methane- air mixture at normal pressure and temperature calculations give $d_{cr} = 1.9$ mm .

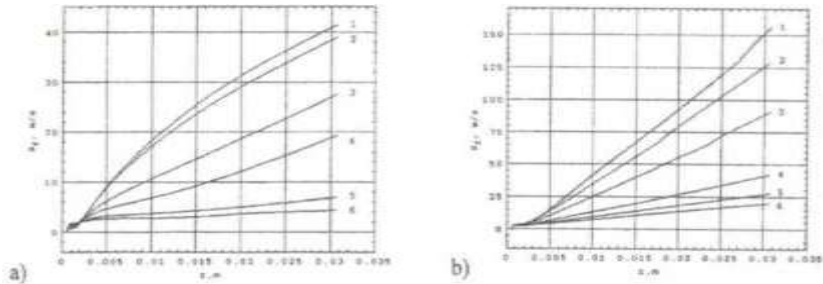


Fig. 1. Flame velocity $S_{f,max}$ as a function of the propagation distance for different diameters of the tube, a) constant temperature walls: 1 - $d_0 = 1.88$, 2 - 1.96, 3 - 2.48, 4 - 2.96, 5 - 3.96, 6 - 4.96 mm ; b) adiabatic walls: 1 - $d_0 = 1$, 2 - 1.46, 3 - 1.96, 4 - 2.96, 5 - 3.96, 6 - 4.96 mm

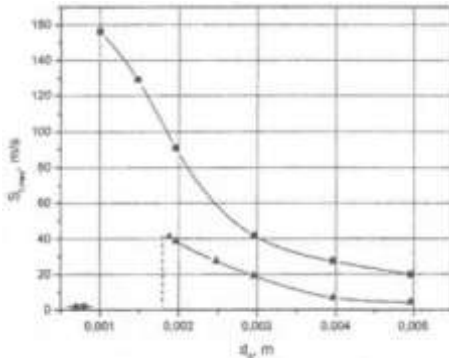


Fig. 2. Flame velocity $S_{f,max}$ at the distance of 3 cm from the closed end as a function of the tube diameter d_0 ■ adiabatic walls; ▲ - non-adiabatic walls. Dashed line - thermal quenching limit

Simulation proves the *flame surface area tow* with high accuracy: flame velocity corresponds to the flame surface area, Fig. 3. At the same time *the flame surface area low* itself doesn't explain mechanisms determining flame velocity and acceleration. Flame surface area grows owing to numerous physical factors: diffusion-thermoconduction and Darreus- Landau instability, interaction with the walls, external perturbations etc.

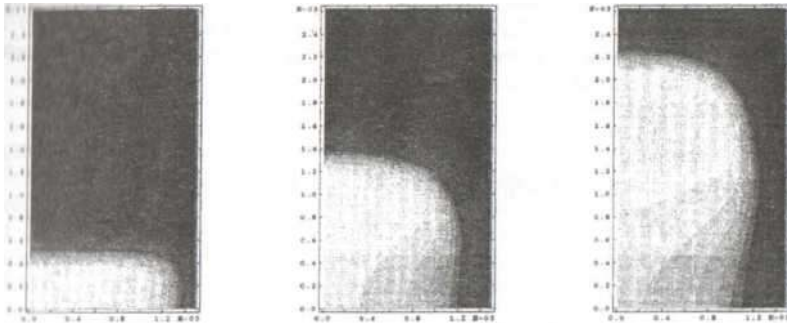


Fig. 3. The sequent shots of the temperature field in the tube at combustion front propagation, $d_0 = 3$ mm. Black solid line - flame front

For observation and analysis of the combustion gas dynamics the streamlines were drawn. Tangents to the streamlines correspond to the momentary velocity field. Note that for the non-steady case the streamlines do not correspond to the trajectories of particles. Nevertheless due to gas local quasi-steady movement in the system of coordinates moving with the front, streamlines effectively represent gas dynamics for the given combustion regime.

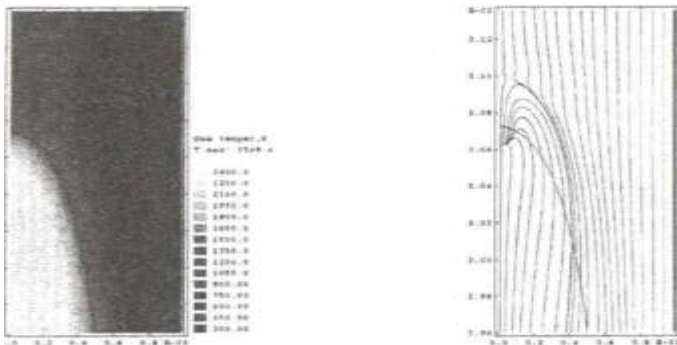


Fig. 4. Temperature field and streamlines in the system of coordinates moving with the front. $d_0 = 2$ mm. Black solid line - flame front

The Fig. 4 shows 2D temperature field and streamlines in the $d_0 = 2$ mm tube at the moment when flame reaches coordinate $z_{fmax} = 30.7$ mm .

Detailed 2D simulation of methane- air mixture combustion in narrow tubes was performed, it revealed complicated gas dynamics of non-steady combustion and gave more clear understanding of front formation mechanisms. Viscous deceleration of gas near the walls is the main factor of front perturbation and front configuration backing. Other mechanisms of front perturbation (diffusion - conduction asymmetry, Darreus-Landau instability) do not develop at least at times and distances of simulated cases. 2D test calculations with zero viscosity resulted in practically one dimensional results and normal laminar flame temperature and flame structure.

Acknowledgements

The work was partially supported by the INTAS grant N 03-51-4736.